GEOLOGICA ULTRAIECTINA

Mededelingen van de
Faculteit Aardwetenschappen der
Rijksuniversiteit te Utrecht

No. 68

THE ROLE OF SOLVENT INTERACTION WITH CRYSTALLINE SURFACES IN CRYSTAL GROWTH

ELLY VAN DER VOORT

GEOLOGICA ULTRAIECTINA

Mededelingen van de
Faculteit Aardwetenschappen der
Rijksuniversiteit te Utrecht

No. 68

THE ROLE OF SOLVENT INTERACTION WITH CRYSTALLINE SURFACES IN CRYSTAL GROWTH

CIP-GEGEVENS KONINKLIJKE BIBLIOTHEEK, DEN HAAG

Voort, Elisabeth van der

The role of solvent interaction with crystalline surfaces in crystal growth / Elisabeth van der Voort. - [Utrecht : Instituut voor Aardwetenschappen der Rijksuniversiteit Utrecht]. - (Geologica Ultraiectina, ISSN 0072-1026 ; no. 68)
Proefschrift Utrecht. - Met samenvatting in het Nederlands.
ISBN 90-71577-21-X
SISO 566 UDC 548.5(043.3)
Trefw.: kristallen.

THE ROLE OF SOLVENT INTERACTION WITH CRYSTALLINE SURFACES IN CRYSTAL GROWTH

DE ROL VAN OPLOSMIDDELINTERACTIE MET KRISTALOPPERVLAKKEN IN DE KRISTALGROEI

(met een samenvatting in het Nederlands)

PROEFSCHRIFT

TER VERKRIJGING VAN DE GRAAD VAN DOCTOR AAN DE RIJKSUNIVERSITEIT TE UTRECHT, OP GEZAG VAN DE RECTOR MAGNIFICUS PROF. DR. J.A. VAN GINKEL, INGEVOLGE HET BESLUIT VAN HET COLLEGE VAN DECANEN IN HET OPENBAAR TE VERDEDIGEN OP MAANDAG 22 OKTOBER 1990 DES NAMIDDAGS TE 4.15 UUR.

DOOR

ELISABETH VAN DER VOORT

GEBOREN OP 11 DECEMBER 1962 TE UTRECHT

PROMOTOR: PROF. DR. P. HARTMAN
verbonden aan de faculteit der Geologie en Geofysica van de Rijksuniversiteit te Utrecht *(em.)*

aan Paul
aan mijn ouders

VOORWOORD

Als ik terug kijk naar de afgelopen vier jaar, kijk ik naar een roerige tijd in "IvA-town" die heel snel voorbij is gegaan. Nu mijn proefschrift klaar is, wil ik een aantal mensen met name bedanken en niet in de laatste plaats mijn ouders die het mij mogelijk hebben gemaakt een wetenschappelijke opleiding te genieten en altijd het volste vertrouwen in mij gehad hebben.

Mijn promotor professor Hartman wil ik bedanken voor de vrijheid om het onderzoek op mijn manier in te richten en het nauwgezet bestuderen van het manuscript.

Mijn collega's Kees Woensdregt, Christina Strom, Nellie Slaats, Marion Sweet, Charles Laman en Vianney Govers bedank ik voor de prettige samenwerking en de gezelligheid.

Bij de vaste 'bemensing' van de op één na achterste tafel in de kantine was het altijd goed koffie drinken en discussiëren over andere dagelijkse dingen dan werk.

Ik ben de glasblazers van de Fysica werkplaats en de mensen van de Audiovisuele dienst van Aardwetenschappen dankbaar voor de snelle en goede service.

De afdeling Kristal- en Structuurchemie ben ik dankbaar voor de gastvrijheid en het mogen gebruiken van de computerfaciliteiten en programma's.

Ik ben de mensen van de vakgroep Fysische en Colloïdchemie, en in het bijzonder de hardlopers, dankbaar voor hun vriendschap en het mogen meeproeven van de goede Van 't Hoffse sfeer.

En Paul, voor jou zijn er geen woorden.....

CONTENTS

The following chapters have been or will be published:

CHAPTER 2
Van der Voort, E. & Hartman, P. (1988). Calculated interfacial tensions for the calcite cleavage rhombohedron and water. *J. Crystal Growth* **89**, 603-607.

CHAPTER 3
Van der Voort, E. (1990). Observations on growth form and habit of potassium nitrate as a function of the temperature. *J. Crystal Growth* **100**, 544.

CHAPTER 4
Van der Voort, E. (1990). The morphology of succinic acid crystals: the role of solvent interaction. Submitted for publication in *J. Crystal Growth.*

CHAPTER 5
Van der Voort, E. (1990). The theoretical growth form of potassium nitrate from an aqueous solution. Submitted for publication in *J. Crystal Growth.*

CHAPTER 6
Van der Voort, E. & Hartman, P. (1990). The role of water in the habit change from cube to octahedron of alkali halide crystals. *J. Crystal Growth.* In press.

CHAPTER 7
Van der Voort, E. & Hartman, P. (1990). Morphology of polar $ASO_3 \cdot 6H_2O$ crystals (A = Ni, Co, Mg) and solvent interaction. Accepted for publication in *J. Crystal Growth.*

CHAPTER 8
Van der Voort, E. & Hartman, P. (1990). The habit of gypsum and solvent interaction. Intended for publication in *J. Crystal Growth.*

CHAPTER 1

INTRODUCTION

1.1 General

The PBC-theory (Hartman & Perdok, 1952, 1955; Hartman, 1973, 1988) has shown to be a powerful tool in understanding and predicting the growth form of crystals (Hartman, 1978, 1980; Dumas, 1980). It is assumed that growth of crystals can be considered as the formation of bonds between growth units (atoms, ions, molecules). If we consider a two dimensional crystal we can derive that the crystal is bounded by edges that are parallel to the directions in which there is an uninterrupted chain of strong bonds (Periodic Bond Chain, PBC). For a layer on a face of a three dimensional crystal holds, that the layer is determined by two PBC's in different directions. Three categories of faces can be distinguished (see figure 1.1):

- F faces or flat faces containing two or more PBCs in a layer (hkl) with

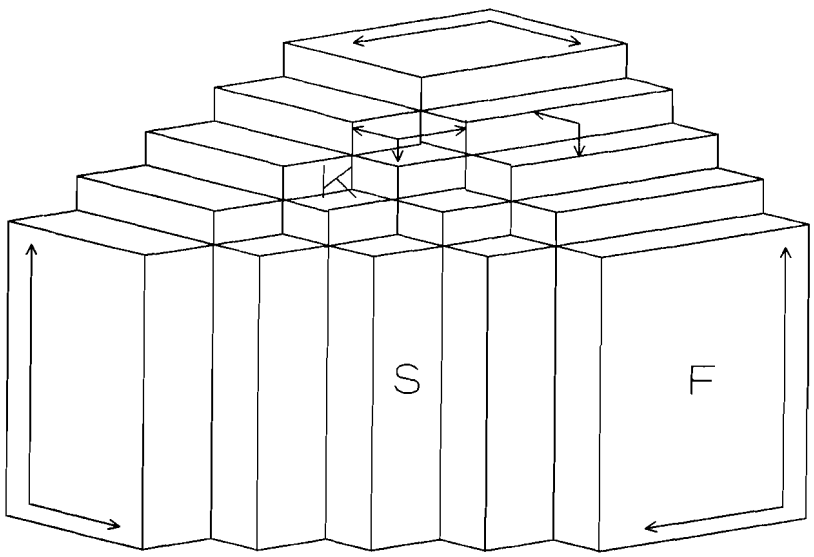

Figure 1.1 Crystal with F,S and K faces and three PBCs as indicated by the arrows.

thickness d_{hkl}. These layers are called slices.

- S faces or stepped faces containing only one PBC in a layer d_{hkl} and,
- K faces or kinked faces containing no PBC at all in a layer d_{hkl}.

F faces grow according to a layer mechanism. They grow slowly and are therefore the most predominant faces present on the crystal. S faces grow according to one dimensional nucleation. K faces need no nucleation at all. Both kinds of faces grow fast and are normally not found on crystals.

The energy released per mole when a slice is attached to a crystal face is defined as the attachment energy E_{att}. The growth rate of a face can be taken proportional with E_{att} (Hartman & Bennema, 1980). The habit of the crystal follows from the relative growth rates of the faces.

Although the PBC-theory can often be used to predict growth forms, sometimes discrepancies are observed between the theoretical and the observed growth forms (Felius, 1976; Woensdregt, 1982). Hartman and Heijnen (1983) discovered that in some of these cases the problematic F forms (*i.e.* the F forms for which an incorrect relative growth rate was predicted) had several possible slice configurations (atomic surface structures with a minimal specific surface energy). It was concluded that such a face can grow by layers of thickness $(1/n)d_{hkl}$. This led to a better agreement between the calculated and observed forms of *e.g.* aragonite (Heijnen, 1986) and calcium oxalate dihydrate (Heijnen & Van Duijneveldt, 1984).

One way to deal with remaining discrepancies is surface relaxation. In the PBC-theory it is assumed that the crystal structure at the surface and in the bulk are the same. Relaxation lowers the surface energy and the attachment energy. Equilibrium habits of corundum and hematite are calculated taking this effect into account (Mackrodt, Davey, Black & Docherty, 1987). Hartman (1989), however, shows that surface relaxation can not account alone for these discrepancies and he concludes that interaction with the solution must play a role.

When crystals of succinic acid are grown from solution, the growth forms depend on the solvent that is used (Davey, Mullin & Whiting, 1982). Only when crystals of succinic acid grow from the vapour they show a very good agreement with the calculated growth form (Berkovitch-Yellin, 1985). It is evident that the origin of these observations has to be sought in the role of the solvent in the crystallization process. It was assumed that the solvent affects the habit of the crystal by preferential adsorption of solvent molecules on specific faces. The stronger the solvent is adsorbed on a face, the more its

growth rate is reduced. Taking this effect into account Berkovitch-Yellin (1985) obtained improved calculated habits for several organic compounds including succinic acid.

Also supersaturation-dependent habit changes may be explained through solvent interaction with the crystal face. Crystals of alkali halides with a NaCl structure grow as cubes from moderately supersaturated solutions. When the supersaturation is increased above a certain level octahedron faces appear on the crystals. The solvent is believed to stabilize the surface structure of the octahedron face (Kern, 1953; Bienfait, Boistelle & Kern, 1965).

The growth rates of crystals of several salts were studied as a function of the temperature (Sipyagin, 1968; Sipyagin & Chernov, 1973; Chernov, Parvov, Eskin & Sipyagin, 1984). It was found that the growth rates of several faces did not increase monotonically with the temperature as one expects. Instead oscillations in the growth rate/temperature dependence were found which are believed to be related to changes in the structure of the solution next to the surface.

In this thesis we want to improve predicted growth forms by taking solvent interaction into account. Also some of the above mentioned effects are explained through solvent interaction. We limit ourselves to the most abundant and most widely used solvent on earth, water. We also limit ourselves to hydrophilic surfaces. In the next section a short overview is given of relevant structural aspects of water and aqueous solutions, because water near a surface is believed to behave as water near a solute molecule in a solution. Drost-Hansen (1969) proposed a model for water near a surface that is analogous to the model of a solution from Frank and Evans (1945).

The molecules of liquid water, their interactions and the processes in which they are involved are inaccessible to direct observation or measurement. We must, therefore resort to considering hypothetical models in order to understand the peculiar observations and measurements upon water, for instance the fact that water shrinks upon warming from the ice point. Over the years water models based on this notion have been put forward.

First, it was suggested that during melting part of the ice was converted into a fluid in which the remainder dissolved (Röntgen, 1892). After the hydrogen bond had been identified (Latimer & Rodebush, 1920), and the structure of ice established (Barua & Das Gupta, 1963), a more structural model was outlined in which melting of ice was described as bending of the tetrahedral hydrogen bonds. The water molecules become surrounded by

neighbours in distorted positions and orientations. This model was already proposed in 1933 by Bernal and Fowler. A third model, as pointed out by Samoilov (1946), describes melting of ice as the migration of water molecules from ice lattice positions to random positions. So disordered water exists between ordered regions and hydrogen bonds are actually broken instead of bent. Raman and infrared spectra confirm that an O-H bond can have two different environments. One has a hydrogen bonded character and the other is more or less free (Frank, 1972). Grunwald (1986) suggested a model containing the familiar tetrahedral four-coordinated species as in ice as well as five-coordinated species. This model can account well for some of the observed peculiar properties of water.

When a polar solute or an ion is dissolved in water the structure of the water changes. Short range solute/water interactions are present which are dominated by electrostatic forces. Frank and Evans (1945) and Frank and Wen (1957) postulated a model for aqueous solutions of ions in which there are three concentric regions around an ion, an innermost region of polarized molecules also known as the primary hydration sphere, an outer region containing bulk water and an intermediate region where the normal liquid structure and the electric field around the ion are in competition (secondary hydration sphere). A simple calculation shows that this model can not be valid for concentrated solutions. These solutions (*e.g.* a saturated solution of NaCl) contain no bulky region, the secondary hydration sphere must be completely absent as well, and water molecules of the primary hydration sphere must be shared by the ions.

It is generally accepted that the properties and the structure of water near a solid surface are different but it is not exactly known how different they are and how far from the surface these differences persist.

Single crystal X-ray diffraction studies of proteins which contain large amounts of water in the crystal structure, have shown that water molecules next to the protein molecules are highly ordered (Johnson, 1985; Savage & Wlodawer, 1986; Savage, 1986). Highly ordered water molecules are also found on surfaces of clays in X-ray diffraction studies (Pons, Tchoubar & Tchoubar, 1980) and NMR-studies (Fripiat, Cases, François & Letellier, 1982).

The structure of the hydration layer immediately adjacent to a hydrophilic (polar) surface is mainly determined by electrostatic forces. When these forces are not too strong the formation of hydrogen bonds between water molecules becomes competitive with water/surface bonding (Thiel & Madey, 1987; Pruppacher & Klett, 1978). The water/surface interaction usually ties the

water through the oxygen to specific cation sites (Kurtz & Henrich, 1982). In crystal structures of proteins water molecules are bonded to exposed polar groups at the surface through hydrogen bonding (Finney, 1979).

Monte Carlo and Molecular Dynamics simulations show anisotropic angular distributions which means that the water molecules near the surface are oriented preferentially with their dipole moment parallel to the surface. The effects are rather weak and penetrate not further than a few molecular diameters into the fluid (Aloisi, Guidelli, Jackson, Clark & Barnes, 1986; Mulla, 1986; Valleau & Gardner, 1987; Gardner & Valleau, 1987).

1.2 Scope of the thesis

The purpose of the research described in this thesis is to obtain more insight and understanding in the interaction of water and aqueous solutions with crystalline surfaces. Furthermore we aim at understanding the role of this interaction in crystal growth processes and the consequences for the habit of the crystals, in order to be able to explain the discrepancies between theoretical growth forms, obtained by a so-called PBC-analysis, and observed growth forms.

Crystal growth from a solution involves much more than simply adding growth units (molecules, ions, complexes) to the growing crystal. It involves complex reactions of which the mechanisms are not known. The reaction pathway consists among other things of (partial) solvation and desolvation steps of both the crystal and growth units. Expressions for linear growth rates of faces in a solution are deduced from those derived for growth from the vapour. These expressions appear very useful but do not tell what is actually happening in the solution or near the crystal surface.

In order to get an insight in the possible strength of solvent interaction for calcite, the electrostatic field near the cleavage rhombohedron was calculated (Chapter 2).

Crystals of potassium nitrate were grown in a flow system at constant supersaturation and different temperatures in order to investigate the influence of previously reported oscillations in growth rate as a function of the temperature on the habit of the crystals (see section 1.1). These oscillations are believed to be caused by changes in the structure of the solution near the crystal faces (Chapter 3).

In Chapters 4, 5, 6, 7 and 8 some case studies in which standard theory and practice do not agree are presented.

In Chapter 4 and 5 the solvent interactions with crystal faces are studied.

In order to understand in what way the solvent interaction influences the growth rate, the solvent interaction with the faces of succinic acid was studied. With the aid of Molecular Mechanics calculations the strength of the solvent interaction was determined and included in the growth rate law (Chapter 4). The same method was applied to potassium nitrate to explain the observed habits (Chapter 5).

In Chapter 6 also the solvent interaction with steps and kinks of some alkali halides is studied. Because the rocksalt structure of these halides is relatively simple it is possible to establish the shape of the steps and kinks.

Chapter 7 and 8 present two case studies of hydrates. The first one involves the polar habit of $MgSO_3 \cdot 6H_2O$. With the PBC-theory it is in principle not possible to predict polar habits. The second case study is focused on gypsum. Several theoretical habits have been derived for gypsum but none of them agrees with the habit from an aqueous solution.

References

Aloisi, G., Guidelli, R., Jackson, R.A., Clark, S.M & Barnes, P. (1986). *J. Electroanal. Chem.* **206**, 131.

Barua, A.K. & Das Gupta, A. (1963). *Trans. Faraday Soc.* **59**, 2243.

Berkovitch-Yellin, Z. (1985). *J. Am. Chem. Soc.* **107**, 8239.

Bernal, J.D. & Fowler, R.H. (1933). *J. Chem. Phys.* **1**, 515.

Bienfait, M., Boistelle, R. & Kern, R. (1965). In *Adsorption et Croissance Cristalline*, Colloques Internationaux du CNRS No. **152**, p. 515. Paris: Edition du CNRS.

Chernov, A.A., Parvov, V.F., Eskin, S.M. & Sipyagin, V.V. (1984). In *Growth of Crystals*, Vol. 12, edited by A.A. Chernov, p. 103. New York: Consultants Bureau.

Davey, R.J., Mullin, J.W. & Whiting, M.J.L. (1982). *J. Crystal Growth* **58**, 304.

Drost-Hansen, W. (1969). *Ind. Eng. Chem.* **61**, 10.

Dumas, A., Ledésert, M., Woensdregt, C.F., Hartman, P. & Monier, J.C. (1980). *J. Crystal Growth* 49, 233.

Felius, R.O. (1976). *Structural Morphology of Rutile and Trirutile type crystals*, Ph.D. Thesis, Leiden.

Finney, J.L. (1979). In *Water, A Comprehensive Treatise*, Vol. **6**, edited by F. Franks, Chapter 2, and references therein. New York: Plenum.

Frank, H.S. (1972). In *Water, A Comprehensive Treatise*, Vol. **1**, edited by F. Franks, Chapter 1. New York: Plenum.

Frank, H.S. & Evans, M.W. (1945). *J. Chem. Phys.* **13**, 507.

Frank, H.S. & Wen, W.Y. (1957). *Disc. Faraday Soc.* **24**, 133.

Fripiat, J.J., Cases, J., François, M. & Letellier, M. (1982). *J. Coll. Interf. Sci.* 89, 378.

Gardner, A.A. & Valleau, J.P. (1987). *J. Chem. Phys.* **86**, 4171.

Grunwald, E. (1986). *J. Am. Chem. Soc.* **108**, 5719.

Hartman, P. (1973). In *Crystal Growth, An Introduction*, edited by P. Hartman, Chapter 14. Amsterdam: North-Holland.

Hartman, P. (1978). *Bull. Minéral.* **101**, 195.

Hartman, P. (1980). *J. Crystal Growth* **49**, 157.

Hartman, P. (1988). In *Morphology of Crystals, Part A*, edited by I. Sunagawa, p. 269. Tokyo: Terrapub and Dordrecht: Reidel.

Hartman, P. (1989). *J. Crystal Growth* **96**, 667.

Hartman, P. & Bennema, P. (1980), *J. Crystal Growth* **49**, 145.

Hartman, P. & Heijnen, W.M.M. (1983). *J. Crystal Growth* **63**, 261.

Hartman, P. & Perdok, W.G. (1952). *Proc. Koninkl. Nederland. Akad. Wetenschap. Ser. B*55, 134.

Hartman, P. & Perdok, W.G. (1955). *Acta Cryst.* **8**, 49.

Heijnen, W.M.M. (1986). *Neues Jahrb. Mineral. Abh.* **154**, 223.

Heijnen, W.M.M. & van Duijneveldt, F.B. (1984). *J. Crystal Growth* **67**, 324.

Johnson, L.N. (1985). In *New Comprehensive Biochemistry*, Vol. **11**A, edited by A. Neuberger & L.L.M. van Deenen. Amsterdam: Elsevier.

Kern, R. (1953). *Bull. Soc. Fr. Minér. Crist.* **76**, 325.

Kurtz, R.L. & Henrich, V.E. (1982). *Phys. Rev.* B**26**, 6682.

Latimer, W.M. & Rodebush, W.H. (1920). *J. Am. Chem. Soc.* **42**, 1419.

Mackrodt, W.C., Davey, R.J., Black, S.N. & Docherty, R. (1987). *J. Crystal Growth* **80**, 441.

Mulla, D.J. (1986). In *Geochemical Processes at Surfaces*, edited by J.A. Davis and K.F. Hayes, Chapter 2. Washington D.C.: American Chemical Society.

Pons, C.H., Tchoubar, C. & Tchoubar, D. (1980). *Bull. Soc. Fr. Minér. Crist.* **103**, 452.

Pruppacher, H.R. & Klett, J.D. (1978). *Microphysics of Clouds and Precipitation*. Dordrecht: Reidel.
Röntgen, W.K. (1892). *Ann. Phys.* **45**, 91.
Samoilov, O. Ya. (1946). *Zh. Fiz. Khim.* **20**, 12.
Savage, H. (1986). *Biophys. J.* **50**, 947.
Savage, H. & Wlodawer, A. (1986). *Methods in Enzymology* **127**, 162.
Schwendinger, M.G. & Rode, B.M. (1989). *Chem. Phys. Lett.* **155**, 527.
Sipyagin, V.V. (1968). *Soviet Physics - Crystallography* **12**, 590.
Sipyagin, V.V. & Chernov, A.A. (1973). *Soviet Physics - Crystallography* **17**, 881.
Thiel, P.A. & Madey, T.E. (1987). *Surf. Sci. Rep.* **7**, 211.
Valleau, J.P. & Gardner, A.A. (1987). *J. Chem. Phys.* **86**, 4162.
Woensdregt, C.F. (1982). *Z. Kristallogr.* **161**, 15.

CHAPTER 2

CALCULATED INTERFACIAL TENSIONS FOR THE CALCITE CLEAVAGE RHOMBOHEDRON AND WATER

Abstract

The interfacial tension for the calcite cleavage rhombohedron and water has been calculated from Coulomb potentials of lattice slices, taking into account the polarizability of water. The water layer is considered as a crystalline structure. It appears that the interfacial tension as measured from nucleation experiments does not refer to the calcite-water interface, but to the interface between water and a calcite surface covered with an either complete or incomplete monolayer of water. In the models used the calcite-water interface has a negative interfacial tension of -556 mJ m^{-2}, whereas the completely hydrated surface-water interface has an interfacial tension of 49 mJ m^{-2}.

2.1 Introduction

Recently the specific surface energies of the major faces of the $CaCO_3$ modifications calcite and aragonite have been calculated (Heijnen, 1985, 1986). The values range from 1089 mJ m^{-2} for the cleavage rhombohedron of calcite to 1752 mJ m^{-2} for (020) and 1787 mJ m^{-2} for (110) of aragonite. These are surface energies with respect to vacuum. Values of the specific surface energies with respect to an aqueous solution, as derived from nucleation experiments, are in the order of 100 mJ m^{-2} (Söhnel & Mullin, 1978). This enormous discrepancy shows that there must be a strong interaction between the crystal surface and the solvent. By calculating this interaction energy it should be possible to obtain calculated values of the interfacial tension between crystal face and solution.

The quantities involved are related by

$$\gamma_{SL} = \gamma_S + \gamma_L - U_{int} \qquad (2.1)$$

where γ_S is the specific surface energy of the crystal face, γ_L that of the surrounding medium, i.e. solution and U_{int} the interaction energy and γ_{SL} the interfacial tension. In this paper we report on calculations for the cleavage rhombohedron of calcite, using two models for the interface structure.

2.2 Interface model I

The face under consideration is the cleavage rhombohedron face (211) of calcite (indexing based on smallest rhombohedral unit cell, the parameters of which are a = b = c = 6.3576 Å, $\alpha = \beta = \gamma = 46.214°$ (Chessin, Hamilton & Post, 1965)). To describe the interface structure, a new set of axes is used: **a'** = [$\bar{1}$11], **b'** = [0$\bar{1}$1] and **c'** = [2$\bar{1}\bar{1}$]. Then (211) becomes (001). The new unit cell is A-centered with a = 8.0821 Å, b = 4.9901 Å, c = 8.6431 Å and β = 135.475°. Atomic coordinates are listed in table 2.1 and an *ac*-projection is depicted in figure 2.1. We assume that the surface is not relaxed and that the water molecules are adsorbed in such a way that the structure of calcite is more or less continued. That is to say, that the coordinations around the calcium ion at the surface and in the bulk are similar. The charge distribution in the

Table 2.1 Fractional atomic coordinates and charges (e) of the transformed calcite unit cell.

Atom	x	y	z	q
Ca1	0	0	0	2
Ca2	1/2	0	0	2
C1	3/4	-1/2	0	1
C2	1/4	-1/2	0	1
O1	1/4	-0.6285	-0.1285	-1
O2	1/4	-0.2429	0	-1
O3	1/4	-0.6285	0.1285	-1
O4	3/4	-0.3715	0.1285	-1
O5	3/4	-0.7571	0	-1
O6	3/4	-0.3715	-0.1285	-1
Ca3	0	1/2	1/2	2
Ca4	1/2	1/2	1/2	2
C3	3/4	0	1/2	1
C4	1/4	0	1/2	1
O7	1/4	-0.1285	0.3715	-1
O8	1/4	0.2571	1/2	-1
O9	1/4	-0.1285	0.6285	-1
O10	3/4	0.1285	0.6285	-1
O11	3/4	-0.2571	1/2	-1
O12	3/4	0.1285	0.3715	-1

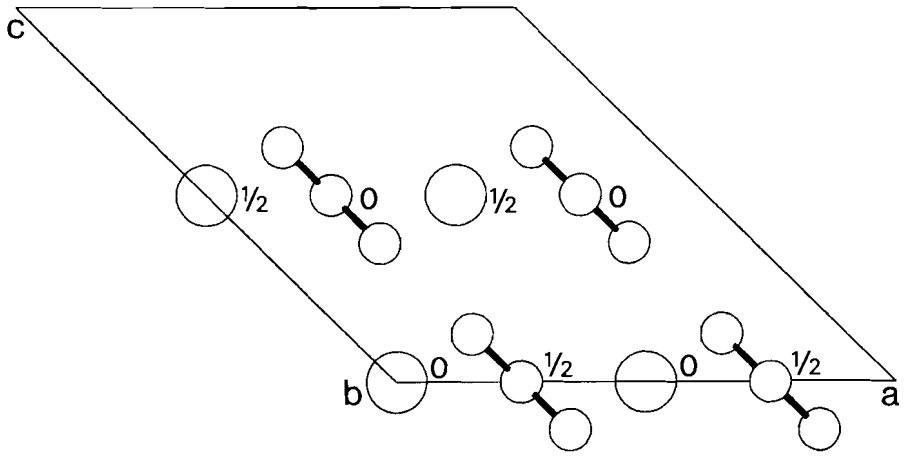

Figure 2.1 ac projection of the transformed unit cell (PLUTON, EUCLID-version (Spek, 1982).

CO_3^{2-}-ion is taken as $C^+O_3^-$ based on the same arguments as given by Heijnen (1985).

The APL-program *SURFPOT* (Strom & Hartman, 1989) was used for the calculation of the Coulomb potentials, energies and fields.

The direction and magnitude of the electric field vector at the position of the oxygen atom of the water molecule have been calculated. The positions of the hydrogen atoms have been chosen such that r(O-H) = 0.96 Å, $\angle$(H-O-H) = 104.5° and the dipole moment of the water molecule is parallel to the electric field vector. The charge distribution within the water molecule was taken to comply with the dipole moment in the gas, leading to q_H = +0.33. The rotational barrier of the water molecule has been calculated by rotating the molecule round its twofold axis and calculating the interaction energies with the electric field of the surface. The interaction energy of the molecule with the electric field of the crystal surface is

$$U_{int} = \sum_i q_i V_i \qquad (2.2)$$

where q_i = electric charge of an ion (e), V_i = electrostatic potential (e Å^{-1}) and U_{int} is the interaction energy (e^2 Å^{-1}). The rotational barrier is 3.1 kJ mole^{-1} and therefore less than 3RT for T = 300 K.

Another water molecule completes the first layer and is placed in the vicinity of the CO_3^{2-}-ion on a position at which the magnitude of the electric

Table 2.2 Atomic coordinates of the first water layer.

Atom	x	y	z
O11	1/4	0.3715	0.8715
H11	0.3716	0.5052	0.9568
H12	0.2848	0.2616	0.9678
O21	3/4	0.6285	0.8715
H21	0.8716	0.4948	0.9568
H22	0.7848	0.7384	0.9678
O31	0.0692	0.8697	0.8715
H31	-0.0167	0.7555	0.7448
H32	-0.0314	1.0255	0.8196
O41	0.5692	0.1303	0.8715
H41	0.4833	0.2445	0.7448
H42	0.4686	-0.0255	0.8196

O21 is generated from O11 and O41 is generated from O31 by the a-glide mirror plane at y=1/2.

field vector is maximal. The positions of the hydrogen atoms of this water molecule have been determined using the same procedure. The resulting atomic coordinates of the water molecules are listed in table 2.2. The second and next layers are identical to the first layer and are stacked upon the first layer and each other such that the interaction between the layers is maximal. The water layers constitute a crystalline structure of which some details are listed in table 2.3. The specific surface energy γ_L is calculated from the interaction energy of the first water layer with the second layer. The energy of a water molecule in the water layers is 37 kJ mole^{-1} and the evaporation enthalpy of ice is 47 kJ mole^{-1} (Washburn & West, 1926).

The specific surface energies of the calcite surface, and the water surface

Table 2.3 Unit cell parameters and atomic coordinates of the crystalline water layer; a = 8.0828, b = 4.9901, c = 2.9 Å, $\alpha = \beta = \gamma = 90°$.

Atom	x	y	z	q
O1	0.5856	0.3715	0	-0.66
H1	0.6421	0.5052	0.1784	0.33
H2	0.5469	0.2616	0.2014	0.33
O2	0.0856	0.6285	0	-0.66
H3	0.1421	0.4948	0.1784	0.33
H2	0.0469	0.7384	0.2014	0.33
O3	0.4048	0.8697	0	-0.66
H5	0.4154	0.7555	-0.2647	0.33
H6	0.3437	1.0255	-0.1083	0.33
O4	-0.0952	0.1303	0	-0.66
H7	-0.0846	0.2445	-0.2647	0.33
H8	-0.1563	-0.0255	-0.1083	0.33

and the interaction energy between the calcite surface and the first water layer, have been calculated and are listed in table 2.4. It is seen that in this case U_{int} exceeds the value of $\gamma_S + \gamma_L$. If we take the polarization of the water molecules into account, the values of γ_L and U_{int} will increase and γ_{SL} will become more negative. The induced dipole moment is given by

$$\mu_{ind} = \alpha F \qquad (2.3)$$

where α is the polarizability of the water molecule, taken as 1.444 $Å^{-3}$ (Bailar, Emelius, Nyholm & Trotman-Dickenson, 1973) and F is the field at the position of the oxygen atom as calculated by the program. The polarization increases the charges which become now $q_O = -1.14$ for O11 and O21 and $q_O = -0.88$ for O31 and O41. The negative value of γ_{SL} corresponds to the heat of immersion of an anhydrous calcite surface into water. Goujon and Mutaftschiev (1976) obtained in their experiments a value of 540 mJ m^{-2}.

Table 2.4 Surface and interaction energies (mJ m^{-2}).

	γ_S	γ_L	U_{int}	γ_{SL}
Model I				
No polarization	1087	69	1170	-14
With polarization	1087	154	1797	-556
Model II				
Calculated	197	69	214	49
Ref. [3]				83

These results led us to the conclusion that interface energies from nucleation data refer to a different system for which we took model II.

2.3 Interface model II

Model II is a hydrated crystal and its surrounding medium. To describe such a different system we use the same crystal surface and the same water layers with the same geometry. But this time γ_S refers to a crystal surface with a monolayer of water, γ_L refers to the second and next water layers and U_{int}

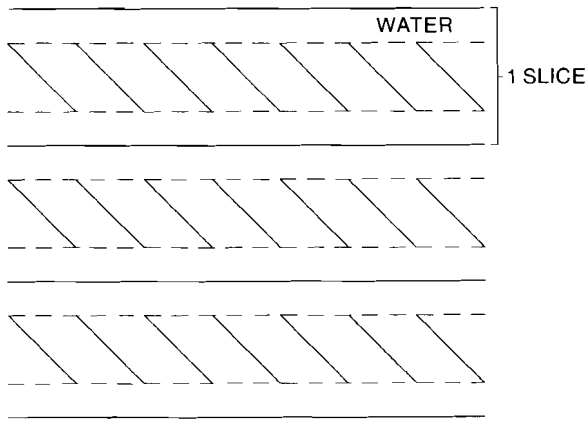

Figure 2.2 The model that is used for the calculation of γ_S (model II).

is the interaction energy of the hydrated crystal and the surrounding medium.

To be able to calculate γ_S, we have to describe the hydrated crystal as a stacking of identical slices. Each slice consists of a layer of calcite which is sandwiched between two layers of water (see figure 2.2). The slices are stacked upon each other such that the interaction between the slices is maximal. Table 2.5 lists the cell parameters and the atomic coordinates and figure 2.3

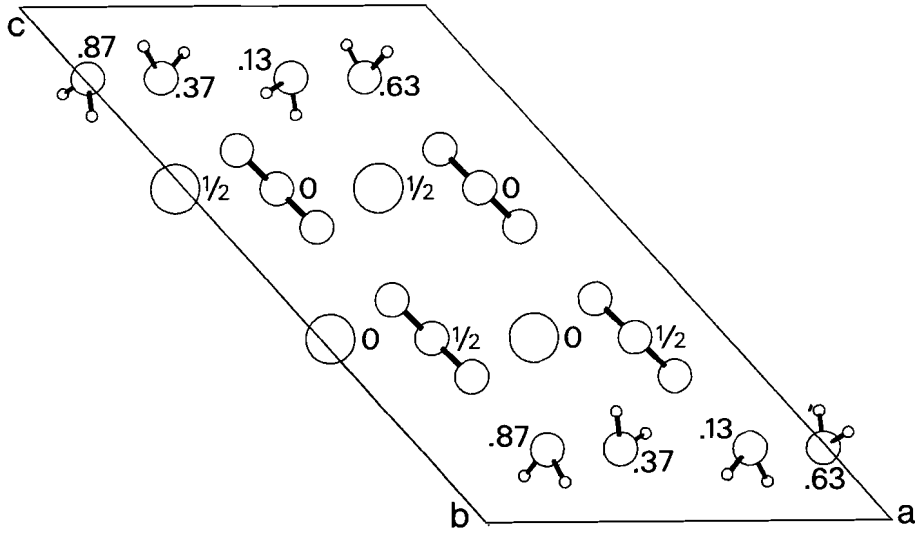

Figure 2.3 ac projection of the sandwich model (PLUTON, EUCLID-version (Spek, 1982).

Table 2.5 Atomic coordinates and charges of the sandwich model, a = 8.0821, b = 4.9901, c = 13.93 Å, $\alpha = \beta = \gamma = 90°$.

Atom	x	y	z	q
Ca1	0.0239	0	0.3544	2
Ca2	0.5239	0	0.3544	2
Ca3	-0.0239	1/2	0.6456	2
Ca4	0.4761	1/2	0.6456	2
C1	0.7739	1/2	0.3544	1
C2	0.2739	1/2	0.3544	1
C3	0.7261	0	0.6456	1
C4	0.2261	0	0.6456	1
O1	0.2861	0.3715	0.2796	-1
O2	0.2739	0.7571	0.3544	-1
O3	0.2616	0.3715	0.4293	-1
O4	0.7616	0.6285	0.4293	-1
O5	0.7739	0.2429	0.3544	-1
O6	0.7861	0.6285	0.2796	-1
O7	0.2384	0.8715	0.5707	-1
O8	0.2261	0.2571	0.6456	-1
O9	0.2139	0.8715	0.7204	-1
O10	0.7139	0.1285	0.7204	-1
O11	0.7261	-0.2571	0.6456	-1
O12	0.7384	0.1285	0.5707	-1
O13	0.1907	0.3715	0.8618	-1.14
H1	0.3041	0.5052	0.9115	0.57
H2	0.2193	0.2488	0.9244	0.57
O14	0.6907	0.6285	0.8618	-1.14
H3	0.8041	0.4948	0.9115	0.57
H4	0.7193	0.7512	0.9244	0.57
O15	0.0099	0.8697	0.8618	-0.88
H5	-0.0639	0.7555	0.7881	0.44
H6	-0.0858	1.0255	0.8316	0.44
O16	0.5099	0.1303	0.8618	-0.88
H7	0.4361	0.2445	0.7881	0.44
H8	0.4142	-0.0255	0.8316	0.44
O17	0.3093	0.8715	0.1382	-1.14
H9	0.1959	1.0052	0.0885	0.57
H10	0.2807	0.7488	0.0756	0.57
O18	0.8093	0.1285	0.1382	-1.14
H11	0.6959	-0.0052	0.0885	0.57
H12	0.7807	0.2512	0.0756	0.57
O19	0.4901	0.3697	0.1382	-0.88
H13	0.5639	0.2556	0.2119	0.44
H14	0.5858	0.5255	0.1684	0.44
O20	0.9901	0.6303	0.1382	-0.88
H15	1.0639	0.7445	0.2119	0.44
H16	1.0858	0.4745	0.1684	0.44

shows an *ac*-projection. Note that in this case the adjacent water layers are symmetrically identical. The charges on the H and O atoms are also given in table 2.5. The values of γ_S, U_{int} and γ_{SL} have been calculated and are listed in table 2.4 as well as the specific surface energy γ_{SL} calculated from nucleation data by Söhnel and Mullin (1978). Both values of γ_{SL} are of the same order of magnitude.

2.4 Discussion and conclusions

It might seem somewhat unlikely that the interaction energy U_{int} is larger than the specific surface energy γ_S. This is due to the fact that the water layer has the negatively charged atoms at its center and the positively charged atoms at its outsides, in contrast to the $CaCO_3$ layer where the opposite situation occurs. Moreover, the distance between the successive carbonate layers is 3.03 Å while the water layer is at 2.25 Å.

The fact that the calculated interfacial energy for calcite is lower than the one derived from experimental data may be due to the assumption that the nucleus has the form of a rhombohedron. When other faces or steps also occur the electrostatic field of the surface will increase, leading to higher values of γ_S which increases quadratically and a U_{int} which increases proportionally with the electrostatic field. The value of γ_{SL} will increase, generally.

During the nucleation process the hydrated ions lose their hydration shells, except the ions at the surface of the nucleus. The latter retain one or two water molecules depending on the geometry and charge of the ions. So we conclude that the interfacial energies calculated from nucleation data are in fact the interfacial energies of an either totally or partially hydrated surface with its surrounding aqueous solution.

Acknowledgements

We are indebted to Dr. C.S. Strom for putting her program *SURFPOT* at our disposal. Thanks are also due to Dr. A.L. Spek for putting programs of the *EUCLID*-package at our disposal.

References

Bailar, J.C., Emelius, H.J., Nyholm, R. & Trotman-Dickenson, A.F. eds. (1973). *Comprehensive Inorganic Chemistry*, Vols. 1 and 2. Oxford: Pergamon.

Chessin, H., Hamilton, W.C. & Post, B. (1965). *Acta Cryst.* **18**, 689.

Goujon, G. & Mutaftschiev, B. (1976). *J. Chim. Physique* **73**, 351.

Heijnen, W.M.M. (1985). *Neues Jahrb. Mineral. Mh.* 357.

Heijnen, W.M.M. (1986). *Neues Jahrb. Mineral. Abh.* **154**, 223.

Söhnel, O. & Mullin, J.W. (1978). *J. Crystal Growth* **44**, 377.

Spek, A.L. (1982). The *EUCLID*-package, in *Computational Crystallography*, ed. D. Sayre, p. 528. Oxford: Clarendon.

Strom, C.S. & Hartman, P. (1989). *Acta Cryst.* A**45**, 371.

Washburn, E.W. & West, C.J., eds. (1926-1933). *International Critical Tables of Numerical Data, Physics, Chemistry and Technology*. New York: McGraw-Hill.

CHAPTER 3

OBSERVATIONS ON GROWTH FORM AND HABIT OF POTASSIUM NITRATE AS A FUNCTION OF THE TEMPERATURE.

Abstract

Crystals of potassium nitrate were grown in a flow system in order to find out whether fluctuations in growth rate of the faces with the temperature as observed by Sipyagin and Chernov (1973) and Chernov *et al.* (1984) lead to expected drastic changes in growth form and habit. Slight changes in both growth form and habit have been observed but they were different from the changes we expected. Discrepancies with the data of Sipyagin and Chernov (1973) are explained by differences in experimental circumstances.

3.1 Introduction

Several scientists have studied the temperature dependence of the normal growth rates V(t) of the faces of single crystals of different salts such as sodium chlorate and potassium chlorate (Sipyagin, 1968), Rochelle salt, sodium perchlorate, sodium nitrite, sodium nitrate and potassium nitrate (Sipyagin & Chernov, 1973) in aqueous solutions at constant supersaturation. The experiments were carried out in a fast moving solution in a flow system. They observed that the V(t) relationships for the crystals studied show sharp minima and maxima superimposed on a systematic increase in the growth rate with temperature. The results were interpreted as due to a structured film of solution, that is adsorbed on the faces of the growing crystal. This film influences the growth kinetics in different ways depending on the temperature and the face.

For potassium nitrate they determined the V(t) dependence of the (110), (010), (001), and (021) faces. From these curves, it appears that at certain temperatures one face can have a maximum in growth rate while another face can have a minimum. This behaviour of the V(t) curves should lead to changes in both habit and growth form of the crystals. Crystal habit is the overall shape

of a crystal and is described in qualitative terms as plate-like needle-like and so on. The term crystal growth form is used to sum up the forms present on the crystal. In this paper we report on experiments that were carried out with potassium nitrate to verify our expectations.

In a later study Chernov *et al.* (1984) determined the V(t) dependence of the (001) and (011) faces in a different experimental setup and with a different supersaturation. Our results will be compared with these growth rate data.

3.2 Experimental

The potassium nitrate crystals were grown in a flow system that was earlier developed by Human (1981). It was rebuilt at our laboratory with slight modifications (figure 3.1). The flow system consists of a storage vessel (SV), two heat exchangers (C and H), an observation cell (OC), a centrifugal pump (P), a flowmeter and three thermostat baths (T1, T2, and T3 with temperatures T_1, T_2, and T_3). The temperatures are set such that $T_3 > T_1 > T_2$. An undersaturated solution is pumped from the storage vessel through the cooler into

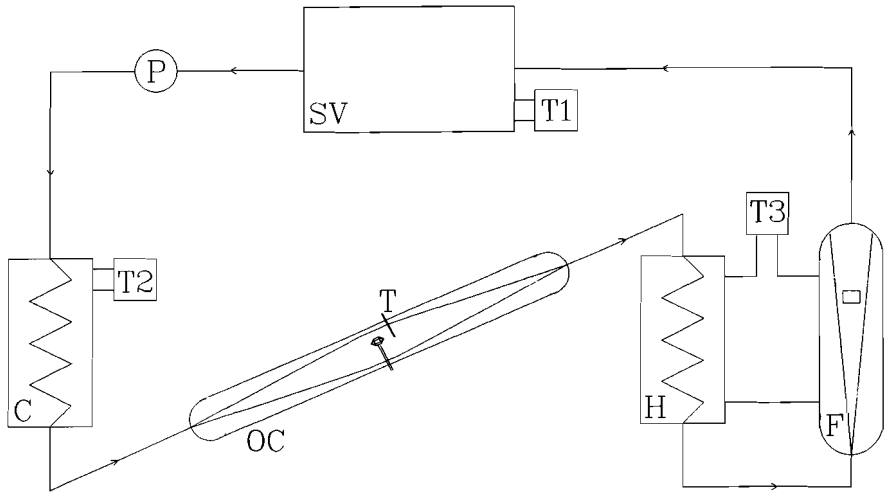

Figure 3.1 Scheme of the flow system; SV = storage vessel; P = pump; C = cooler; OC = observation cell; H = heater; F = flow meter; T = thermometer; T1, T2, and T3 = thermostats of which the temperatures are T_1, T_2, and T_3 and $T_3 > T_1 > T_2$.

the observation cell, in which the crystal grows. The solution, that has become supersaturated, is pumped back into the storage vessel through the heater and the flow meter. Growth can only take place in the cell. The materials of which the flow system is made are glass, Teflon and polypropene. The volume of the solution in the flow system is approximately 10 litres. The temperature in the cell was measured with a Pt-100 resistance with a resolution of 0.01 K. The flow system was equipped with a microscope with a time lapse photography setup to follow the growth experiments.

The solutions were prepared by dissolving potassium nitrate (Merck zur Analyse) in deionised water purified in a Millipore Milli-Q2 system. The appropriate amounts of potassium nitrate and water were determined from the solubility data of Washburn & West (1926-1933), Linke (1958) and Stephen & Stephen (1962). The solution was filtered through 0.22 μm Millipore filters.

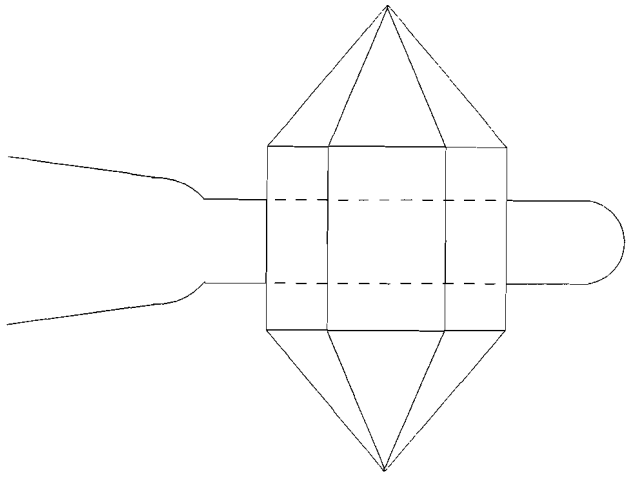

Figure 3.2 Crystal glued on a crystal holder.

Seed crystals were grown from an aqueous solution by slow evaporation at a constant temperature of 20.0 ± 0.2 °C. For an experiment a crystal of (3-4) x (1-2) mm with well-formed external faces was chosen. It was glued on the crystal holder as shown in figure 3.2 with a cyanoacrylate cement and thereafter mounted in the cell. The saturation temperature of the solution was determined by minimizing the temperature interval between growth and dissolution until no change could be observed. The saturation temperature could be determined with an accuracy of about ± 0.02 K. After determination

of the saturation temperature the temperature in the cooler was lowered until the temperature in the cell had reached a value of 0.15 K below saturation temperature. The crystal was allowed to grow for eight hours. Every hour a photograph was taken for checking purposes. Thereafter the crystal was taken out of the cell and dried. The faces of the crystal were indexed by measuring their angular coordinates on a two-circle goniometer.

Experiments were carried out at temperatures between 30 and 42 °C. At each of the temperatures two experiments were done. For each experiment a new seed crystal was used. The absolute supersaturation in all experiments was 0.15 ± 0.02 K. The flow rate of the solution was during all the experiments approximately 35 cm s^{-1}, well above flow rates at which volume diffusion may play a role (Sipyagin & Chernov, 1973).

3.3 Results

Only the "upstream" side of the crystals were considered in our observations because this side grew much faster than the "downstream" side. On the seed crystals the pinacoid {010}, the prisms {021} and {110}, and the dipyramid {111} were present (a : b : c = 0.5910 : 1 : 0.7011, space group Pmcn). During the growth period these forms remained on the crystals and at certain temperatures the pinacoid {001} and the prism {011} appeared. In table 3.1 the results concerning the presence of the (001) and (011) faces are listed. Figure 3.3 shows some typical crystals we have grown with indexing of the faces. The length/thickness ratios of the crystals were measured and are presented in a

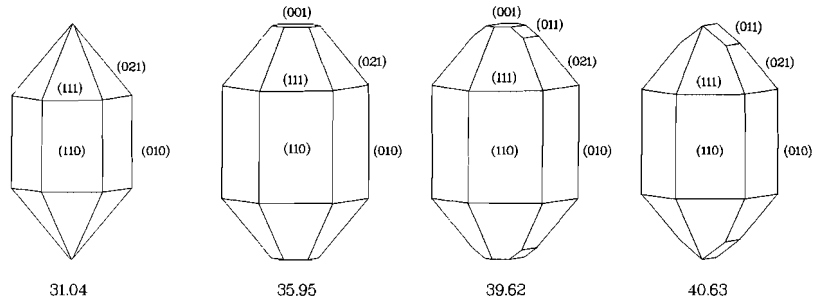

Figure 3.3 Selected observed growth forms together with the temperature (in ° C) at which they grew. Plots made with ABSORB (Spek, 1983).

Table 3.1 Occurrence of the (001) and (011) faces and length/thickness ratio as a function of the temperature.

t(°C)	(001)		(011)		length/thickness	
	I	II	I	II	I	II
30.05	-	-	-	-	2.1	1.8
31.04	-	-	-	-	2.1	2.3
31.93	-	-	-	-	2.3	2.3
32.90	•	•	-	••	1.8	2.3
33.90	••	•	••	-	1.9	1.5
34.92	••	-	-	•	1.6	2.0
35.52	•	•	-	-	3.0	2.9
35.95	•••	•••	-	-	1.9	2.1
36.44	••	••	-	-	2.3	2.1
36.85	••	•	-	-	2.1	2.1
37.50	•	-	-	-	2.1	1.9
38.07	•••	•••	-	-	2.5	2.3
38.38	••	••	••	•	1.8	1.9
38.85	•	-	•	-	3.0	2.7
39.62	•	••	••	••	1.8	1.9
40.13	-	-	-	-	1.8	1.8
40.63	-	-	•	-	2.5	2.5
40.88	-	-	•	-	1.9	2.0
42.23	-	-	-	-	1.9	1.9

I and II represent crystal I and II, "-" means that the face is not observed. The larger the number of dots the larger the face.

graph (figure 3.4). It can be seen from table 3.1 that the changes we have observed in growth form and habit are reasonably reproducible. The changes are slight and therefore not as drastic as expected.

Sipyagin & Chernov (1973) measured the growth rates of the (010), (110), (021) and (001) faces. The growth rates of the (011) and (001) faces were measured in a later study by Chernov *et al.* (1984). These data cannot be merged because the growth rates were measured at different supersaturations and in different experimental setups. Furthermore, the growth rate data of the (001)-face do not agree. Therefore the results of Sipyagin & Chernov (1973) and those of Chernov *et al.* (1984) are compared separately with our results.

From the growth rates as determined by Sipyagin & Chernov (1973) for the (010), (110), (021) and the (001) faces growth forms were constructed by taking the central distance of a face proportional to the growth rate and by assuming that the growth rates of the (111) and (021) faces are equal. The growth rates of the faces are listed in table 3.2 together with the faces that are present on the constructed growth forms. The most illustrative constructed forms are depicted in figure 3.5.

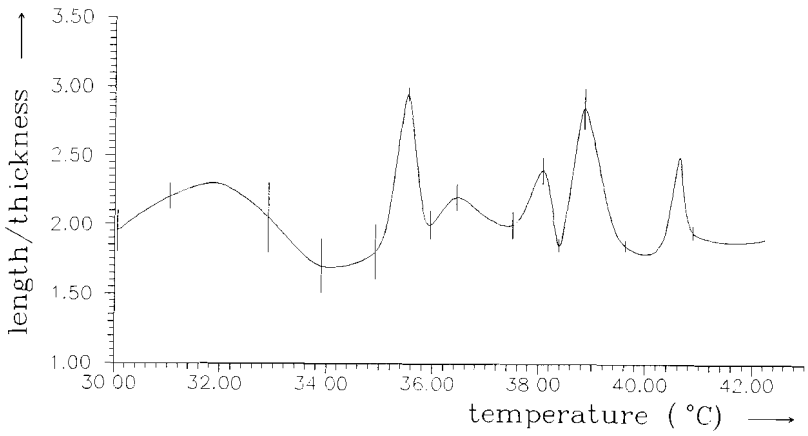

Figure 3.4 Length/thickness ratio of the crystals versus temperature.

3.4 Discussion

From table 3.2 it can be seen that the published growth rates of the (001) face are low when compared with the growth rates of the (021) face. In the whole temperature interval between 30 and 42 °C the (001) face is present as an important form. The (021) face is sometimes not present on the constructed growth forms. No growth rates have been determined for the (111) face. The crystals that are grown in our experiments have large (111) and (021) faces and small (001) faces, if any. Furthermore, the habit of the crystals is more

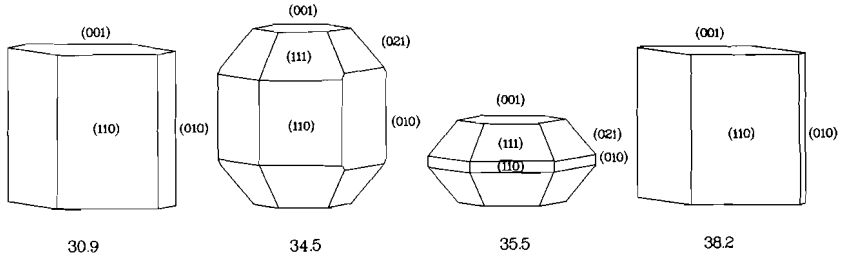

Figure 3.5 Selected constructed growth forms from the data of Sipyagin and Chernov (1973) together with the temperature (in ° C). Plots made with ABSORB (Spek, 1983).

Table 3.2 Growth rates of the (110), (010), (001) and (021) faces in 10^{-5} cm s^{-1} as determined by Sipyagin and Chernov (1973) and forms present on the constructed growth forms.

t(°C)	V_{110}	V_{010}	V_{001}	V_{021}	Forms present {110}	{010}	{001}	{021}	{111}
30.9	3.5	5.0	4.5	8.1	x	x	x		
33.4	5.0	5.9	7.5	8.7	x	x	x	x	x
34.5	7.0	6.6	8.2	8.0	x	x	x	x	x
35.5	8.3	8.3	4.7	7.1	x	x	x	x	x
36.6	7.8	6.4	2.8	5.3	x	x	x	x	x
37.2	5.0	6.0	3.0	6.0	x	x	x	x	x
38.2	3.5	6.2	5.0	10.0	x	x	x		
39.3	6.6	6.5	10.0	8.0	x	x	x	x	x
40.6	4.2	10.0	8.2	14.0		x	x		
42.2	5.0	5.5	4.1	9.0	x	x	x		

elongated than the habit of the constructed growth forms. Our results cannot be brought into agreement with the results of Sipyagin & Chernov (1973). This may be due to the accuracy in their temperature measurements, which was ± 0.1 K. The supersaturation they worked with was 0.2 K. The relative error in the supersaturation was thus quite large, which can lead to a large scatter in growth rates and spurious results. Sipyagin & Chernov (1973) used a supersaturation of 0.2 K whereas in our experiments the supersaturation was 0.15 K. This difference in supersaturation, although small, may also be the cause of the discrepancies. In our experiments nucleation in the cooler occurred at a supersaturation of 0.20 K, and on the seed crystals small crystals started to grow. At a higher supersaturation the rate determining step in the growth of one or more faces may change, which may result in a change in growth rates.

Sipyagin & Chernov (1973) have not mentioned the duration of their experiments but a remark can be placed. If the duration of the experiments is short, for example half an hour, one may find an average growth rate that differs from average growth rates as determined in long term experiments, for example eight hours in our experiments. Human (1981), Chernov *et al.* (1984), Jetten, van der Hoek & van Enckevort (1983) and Chernov & Malkin (1988) mention that crystal faces can grow irregularly in time. This means that a period of growth is alternated by a period of very slow growth or even complete absence of growth. In long term experiments this effect will be averaged. The photographs taken during our experiments did not show such temporal fluctuations in growth rate, which means that these fluctuations average out within an hour.

The orientation of the crystal in the stream may have been different in our

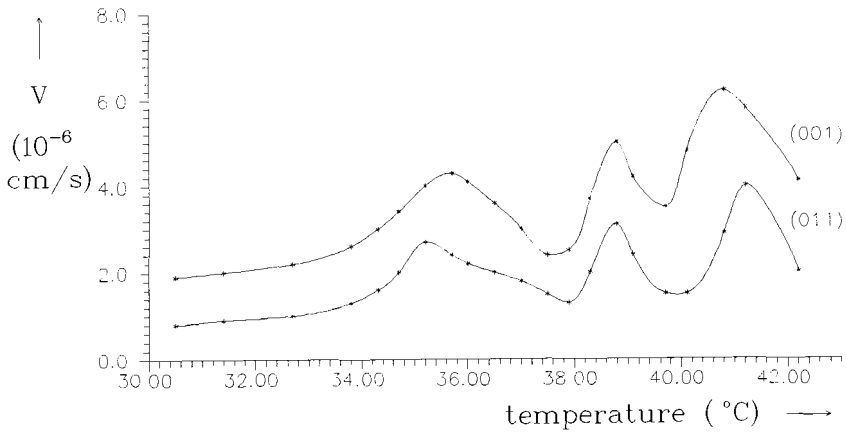

Figure 3.6 Growth rate of the (001) and (011) faces as measured by Chernov et al. (1984) versus temperature.

series of experiments, but this can only account for small differences in the constructed and observed growth forms.

The growth rates of the (011) and (001) faces as measured by Chernov *et al.* (1984) are plotted in figure 3.6. It is found that the maxima in growth rate of the (001) face coincide with the maxima in length/thickness ratio of our crystals. It can be derived that the (001) face disappears when $V_{001} > 1.22\ V_{011}$, unless the (021) face grows very slowly. In that case neither (011) nor (001) are present. At 40.63 °C and 40.88 °C the crystals have (011) faces without (001) being present. At these temperatures Chernov *et al.* (1984) found that V_{001} is about twice as large as V_{011}, which obeys the requirement mentioned above. Our results are not in contradiction with the results of Chernov *et al.* (1984) but it is not possible to decide whether the results agree or not, because the faces that are studied by Chernov *et al.* (1984) are not present on our crystals as important forms.

The cause of the fluctuations in growth rate is not known, but several possible causes were already suggested (Petrov, 1965; Sipyagin, 1968; Sipyagin & Chernov, 1973). The fluctuations may be caused by air bubbles at the growth front or adsorbed gases and impurities on the surface. Several authors mention that there is a layer of physically adsorbed, structured water or solution on the surface. The fluctuations in the growth rate are due to changes in the structure of that layer. When the structure of that layer changes, the rate

determining step in the growth process may become a different one. Changes in the structure of the layer may also affect the rate of diffusion and when surface diffusion or volume diffusion is the rate determining step in the growth process, the growth rate changes.

Flaws in the crystal may also be a cause for the fluctuations (Chernov *et al.*, 1984). It is well known that flaws, which differ from crystal to crystal, affect the growth rate (Ristić, Sherwood & Wojciechowski, 1988). Although we used only two crystals in our study at each temperature, out results are reasonably reproducible. This makes flaws as a cause of the fluctuations questionable.

3.5 Conclusions

The fluctuations in growth rate as a function of the temperature, observed by Sipyagin & Chernov (1973) are not expressed in the expected spectacular changes in growth form and habit. Instead we found slight and different changes from those we expected on account of their results. Our results are not in contradiction with the growth rate data from Chernov *et al.* (1984).

In view of the reproducibility of our results we may conclude that the fluctuations in growth rates are not caused by flaws in the crystals. Fluctuations can also be caused by gas bubbles at the growth front, impurities and changes in the structure of the solution near the structure of the solution near the surface of the crystal. The latter is probably only important if the growth rate is determined by volume or surface diffusion.

Acknowledgements

The author wishes to thank Professor P. Hartman for stimulating discussions and reading the manuscript. Thanks are also due to Mr. C.D. Laman for his help and advice during the building of the flow system.

References

Chernov, A.A. & Malkin, A.I. (1988) *J. Crystal Growth* **92**, 432.

Chernov, A.A., Parvov, V.F., Eskin, S.M. & Sipyagin, V.V. (1984). In *Growth of Crystals*, Vol. 12, ed. A.A. Chernov, p. 103. New York: Consultants Bureau.

Human, H.J. (1981). Ph.D. Thesis, Nijmegen.

Jetten, L.A.M.J., van der Hoek, B. & van Enckevort, W.J.P. (1983). *J. Crystal Growth* 62, 603.

Linke, W.F. (1958). *Solubilities of Inorganic and Metalorganic Compounds*, 4th ed. Princeton: Van Nostrand.

Petrov, T.G. (1965). *Soviet Physics - Crystallography* **9**, 448.

Ristić, R.I., Sherwood, J.N. & Wojciechowski, K. (1988). *J. Crystal Growth* **91**, 163.

Sipyagin,V.V. (1968). *Soviet Physics - Crystallography* 12, 590.

Sipyagin, V.V. & Chernov, A.A. (1973). *Soviet Physics - Crystallography* **17**, 881.

Spek, A.L. (1983). *ABSORB, A Program for Absorption Correction*. University of Utrecht, The Netherlands.

Stephen, H. & Stephen, T. eds. (1962). *Solubilities of Inorganic and Organic Compounds*. Oxford: Pergamon.

Washburn, E.W. & West, C.J. eds. (1926-1933). *International Critical Tables of Numerical Data; Physics, Chemistry and Technology*. New York: McGraw-Hill.

CHAPTER 4

THE MORPHOLOGY OF SUCCINIC ACID CRYSTALS: THE ROLE OF SOLVENT INTERACTION

Abstract

Succinic acid crystals grown from aqueous solutions are platy with a (100) basal plane and side faces (111) and (011) while crystals grown from *iso*-propanol are needle-like with (100) and (010) planes. These habits are not predicted from PBC-analyses. In this study, the role of solvent interaction is related to habit controlling factors in the screw dislocation mechanism. The solvent interaction with various faces of succinic acid crystals was determined with the aid of molecular mechanics calculations. The observed habits from water and from *iso*-propanol could be explained satisfactorily in a semi-quantitative way.

4.1 Introduction

It has been known for some time that the habit of crystals depends on the solvent from which they are grown. In previous papers the influence of solvent interaction on the crystal habit has been studied by several workers and some of them have already tried to understand this solvent effect in order to predict growth habits from different solvents (Garti, Leci & Sarig, 1981; Davey, Mullin & Whiting, 1982; Saska & Myerson, 1983; Berkovitch-Yellin, 1985; Aquilano *et al.*, 1986).

Succinic acid crystallizes in the monoclinic space group $P2_1/c$ (a = 5.519, b = 8.862, c = 5.102 Å, β = 91.59°, Z = 2) (Leviel, Auvert & Savariault, 1981). Figure 4.1 shows the molecular structure of succinic acid. In the crystal structure planar acid molecules are interlinked by a translation along the $[10\bar{1}]$ direction to form infinite H-bonded chains.

Crystals of succinic acid grown from the vapour have predominant (010) faces and smaller (100), (111), (110) and (011) faces, which is in good agreement with the habit predicted from PBC-analyses (Hartman & Perdok,

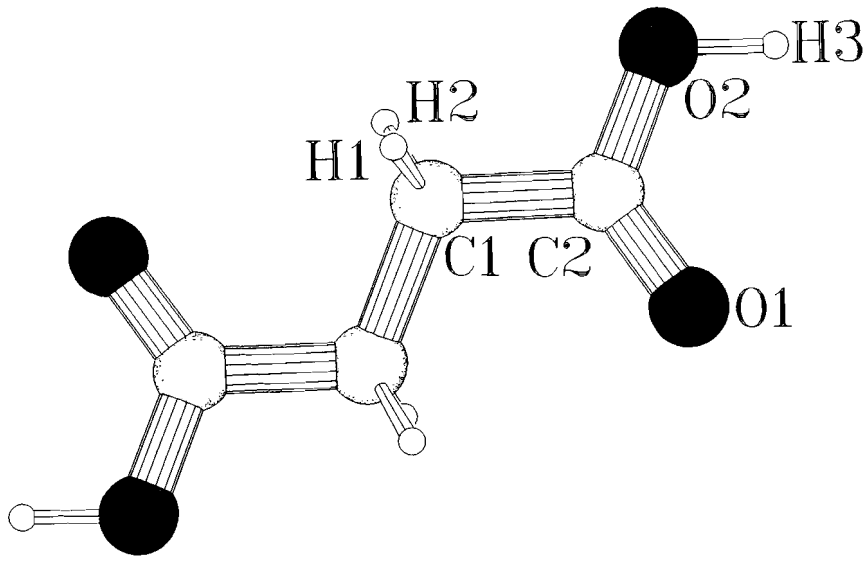

Figure 4.1 PLUTON-plot (Spek, 1982) of succinic acid with atomic labelling. Atom code: black, oxygen; dotted, carbon; white hydrogen.

1952, 1955; Hartman, 1973, 1988) (Berkovitch-Yellin, 1985) (figure 4.2a). When grown from an aqueous solution, they have a predominant (100) basal plane bounded by (010), (111) and (011) faces (Davey, Mullin & Whiting, 1982) (figure 4.2b). From *iso*-propanol they grow as needle-like crystals with major (100) and (010) faces (figure 4.2c).

Davey, Mullin and Whiting (1982) calculated the surface entropy factor α by including the solubility of the compound in the calculations as was earlier done by Human *et al.* (1981). Knowing α, it was possible to predict the growth mechanism of the face and its relative growth rate. The results were, however, not satisfactory.

Berkovitch-Yellin (1985) calculated the electrostatic potential on closest approach points of the crystal faces. The root-mean-square of the potentials was taken as a measure for the polarity of that face. The growth rate reduction of the polar faces is largest when a polar solvent is used. Predictions made on this basis were in nice agreement with the observed forms.

Saska and Myerson (1983) and Aquilano *et al.* (1986) used a more quantitative approach and calculated the interaction of water with the faces of sucrose crystals by counting the number of unsaturated hydrogen bonds on

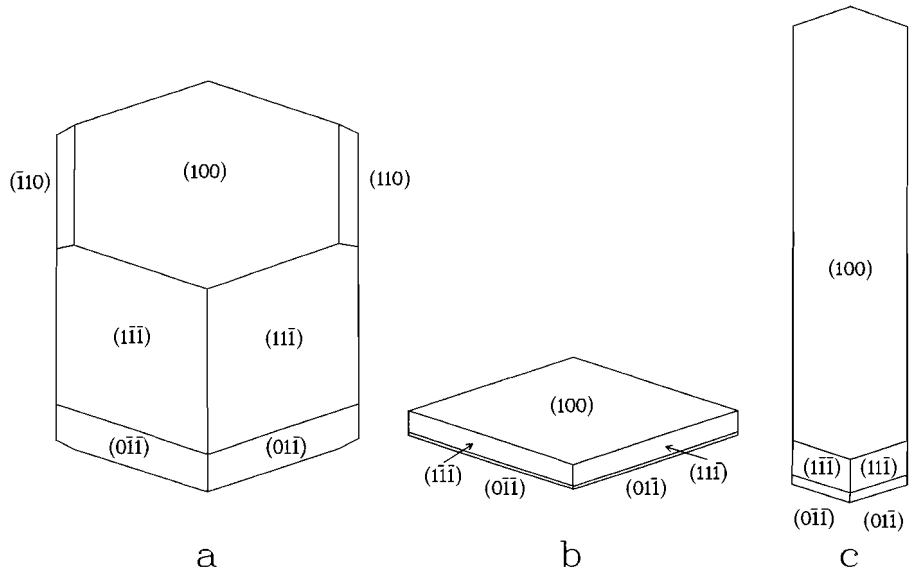

Figure 4.2 a) Crystal of succinic acid grown from the vapour; b) from an aqueous solution; c) from iso-propanol.

the crystal faces and used the potential functions of Rao *et al.* (1967) to calculate the interaction energy. The obtained interaction energy was subtracted from the specific surface energy with respect to vacuum and a modified habit was constructed by making Wulff-plots using the modified surface energies.

Recently, we (Van der Voort & Hartman, 1988) used an approach like those described above for an ionic crystal and we found that the solvent interaction (especially water) can be much stronger than the intermolecular interactions in the crystal and therefore this approach did not work. This result may indicate that this method is, in general, even not valid. We are of the opinion that it is important to find out what role the solvent interaction plays in the growth process.

In this paper, it will be shown that it is possible to include the solvent interaction in the growth law of the screw dislocation mechanism. Furthermore, an application to succinic acid is shown and discussed.

4.2 Theory

In the following part an expression for the reduced growth rate (Hartman & Bennema, 1980) will be derived in which the solvent interaction will be included. The growth rate R of a face growing by the screw dislocation mechanism (Burton, Cabrera & Frank, 1951) is given by

$$R = C\,(\sigma^2/\sigma_1)\tanh\,(\sigma_1/\sigma) \tag{4.1}$$

where σ is the relative supersaturation. σ_1 and C are defined as

$$\sigma_1 = 9.5\,\kappa\,\Omega/kT\;\lambda_s\,s \tag{4.2}$$

and

$$C = \zeta\,n_{s0}\,\Omega/\tau_{de\text{-}ads} \tag{4.3}$$

where κ is the specific edge energy, Ω is the molecular volume, k is the Boltzmann factor, T is the absolute temperature, λ_s is the mean displacement of an ad-atom on the face, s is the number of cooperating spirals, ζ is a retardation factor, n_{s0} is the concentration of ad-atoms, and $\tau_{de\text{-}ads}$ is the relaxation time for de-adsorption of an ad-atom from the face.

For n_{s0} we can write according to Bennema and Gilmer (1973)

$$n_{s0} = l\,N_0\,\exp\,(\Delta G^{\neq}_{de\text{-}ads} - \Delta G^{\neq}_{de\text{-}solv})/kT \tag{4.4}$$

where l is the mean free path of a growth unit in a solution, N_0 is the concentration of growth units, $\Delta G^{\neq}_{de\text{-}ads}$ is the activation energy for de-adsorption and $\Delta G^{\neq}_{de\text{-}solv}$ is the activation energy for de-solvation of a growth unit.

For $1/\tau_{de\text{-}ads}$ we can write

$$1/\tau_{de\text{-}ads} = \nu_0\,\exp(-\Delta G^{\neq}_{de\text{-}ads}/kT) \tag{4.5}$$

where ν_0 is the atomic frequency factor, often taken as kT/h where h is Planck's constant. So C becomes

$$C = \zeta \nu_0 \Omega l N_0 \exp(-\Delta G^{\neq}_{de\text{-}solv}/kT) \quad (4.6)$$

and in fact C/ζ equals the number of growth units that hits the surface per unit area and time.

σ/σ_1 can be related to the attachment energy, E_{att}, and the solvent interaction as follows:

κ is the specific edge energy. On a crystal face with monatomic steps the spirals are rounded (Human *et al.*, 1981). The specific edge energy can be considered as the average energy required to split a slice of thickness d_{hkl} along an arbitrary direction.

$$\kappa = 2 Z E_{slice}/\sqrt{(V d_{hkl})} \quad (4.7)$$

where V is the unit cell volume and Z is the number of formula units in the unit cell. The specific edge energy will be lower when the slice is split in a solution. We assume that E_{slice} will be lowered by a factor k', which is between 0 and 1. So the expression for κ becomes

$$\kappa = 2 k' Z E_{slice}/\sqrt{(V d_{hkl})} \quad (4.8)$$

We can express λ_s as

$$\lambda_s = \sqrt{(D_s \tau_{de\text{-}ads})} \quad (4.9)$$

and

$$D_{sdiff} = a^2/\tau_{sdiff} \quad (4.10)$$

so

$$\lambda_s = a \sqrt{(\tau_{deads}/\tau_{sdiff})} \quad (4.11)$$

where τ_{deads} is the relaxation time for de-adsorption of the molecules from a mesh (unit cell area), τ_{sdiff} is the relaxation time for a surface diffusion jump as big as a mesh and a is the length of a molecular jump. Because the molecules

on a mesh do not de-adsorb or jump simultaneously, we can write the relaxation times as the sum of the relaxation times of the individual molecules.

$$\tau_{deads} = \sum_{i=1}^{n} \tau_i \tag{4.12}$$

$$\tau_{sdiff} = \sum_{j=1}^{m} \tau_j \tag{4.13}$$

and n is the number of molecules of the crystal on a mesh and m is the number of water molecules on a mesh. So

$$\lambda_s = \frac{a \sqrt{\sum_{i=1}^{n} \exp(\Delta G^{\neq}_{de\text{-}ads,i}/kT)}}{\sqrt{\sum_{j=1}^{m} \exp(\Delta G^{\neq}_{sdiff,j}/kT)}} \tag{4.14}$$

The de-adsorption of an ad-atom or molecule into a solution may be described as moving a (partly) solvated ad-atom or molecule away from the face and subsequent hydration of it and of the face. The energy required for the first step is assumed to be proportional to $E_{att,i}$. $E_{att,i}$ is defined as the energy released when a growth unit i crystallizes on a face. The system gains energy in the second step so $\Delta G^{\neq}_{de\text{-}ads,i}$ can be expressed as

$$\Delta G^{\neq}_{de\text{-}ads,i} = c_i E_{att,i} \tag{4.15}$$

where c_i is a constant between 0 and 1. A similar approach is used for the surface diffusion process on a solvated face. The rate determining step in this process is assumed to be moving the adsorbed solvent molecules and we substitute $c_j U_{int,j}$ for $\Delta G^{\neq}_{sdiff,i}$ where $U_{int,j}$ is the interaction energy of a single water molecule with the face and c_j is a constant with a value between 0 and 1.

Recalling that $\Omega = V/Z$, we find

$$\frac{\sigma}{\sigma_1} = \frac{\sigma\, a k T s \sqrt{d_{hkl}} \sqrt{\sum_{i=1}^{n} \exp(c_i E_{att,i}/kT)}}{19\, Z\, k' \sqrt{V}\, E_{slice} \sqrt{\sum_{j=1}^{m} \exp(c_j U_{int,j}/kT)}} \tag{4.16}$$

The face dependent factors are separated from the others by introducing

$$B = \sigma a\ kT\ s/19\ k'\ \sqrt{V} \tag{4.17}$$

and

$$G = \frac{\sqrt{d_{hkl}} \sum_{i=1}^{n} \exp(c_i\ E_{att,i}/kT)}{Z\ E_{slice} \sqrt{\sum_{j=1}^{m} \exp(c_j\ U_{int,j}/kT)}} \tag{4.18}$$

We arrive at the expression for the relative growth rate of a face

$$R_{rel} = BG \tanh (1/BG) \tag{4.19}$$

where we have taken ζ and C independent of the face.

4.3 Results

R_{rel} is calculated for the (100), (011), (111), and (010) faces of succinic acid. For the calculation of B we substituted the following values in (4.17), $\sigma = 0.01$, a = 10 Å, R = 8.314 J mole^{-1} K^{-1}, T = 300 K, s = 1, and V = 249.3 Å^3, we find B = $8.314 \cdot 10^5$ J mole m$^{-\frac{1}{2}}$. Edge energies in an aqueous solution are a factor 5 to 10 lower than those with reference to vacuum, and in this case k' is chosen as 0.1 for all faces. Figure 4.3 shows space-filling plots of the (100) and (010) faces. The atomic structure of the surface is assumed to be the same as in the bulk crystal, which is quite reasonable. Atomic force microscopy shows that this is indeed the case for the in plane structure of the amino-acid *dl*-leucine (Hansma & Salisbury, 1989). The carboxyl groups project normal to the (011) and (100) faces. The (010) face is parallel to the [10$\bar{1}$] chain. Carboxyl oxygens and the -CH_2- groups are exposed.

Interaction energies, $U_{int,j}$ of water with the faces of succinic acid were determined with molecular mechanics calculations. First, closest approach points of the faces were calculated with the "Molecular Surface Program" (Connolly, 1981) and the electrostatic field at these point was calculated with *SURFPOT* (Strom & Hartman, 1989). This program calculates electrostatic potentials and fields of infinite lattice slices. At the positions with the strongest electrostatic field water molecules were placed and thereafter the positions were optimized with *AMBER* (Weiner & Kollman, 1981). This program

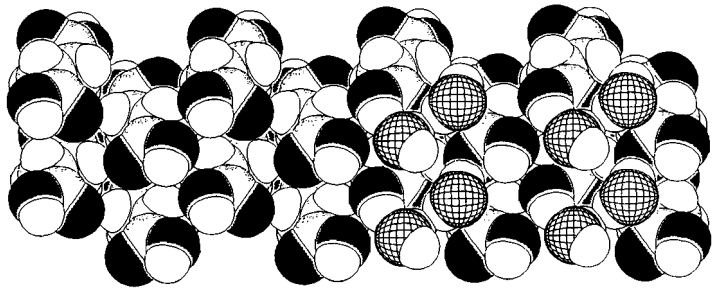

(100)

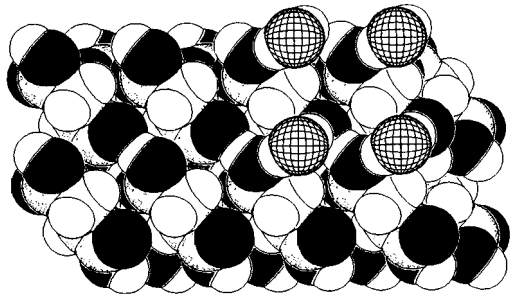

(010)

Figure 4.3 Space-filling plots (Spek, 1982) of the (100) and (010) face. The left halves show the uncovered faces and the right halves show the faces with adsorbed water molecules. Atom code: black, oxygen; dotted, carbon; white, hydrogen; net oxygen, water.

package uses an energy function of the form

$$E = \sum_{\text{bonds}} k_b(r-r_b)^2 + \sum_{\text{angles}} k_a(\theta-\theta_a)^2 + \sum_{\text{dihedrals}} k_d/2[1+\cos(n\phi-\gamma)] + \sum_{\text{non-bonded}} [Br^{-12}-Ar^{-6}-q_iq_j/r] \qquad (4.20)$$

The first three terms represent the difference in energy between the actual geometry and the geometry in which the bond lengths, bond angles and dihedral angles have ideal values. The remaining terms represent non-bonded Van der Waals and electrostatic interactions.

Table 4.1 Force field parameters and non-bonded interactions.

bond	k_b(kcal Å^{-2} mole^{-1})	r_b(Å)
H-O	553	1.00

angle	k_a(kcal radian^{-2} mole^{-1})	θ_a(°)
H-O-H	47	109.3

non-bonded	r(Å)	ϵ(kcal mole^{-1})	q(e)
H(water)	0.01	0.000	0.41
O(water)	1.78	0.155	-0.82
C2	1.94	0.044	0.1839
H3	0.90	0.015	0.1493
O1	1.74	0.066	-0.2214
O2	1.74	0.050	-0.1393
C1	1.90	0.044	0
H1 and H2	1.50	0.047	0

The relation between r, ϵ and A_{ij} and B_{ij} is given by $A_{ij} = 2\ \epsilon_{ij} r_0^6$, $B_{ij} = \epsilon_{ij}\ r_0^{12}$ and $\epsilon_{ij} = \sqrt{\epsilon_i \epsilon_j}$ and $r_0 = r_i + r_j$.

[a]Water parameters from GROMOS (Van Gunsteren, 1986); succinic acid parameters from AMBER (Weiner & Kollman, 1981) and charges from Berkovitch-Yellin & Leiserowitz (1982).

To obtain the most favourable position for the water molecule E was minimized with respect to all degrees of freedom until the change in energy became less than 0.01 kcal mole^{-1} or the gradient became less than 0.1 kcal Å^{-1}. The crystal was kept rigid during the minimization and the minimizations were carried out with different start geometries. The parameters we used in the energy function are listed in table 4.1.

Table 4.2 Attachment energies, slice energies and interaction energies (in kJ mole^{-1}).

face	$E_{att,i}$		E_{att}	E_{slice}	$U_{int,j}$	
	i=1	i=2			j=1	j=2
(100)	34.1	35.4	34.7	25.4	28.6	29.7
(010)	25.6	-	25.6	34.5	15.8	-
(011)	39.3	39.4	39.3	20.8	24.4	18.9
(111)	35.2	36.2	35.7	24.5	20.9	-

E_{cr} = 60.2 kJ mole^{-1}

The attachment energies of the (100), (010), (011) and (111) faces were also calculated with *AMBER* and are listed in table 4.2. Figure 4.2 shows the adsorbed water molecules on the (100) and (010) faces. The interaction energies are also shown in table 4.2. The (100) and (011) face have two favourable sites for water molecules whereas the (010) and (111) face have only one.

Table 4.3 De-adsorption relaxation times (s), surface diffusion relaxation times (s) and relative growth rates of the (100), (010), (011) and (111) faces.

face	$\upsilon_{de\text{-}ads}$	υ_{sdiff}	d_{hkl}	G	R_{rel}	R_{rel}/R_{min}
(100)	$3.57 \cdot 10^{-7}$	$3.75 \cdot 10^{-8}$	5.52	$1.42 \cdot 10^{-9}$	$1.19 \cdot 10^{-3}$	1.00
(010)	$4.41 \cdot 10^{-9}$	$8.66 \cdot 10^{-11}$	4.43	$2.17 \cdot 10^{-9}$	$1.81 \cdot 10^{-3}$	1.52
(011)	$2.18 \cdot 10^{-6}$	$3.02 \cdot 10^{-9}$	4.42	$1.36 \cdot 10^{-8}$	$1.13 \cdot 10^{-2}$	9.53
(111)	$5.16 \cdot 10^{-7}$	$6.56 \cdot 10^{-10}$	3.41	$1.06 \cdot 10^{-8}$	$8.81 \cdot 10^{-3}$	7.42

In table 4.3 are shown the results of the calculation of G according to (4.18). The c_i and c_j are taken as 1, which means in fact that the activation energies $\Delta G^{\neq}_{de\text{-}ads,i}$ and $\Delta G^{\neq}_{sdiff,j}$ equal $E_{att,i}$ and $U_{int,j}$ respectively. This is reasonable because in the case of succinic acid the non-bonded interactions (electrostatic and Van der Waals) vanish when the distance from the surface is more than a few Å. It can be seen that BG is so small that $\tanh(1/BG) = 1$ so

$$R_{rel} = BG \tag{4.21}$$

The values of R_{rel} are also listed in table 4.3. If a habit is constructed from the relative growth rates a needle is obtained (see figure 4.2c) with predominant (100) and (010) faces and small (111) and (011) faces, which does not agree with the observed growth habit from an aqueous solution. In this approach we took $\Delta G^{\neq}_{de\text{-}ads,i} = E_{att,i}$, which may be a good approximation if the adsorbed succinic acid molecules have the same conformation and orientation as those in the crystal. For the (100), (011) and (111) faces this may be true, but for the (010) face, there are positions that are more favourable for the adsorbed molecule than the crystallographic position, so $\Delta G^{\neq}_{de\text{-}ads,i}$ for this face might be too low. If we take $\Delta G^{\neq}_{de\text{-}ads,i}$ for (010) as 35 kJ $mole^{-1}$ we find $BG = 2.98 \cdot 10^{-3}$ for which a constructed growth form agrees better.

Furthermore, the relatively weak interaction of water with the (010) face may enhance the growth rate instead of reducing it by changing the growth mechanism from *e.g.* spiral growth to 2D-nucleation (Birth & Spread).

The growth habit from *iso*-propanol can be explained when we look closely at the solvent interaction. The interaction of *iso*-propanol with the (010) and (111) face, which contain both polar and non-polar regions, consists of electrostatic and H-bond interactions of the hydroxyl group with the polar region and of Van der Waals interaction of the *iso*-propyl group with the non-polar region. So the (010) face becomes more important on the growth form from *iso*-propanol than on the growth form from water. The same goes for the (111) face. On the crystals grown from aqueous solutions, both (111) and (011) are present. The (011) face is absent on crystals grown from *iso*-propanol.

4.4 Conclusions

In this paper a new expression for the relative growth rate is derived in which the solvent interaction with the crystal faces is included. It was assumed that the solvent interaction determines the rate of surface diffusion. The results for the (100), (111) and (011) faces are satisfactory. The too low relative growth rate of the (010) face can be explained, because for this face $E_{att,i}$ is not a good measure for $\Delta G^{\neq}_{de\text{-}ads,i}$. Furthermore, the weak solvent interaction with the (010) face may enhance the growth rate of the (010) face. The habit of crystals grown from *iso*-propanol could also be explained on this basis. It is, however, difficult to predict growth habits, due to the low precision of the interaction energy calculations.

Acknowledgements

The author wishes to thank Professor P. Hartman for stimulating discussions and conscientiously reading the manuscript. Thanks are also due to Dr. L.M.J. Kroon-Batenburg for introducing the author into the molecular mechanics method and software and Dr. A.L. Spek and Dr. C.S. Strom for their permission to use the computer programs *PLUTON*, *ABSORB* and *SURFPOT*.

References

Aquilano, D., Rubbo, M., Mantovani, G., Sgualdino, G. & Vaccari, G. (1986). *J. Crystal Growth* 74, 10.

Bennema, P. & Gilmer, G.H. (1973). In *Crystal Growth, An Introduction*, edited by P. Hartman, Chapter 10. Amsterdam: North-Holland.

Berkovitch-Yellin, Z. (1985). *J. Am. Chem. Soc.* **107**, 8239.

Berkovitch-Yellin, Z. & Leiserowitz, L. (1982). *J. Am. Chem. Soc.* **104**, 4052.

Burton, W.K., Cabrera, N. & Frank, F.C. (1951). *Phil. Trans. Roy. Soc.* A**243**, 299.

Connolly, M.L. (1981). "Molecular Surface Program", *QCPE Bull.* **1**, 74. It may be obtained by writing to Quantum Chemistry Program Exchange, Department of Chemistry, Indiana University, Bloomington, IN 47405, USA.

Davey, R.J., Mullin, J.W. & Whiting, M.J.L. (1982). *J. Crystal Growth* **58**, 304.

Garti, N. Leci, C.L. & Sarig, S. (1981). *J. Crystal Growth* **54**, 227.

Hansma, P.K. & Salisbury, D. (1989). *New Scientist* **122**, 52.

Hartman, P. (1973). In *Crystal Growth, An Introduction*, edited by P. Hartman, Chapter 14. Amsterdam: North-Holland.

Hartman, P. (1988). In *Morphology of Crystals, Part A*, edited by I. Sunagawa, p. 269. Tokyo: Terrapub and Dordrecht: Reidel.

Hartman, P. & Bennema, P. (1980). *J. Crystal Growth* **49**, 145.

Hartman, P. & Perdok, W.G. (1952). *Proc. Koninkl. Nederland. Akad. Wetenschap. Ser. B***55**, 134.

Hartman, P. & Perdok, W.G. (1955). *Acta Cryst.* **8**, 49.

Human, H.J., van der Eerden, J.P., Jetten, L.A.M.J. & Odekerken, J.G.M. (1981). *J. Crystal Growth* **51**, 589.

Leviel, J.-L., Auvert, G. & Savariault, J.-M. (1981). *Acta Cryst. B***37**, 2185.

Rao, V.S.R., Sundarajan, P.R., Ramakrishman, C. & Ramachandran, C.N. (1967). In *Conformation of Biopolymers*, Vol. 2, edited by C.N. Ramachandran. New York: Academic Press.

Saska, M. & Myerson, A.S. (1983). *J. Crystal Growth* **61**, 546.

Spek, A.L. (1982). The *EUCLID* package, In *Computational Crystallography*, edited by D. Sayre. Oxford: Clarendon, Oxford.

Strom, C.S. & Hartman, P. (1989). *Acta Cryst.* A**45**, 371.

Van Gunsteren, W.F. (1986). *GROMOS86*. Groningen Molecular Simulation program package. University of Groningen, The Netherlands.

Van der Voort, E. & Hartman, P. (1988). *J. Crystal Growth* **89**, 603.

Weiner, P.K. & Kollman, P.A. (1981). *J. Computational Chemistry* 2, 287.

CHAPTER 5

THE THEORETICAL GROWTH FORM OF POTASSIUM NITRATE FROM AN AQUEOUS SOLUTION

Abstract

The theoretical growth form of potassium nitrate, obtained from a PBC analysis, is compared to the growth forms obtained from aqueous solutions. The discrepancies are explained satisfactorily in a semi-quantitative way by taking the solvent interaction into account. It was assumed that the desolvation of the crystal surface determines the growth rate. The solvent interaction was obtained from molecular mechanics calculations on water molecules at the solvent accessible surfaces of the crystal faces. It was observed that the water molecules orient preferentially with their dipole moments parallel to the surface to form a 'skin', kept together by hydrogen bonds.

5.1 Introduction

The morphology of crystals is determined by internal factors such as the crystal structure, and external factors such as supersaturation, temperature and the presence of impurities. A solvent, if employed, should in this perspective also be considered as an impurity. The Hartman-Perdok theory (Hartman & Perdok, 1952, 1955; Hartman, 1973, 1988) enables us to calculate a theoretical habit from the crystal structure, completely neglecting the external factors. The agreement between calculated and observed growth forms is, however, generally quite good.

Potassium nitrate crystallizes from aqueous solutions at room temperature in the orthorhombic space group Pmcn (a = 5.414, b = 9.166, c = 6.431 Å) (Nimmo & Lucas, 1973). Figure 1a shows a typical crystal with the pinacoids {010} and {001}, the prisms {021}, {011} and {110} and the dipyramid {111} (Groth, 1908; Van der Voort, 1990a, Chapter 3).

The theoretical growth form of potassium nitrate can be deduced from that of aragonite ($CaCO_3$) as determined by Heijnen (1986) because potassium

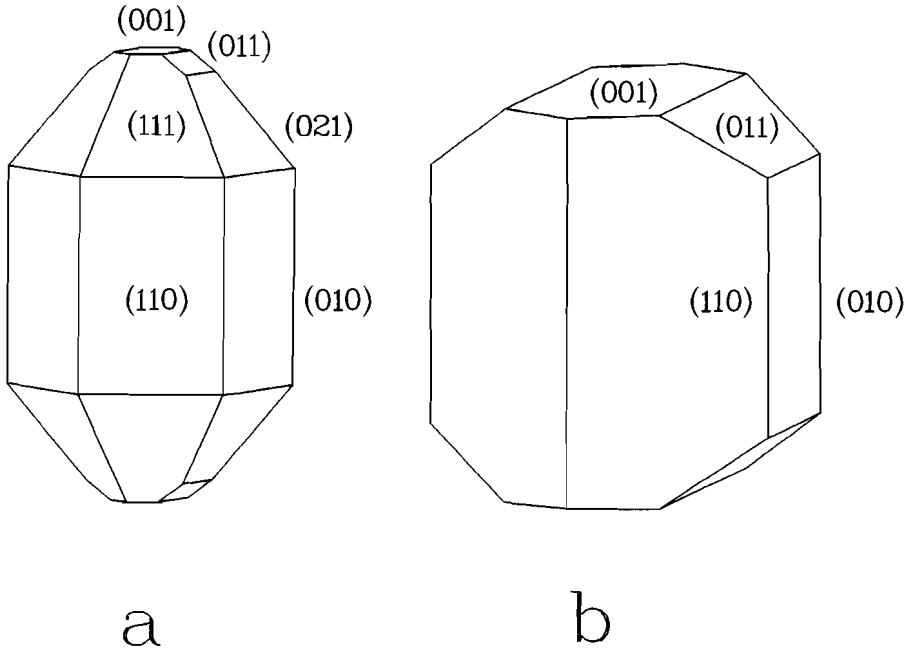

Figure 5.1 Habit of a crystal of KNO_3 grown from an aqueous solution (a) and the theoretical growth form of aragonite (Heijnen, 1986).

nitrate is isostructural with aragonite. Heijnen (1986) established the order of morphological importance of the crystal faces by identifying the Periodic Bond Chains. The faces which are parallel to at least two non-parallel PBCs are called F-faces. They grow slowly, according to a layer mechanism. The relative growth rates of the faces were taken proportional with the attachment energy E_{att} (Hartman & Bennema, 1980). E_{att} is defined as the energy released per molecule when as slice of thickness d_{hkl} crystallizes on a crystal face. The calculations were carried out in an electrostatic point charge model (Ca, 2e; C, 1e; O, -1e). Heijnen (1986) found that the (011) face can have two slice configurations (*i.e.* atomic surface structures with a low surface energy), (011)a and (011)b, differing $\frac{1}{2}\, d_{011}$ in height. The (011) face can grow by layers d_{011} or, much faster, by layers $\frac{1}{2}\, d_{011}$ or by a mixture of both. In figure 1b is shown the theoretical growth form of aragonite. For the attachment energy of (011) the average of those for d_{011} and $\frac{1}{2}\, d_{011}$ was taken, which agreed best with the observed habit. For potassium nitrate a somewhat more elongated habit is

expected. Heijnen (1986) calculated the attachment energies of the aragonite faces as a function of the charge distribution on the CO_3^{2-} ion. The charges on the NO_3^- ion (N 1.5; O -0.8333/4) (Heijnen, 1986) correspond with C 3+; O -1.6666/7 on the CO_3^{2-} ion, which leads to a more elongated habit in the [001] direction.

From figures 1a and b it can be seen that there is some disagreement between the calculated and observed habits. The most striking difference concerns the {021} and the {111} forms. These are important forms on the crystals grown from solution but they are completely absent on the calculated growth form. This may be understood and even predicted if the interaction of the crystal with the solvent is taken into account.

In this study models of adsorbed water layers are constructed for various faces of KNO_3, and the interaction of these water layers with the faces and its role in the growth processes are investigated.

5.2 Method

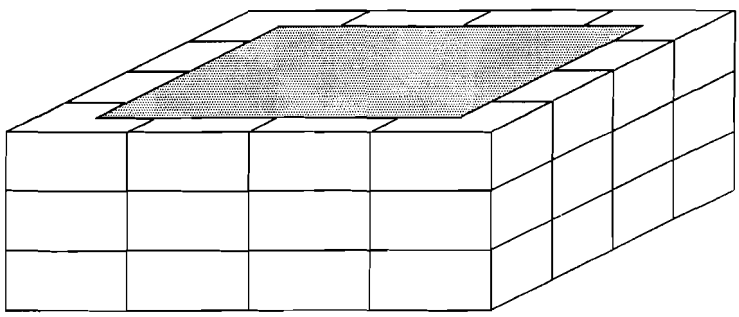

Figure 5.2 The model of the crystal with nine unit cells for the water molecules superimposed.

Water layers are constructed for the (110), (021), (111), (001) and (011) faces. No water layers were constructed for the (010) face because the surface structures of (010) and (110) are similar. The crystal structure of potassium nitrate is pseudo-hexagonal. For the (011) face both slice configurations (011)a and (011)b are considered. It is assumed that the faces are not relaxed *i.e.* the surface and bulk structures are identical (Hansma & Salisbury, 1989). For each face a new set of axes was chosen such that (hkl) becomes (001). For the crystal a block of 4 x 4 x 3 unit cells in the new *a*, *b* and *c* direction was used as shown in figure 2. Figure 3 shows *PLUTON* space filling-plots (Spek, 1982) of the KNO_3 faces, viewed perpendicular to them.

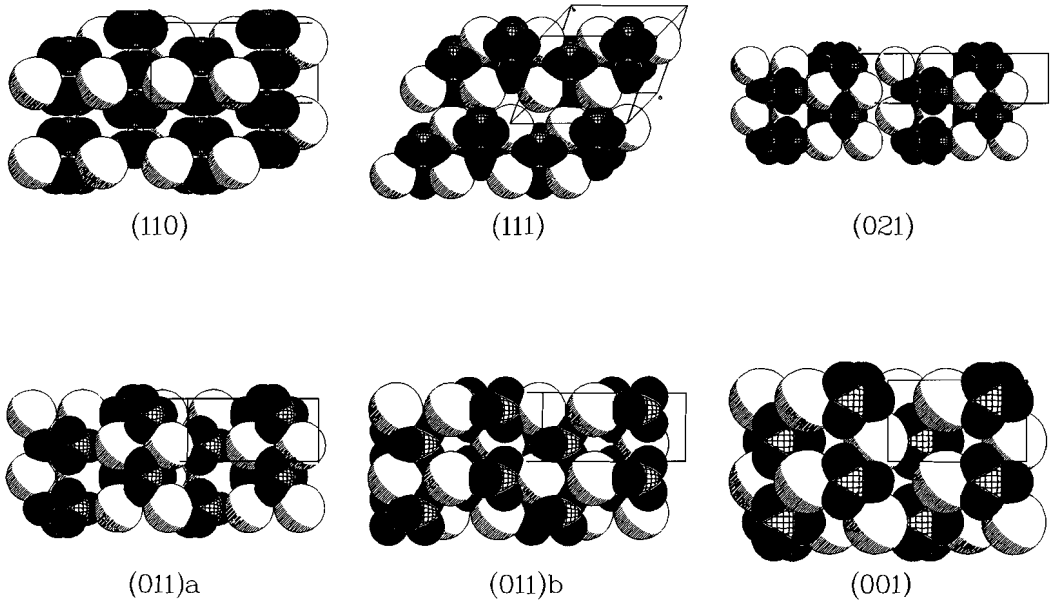

Figure 5.3 Space-filling plot (PLUTON (Spek, 1982)) of the KNO_3 faces. Atom code: black, oxygen; shade, potassium; net, nitrogen.

The (110) face is flat. The K^+ ions are somewhat more exposed than the oxygens. The (021) face is undulated and shows relatively large positively and negatively charged regions. In the middle of the figure neighbouring K^+ ions, that repel each other are shown. The (111) face is also undulated and shows some similarity with the (021) face. The (011)a face shows some similarity with the (021) face but on this face the K^+ and the NO_3^- are shielded by each other.

The (011)b face is not as flat as the (011)a face. The K^+ and the NO_3^- are somewhat more exposed. The (001) face shows NO_3^- ions lying flat on the face. the K^+ ions are partly shielded by the NO_3^- ions.

The construction of the water layers consists of several steps, which are described below.

5.2.1 Solvent accessible surface

As a starting point it was assumed that the most favourable positions of the water molecules are as close as possible to the surface. A solvent accessible surface (based on the geometry of the surface) was calculated with the "Molecular Surface" program (Connolly, 1981). The ions of the crystal face are considered as hard spheres with radii equal to the ionic radii. A water molecule is taken as a sphere with a radius of 1.5 Å. The points of the solvent accessible surface are obtained by rolling the water molecule across the surface and taking the centre of the water molecule as a point. The result is a grid of points (4 points $Å^{-2}$) that are accessible for water molecules (closest approach points).

5.2.2 Electrostatic field

In order to obtain more insight in the configurational space the electrostatic field at each point was calculated with the APL-program *SURFPOT* (Strom & Hartman, 1989). This program calculates Coulomb potentials and fields of stackings of infinite lattice slices, based on the Ewald method (1921). The point charges that are used are listed in table 1 and the atomic coordinates of the KNO_3 structure were taken form Nimmo & Lucas (1973). The first water molecule was placed on the position with the highest field strength with its dipole moment parallel with the direction of the electrostatic field. One degree of freedom remains. The water molecule can spin around its two-fold axis. Therefore minimizations (*vide infra*) were carried out with different start configurations of the newly added water molecules.

5.2.3 Minimizations

The minimization of the position, rotation and geometry of the water molecules was carried out with the use of the molecular mechanics program *AMBER* (Weiner & Kollman, 1981), which uses an energy function of the form

$$E = \sum_{\text{bonds}} k_b(r-r_b)^2 + \sum_{\text{angles}} k_a(\theta-\theta_a)^2 + \sum_{\text{dihedrals}} k_d/2[1+\cos(n\phi-\gamma)] + \sum_{\text{non-bonded}} [Br^{-12}-Ar^{-6}-q_iq_j/r] \qquad (5.1)$$

The first three terms represent the difference in energy between a geometry in which the bond lengths, bond angles, and dihedral angles have ideal values and the actual geometry. The remaining terms represent non-bonded Van der Waals and electrostatic interactions. The parameters used are listed in table 1. Parameters for the dihedral angles are not listed because the geometry of our system is not described with dihedral angles. For K the parameters of Wipff, Weiner and Kollman (1982) were used. The ionic radius was changed from 2.0 to 1.9 Å to fit the quantum mechanically calculated $\Delta H_{formation}$ for the K^+ - H_2O complex and the $K^+ \cdots O$ distance (Kistenmacher, Popkie & Clementi, 1973). For N, H, and O parameters were taken from the *GROMOS* force field (Van Gunsteren, 1986) as well as the point charges of the water molecules. For N the radius was lowered to 1.75 Å because the charge on N was taken more positive. The point charges for potassium nitrate were taken from Heijnen (1986).

For the calculation of the geometries the energy E was minimized with respect to all degrees of freedom by using the conjugate gradient method, the calculations were terminated when the gradient became less than 0.1 kcal $Å^{-1}$ or when the change in energy was less than 0.01 kcal $mole^{-1}$.

It was assumed that the water layer had the same periodicity as the crystal surface. Because periodicity is not yet provided by the *AMBER* software, the water molecule was placed in nine unit cells (figure 2). The crystal was kept rigid during minimization.

Table 5.1 Force field parameters and non-bonded interactions.

bond	k_b(kcal $Å^{-2}$ $mole^{-1}$)	r_b(Å)	
H-O	553	1.00	
angle	k_a(kcal $radian^{-2}$ $mole^{-1}$)	θ_a(°)	
H-O-H	47	109.3	
non bonded	r(Å)	ϵ(kcal $mole^{-1}$)	q(e)
K	1.90	0.739	1
N	1.75	0.090	1.5
O	1.78	0.155	-0.8333
O(water)	1.78	0.155	-0.82
H	0.01	0.000	0.41

The relation between r, ϵ and A_{ij} and B_{ij} is given by $A_{ij} = 2\,\epsilon_{ij} r_0^6$, $B_{ij} = \epsilon_{ij}\, r_0^{12}$ and $\epsilon_{ij} = \sqrt{\epsilon_i \epsilon_j}$ and $r_0 = r_i + r_j$.

Point charges on KNO_3 from Heijnen (1986). Other parameters from GROMOS (Van Gunsteren, 1986).

After the minimization again closest approach points were calculated followed by calculation of the electrostatic field and minimization. This procedure was repeated until the nine unit cells were completely covered with a single layer.

5.3 Results and discussion

5.3.1 Minimization

The minimizations were carried out with different start geometries. In practically all cases the start geometries converged to one single geometry. Apparently, the potential energy surfaces do not have many local minima.

After the surfaces were covered with a layer of water, closest approach points and the contribution of only the crystal to the electrostatic field were calculated. The electrostatic field corresponded to an interaction energy of a water molecule with the surface of less than 5 kJ $mole^{-1}$. So the KNO_3 faces influence a second water layer far less directly through the electrostatic field. The second water layer can however be influenced by the crystal face *via* the first water layer.

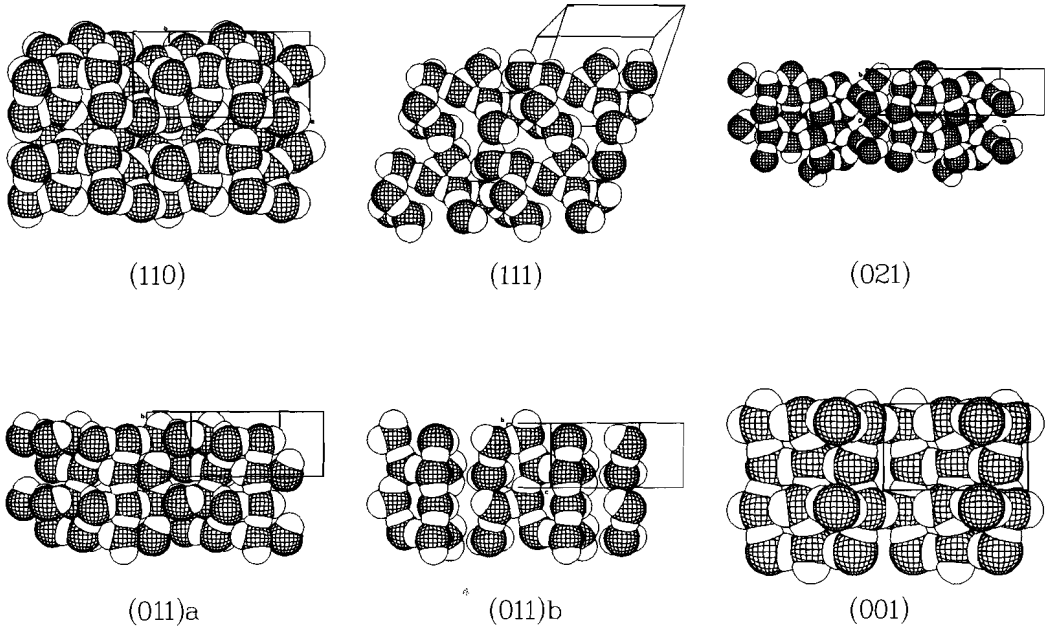

Figure 5.4 Space-filling plot (PLUTON (Spek, 1982)) of the water layers near the KNO_3 faces. Atom code: net, oxygen; white, hydrogen.

The faces covered with a single water layer are depicted in figure 4. It was observed that when a new water molecule was added to the model, loosely bound water molecules and the newly added molecule rotated and moved to form intra layer hydrogen bonds. This results in a water layer with the dipole moments of the molecules oriented more or less parallel with the crystal surface. This was also observed in computer simulations of water near a NaCl(001) face (Anastasiou, Fincham & Singer, 1983) and of water near neutral planar faces (Aloisi *et al.*, 1986; Valleau & Gardner, 1987).

The geometry of the water molecules was slightly disturbed during the minimizations. The bond lengths increased or decreased by approximately 0.02 Å and the bond angle decreased to 105°.

Table 2 lists the attachment energies, the specific surface energies γ of the uncovered faces, and the interaction energies, U_{int}, of the water layers with the faces. Table 2 shows that the interaction of the water molecules with the faces increases on the whole with the attachment energy and the specific surface energy of the faces. This is not unlikely because both quantities are

Table 5.2 Surface energies (electrostatic) E_s and γ of the KNO_3 faces, interaction energies (electrostatic and non-bonded) U_{int} of the water molecule with the faces and mesh areas A.

face	A	$4E_s$	γ	U_{int}	U_{int}
	($Å^2$)	(kJ $mole^{-1}$)	(mJ m^{-2})	(kJ per mesh area)	(mJ m^{-2})
(110)	68.757	254.0	306	380.9	920
(021)	85.941	477.1	460	561.6	1084
(111)	84.874	396.5	387	437.5	855
(011)a	60.876	175.6	239	213.4	582
(011)b	60.876	294.5	401	319.3	871
(001)	49.793	172.5	287	169.9	567

related to the field strength.

The interaction of the water molecules with the faces of potassium nitrate is stronger than the interaction of the next growth layer, E_{att}, with the faces. The interaction of the individual molecules with the faces are listed in table 3. Each face has a few water molecules that interact very strongly with the face when compared with the other water molecules.

5.3.2 The (021) face

Table 5.3 Interaction energies (electrostatic + non-bonded) of the individual water molecules with the crystal faces (in kJ $mole^{-1}$).

water	(110)	(021)	(111)	(011)a	(011)b	(001)
1	86.4	117.2	50.2	57.1	89.7	51.3
2	86.4	59.2	79.8	13.1	42.6	56.4
3	53.9	45.8	49.8	43.5	62.5	31.5
4	48.8	41.4	59.0	2.4	25.5	1.2
5	27.6	68.6	49.8	28.0	4.8	13.1
6	21.9	28.6	29.8	45.1	32.1	3.7
7	18.9	32.4	23.0	6.8	62.1	12.7
8	6.3	59.6	48.7	11.2		
9	4.0	39.9	43.8	6.2		
10	8.7	43.3	46.1			
11	12.1	14.6				
12	5.9	11.2				
Total	380.9	561.6	437.5	213.4	319.3	169.9

Table 5.4 Slice and chain energies of the (021) face (in **kJ** per 4 moles of KNO_3).

	electrostatic	non-bonded	total
(unrelaxed)			
E_{sl}	2408.6	-92.0	
E_{chain}	2461.9	-20.9	
E_{sl}-E_{chain}	-53.3	-71.1	-124.4
(relaxed)			
E_{sl}	2402.5	-188.1	
E_{chain}	2435.8	-208.2	
E_{sl}-E_{chain}	-33.3	20.1	-13.2
(with water)			
$E_{sl+water}$	3270.8	-272.9	
E_{water}	236.6	-133.6	
$E_{sl+water}$- (E_{water}+E_{chain})	572.4	-47.3	525.1

The (021) face is not an F face. It contains only one PBC, in the [100] direction and is therefore an S face. S faces normally grow by one dimensional nucleation. They grow fast and are present as unimportant faces on a crystal, if present at all. These faces are therefore not considered in PBC-analyses. Even if such a face would be considered, it would not be present on the calculated growth form because E_{att} is too high. In table 4 are listed the chain energy and the slice energy. E_{chain} is the total energy of all bonds in a chain per stoichiometric unit and E_{sl} is the total energy of all bonds in a slice per stoichiometric unit. The electrostatic parts of these energies were calculated with *ENERGY* (Woensdregt, 1971) and the non-bonded contribution with *AMBER*.

The chain energy of the [100] chain is higher than the slice energy of the (021) slice. This means that the chains repel each other. The edge energy of the [100] edge is negative and the face can not grow in layers.

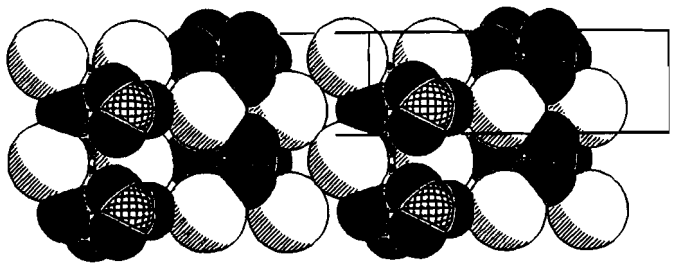

Figure 5.5 Space filling-plot (PLUTON (Spek, 1982)) of the (021) face after relaxation.

Possibly, relaxation can keep the slice together, so we allowed the top layer of the crystal to relax by minimizing the geometry with *AMBER*. Slice and chain energies were calculated and are also listed in table 4. Figure 5 shows the crystal face after relaxation. The NO_3^- ions that are pointing outwards on the unrelaxed (021) face are now lying more or less flat on the face. During relaxation the geometry of the nitrate ions becomes disturbed. Deviations from planarity are observed as well as small changes (0.01 Å) in N-O bond length. The results show that even when the surface is relaxed the slice can not be kept together. The chains still repel each other, albeit by a lesser amount. In table 4 are listed the slice energy of the unrelaxed (021) slice with the water layer on top of it ($E_{sl+water}$) and the slice energy of the water layer (E_{water}). Because $E_{sl+water} > E_{chain} + E_{water}$, the water layer can keep the slice together. This is due to the fact that lateral bonds, the hydrogen bonded network, are formed within the water layer. A temporary PBC is furnished by the water molecules (Hartman, 1988). The [100] edge energy becomes positive so layers of thickness d_{021} can exist on the (021) face.

In a highly concentrated solution, the water layer will be disturbed by the ions. In that case, the temporary PBC will be furnished by a mixture of water molecules and ions.

5.3.3 Crystal growth

The influence of solvent interaction with crystal surfaces on the growth habit of a crystal has been studied by Saska & Myerson (1983), Berkovitch-Yellin (1985) and Aquilano *et al.* (1986).

Berkovitch-Yellin (1985) studied organic compounds such as glycine, cinnamid and succinic acid. The interaction of the solvent with the faces was deduced qualitatively from the polarity of the solvent. The reduction in growth rate was largest for the faces with the strongest solvent interaction.

Saska & Myerson (1983) and Aquilano *et al.* (1986) studied the interaction of water with the faces of sucrose. They calculated the interaction energy and subtracted it from the attachment energy. New growth forms were constructed from the modified attachment energies by taking the central distances of the faces proportional to their attachment energies. The interaction energies of water with the KNO_3 faces is greater or equal to the attachment energies. Subtraction of the interaction energies from the attachment energies yields negative modified attachment energies, so this correction method does not work in this case.

In a preceding paper (Van der Voort, 1990b) it was justified that under certain conditions the interaction of the solvent with the crystal surface may be subtracted from the attachment energy and that

$$R \propto \frac{\sum_{i=1}^{n} \exp(c_i E_{att,i}/kT)}{\sum_{j=1}^{m} \exp(c_j U_{int,j}/kT)} \qquad (5.2)$$

where $E_{att,i}$ is the attachment energy of a single growth unit, not necessarily the unit cell contents, and $U_{int,j}$ is the interaction energy of a single water molecule with a face. In this approach only the strongly adsorbed molecules and growth units count. If we take the K^+ and NO_3^- ions as growth units, we find that this approach does not work. This can have several causes. First, the growth units may consist of clusters instead of single ions (McMahon, Berglund & Larson, 1984; Schwendinger & Rode, 1989). Second, there is no certainty about the shape of the slice (*i.e.* the atomic structure). Third, the role of surface diffusion may be different. Perhaps it does not determine the growth rate. The water molecules are arranged on the faces like a 'skin', and surface diffusion may happen on top of the skin and then E_{att} is no longer a parameter that determines the rate of surface diffusion.

However, because of the very high concentration of KNO_3 (one molecule of KNO_3 per ten molecules of water) in a saturated solution, the existence of

such a complete skin is doubtful. More probable is the assumption that surface diffusion does not occur, due to the strong adsorption of the water molecules, and that the growth rate is determined by the integration of growth units in the kinks. The growth rate may then be expressed as

$$R = \frac{l\, N_0\, s\, kT\, \Omega}{\tau_k\, 19\, \kappa} \tag{5.3}$$

where N_0 is the concentration of growth units in the solution, l is the mean free path of a growth unit in the solution, s is the number of cooperating spirals, k is the Boltzmann factor, T is the absolute temperature, Ω is the molecular volume and τ_k is the relaxation time for entering a kink (Bennema & Gilmer, 1973). τ_k may be expressed as

$$\tau_k = \nu_0^{-1} \exp(\Delta G_k^{\neq}/kT) \tag{5.4}$$

where ν_0 is the atomic frequency factor, often taken as kT/h, where h is Planck's constant. Before a growth unit can enter a kink, the water molecules must be removed. We assume that this process governs the rate. Furthermore, it is assumed that the interaction energy of a water molecule with a face is related to the activation energy of removing a water molecule from a kink, so τ_k can be expressed as

$$\tau_k = \nu_0^{-1} \sum_{i=1}^{n} \exp(c_i\, U_{int,i}/kT) \tag{5.5}$$

where c_i is a constant between 0 and 1 (Van der Voort, 1990b).

For κ we can write

$$\kappa = 2\, k'\, Z\, E_{sl} / \sqrt{(V\, d_{hkl})} \tag{5.6}$$

so we obtain

$$R = \frac{l\, N_0\, s\, kT\, \Omega\, \nu_0\, \sqrt{(V\, d_{hkl})}}{38\, k'\, Z\, E_{sl} \sum_{i=1}^{n} \exp(c_i\, U_{int,i}/kT)} \tag{5.7}$$

By introducing

$$B = \frac{l\, N_0\, s\, kT\, \Omega\, \nu_0\, \sqrt{V}}{38\, k'} \tag{5.8}$$

and

$$G = \frac{\sqrt{d_{hkl}}}{Z\, E_{sl} \sum_{i=1}^{n} \exp(c_i\, U_{int,i}/kT)} \tag{5.9}$$

the face dependent factors are separated from the others. In table 5 are listed the calculated G's for the KNO_3 faces, c_i is taken as a constant. The table shows that

$$R_{(001)} \geq R_{(011)a} > R_{(111)} > R_{(110)} \geq R_{(011)b} > R_{(021)} \tag{5.10}$$

Table 5.5 Calculated G values for the KNO_3 faces.

face	c = 1.0	c = 0.5
(110)	$1.6 \cdot 10^{-18}$	$5.3 \cdot 10^{-11}$
(021)	$1.6 \cdot 10^{-23}$	$2.1 \cdot 10^{-13}$
(111)	$4.4 \cdot 10^{-17}$	$3.6 \cdot 10^{-10}$
(011)a	$4.1 \cdot 10^{-13}$	$3.3 \cdot 10^{-8}$
(011)b	$8.6 \cdot 10^{-19}$	$5.8 \cdot 10^{-11}$
(001)	$8.6 \cdot 10^{-12}$	$3.7 \cdot 10^{-8}$

Furthermore, these results suggest that the (011) face grows by (011)b slices at the condition where the presented theory is valid. At higher supersaturations the formation of 2D nuclei of thickness $\frac{1}{2}\, d_{011}$ becomes more likely and the face can grow by layers $\frac{1}{2}\, d_{011}$. The (011) face will grow faster and the morphological importance will decrease. The observed growth habit suggest that the (011) face indeed grows (partly) by layers of thickness $\frac{1}{2}\, d_{011}$. The calculated relative growth rate of the (021) face is smallest, which does not agree with the observed habit. Yet, the (021) face is a temporary F-face and the slice energy is probably no longer a good measure for the kink density on the face. The kink density is so large that the growth rate is larger than expected.

5.3.4 Aragonite and cerussite

Although aragonite and KNO_3 have the same crystal structure, they have different observed growth habits. This means that the results from the calculations on KNO_3 do not apply for aragonite. This is not strange because all charges on the ions of aragonite are twice as large as the charges on KNO_3. So the surface energies, slice energies and the crystal energy are four times as large as those for KNO_3. The interaction energies of the water molecules with the faces of aragonite are approximately twice as large. In the case of aragonite the growth rate of the faces may be governed by other processes. Furthermore, the (021) slice can not be kept together by the water molecules because the chains repel each other too strongly.

Cerussite ($PbCO_3$) also has the same structure as KNO_3 and aragonite. The most important forms on the crystals are {110}, {010}, {111} and {021}, the same as those on KNO_3. This can be expected because the influence of the ionic charges is much less than for aragonite, mainly due to the more covalent character of the Pb · · · O bond (Hartman, 1953).

5.4 Conclusions

We have shown that despite the limitations of the method, it is possible to get an estimation of the interaction of water molecules with the faces of KNO_3. It is found that on each face a few water molecules adsorb very strongly. By assuming that de-adsorption of these water molecules governs the growth rate, the observed growth form can be predicted semi-quantitatively.

The agreement between observed and theoretical growth forms obtained from the relation $R \propto E_{att}$ is often remarkably good. This is especially the case for growth from the vapour and very often for solution growth. This can only be explained when surface diffusion plays an important role and when there is no preferential solvent adsorption.

Acknowledgements

The author wishes to thank Professor P. Hartman for stimulating discussions and conscientiously reading the manuscript and Dr. A.L. Spek, Dr. C.S. Strom and Drs. C.F. Woensdregt for their permission to use the computer programs *PLUTON*, *ABSORB*, *SURFPOT* and *ENERGY*.

References

Aloisi. G, Guidelli, R., Jackson, R.A., Clark, S.M. & Barnes, P. (1986). *J. Electronal. Chem.* **206**, 131.

Anastasiou, N., Fincham, D. & Singer, K. (1983). *J. Chem. Soc. Farad. Trans. 2* 79, 1639.

Aquilano, D., Rubbo, M., Mantovani, G., Sgualdino, G. & Vaccari, G. (1986). *J. Crystal Growth* 74, 10.

Bennema, P. & Gilmer, G.H. (1973). In *Crystal Growth, an Introduction*, edited by P. Hartman, Chapter 14. Amsterdam: North-Holland.

Berkovitch-Yellin, Z. (1985). *J. Am. Chem. Soc.* **107**, 8239.

Connolly, M.L. (1981). "Molecular Surface Program", *QCPE Bull.* **1**, 74. It may be obtained by writing to Quantum Chemistry Program Exchange, Department of Chemistry, Indiana University, Bloomington, IN 47405, USA.

Ewald, P.P. (1921). *Ann. Phys. (Leipzig)* **64**, 253.

Groth, P. (1908). *Chemische Krystallographie*. Vol. 2, p. 74. Leipzig: Wilhelm Engelman.

Hansma, P.K. & Salisbury, D. (1989). *New Scientist* 122, 52.

Hartman, P. (1953). Ph.D. Thesis, Groningen.

Hartman, P. (1973). In *Crystal Growth, An Introduction*, edited by P. Hartman, Chapter 14. Amsterdam: North-Holland.

Hartman, P. (1988). In *Morphology of Crystals* Part A, edited by I. Sunagawa, p.269. Tokyo: Terrapub and Dordrecht: Reidel.

Hartman, P. & Bennema, P. (1980). *J. Crystal Growth* **49**, 145.

Hartman, P. & Perdok, W.G. (1952). *Proc. Koninkl. Nederland. Akad. Ser. B.*, 55, 134.

Hartman, P. & Perdok, W.G. (1955). *Acta Cryst.* **8**, 49.

Heijnen, W.M.M. (1986). *Neues Jahrb. Mineral. Abh.* **154**, 223.

Kistenmacher, H., Popkie, H. & Clementi, E. (1973). *J. Chem. Phys.* **59**, 5842.
McMahon, P.M., Berglund, K.A. & Larson, M.A. (1984). In *Industrial Crystallization 84*, edited by S.J. Jančić & E.J. de Jong. Amsterdam: Elsevier.
Nimmo, J.K. & Lucas, B.W. (1973). *J. Phys. C.* **6**, 201.
Saska, M. & Myerson, A.S. (1983). *J. Crystal Growth* **61**, 546.
Schwendinger, M.G. & Rode, B.M. (1989). *Chem. Phys. Lett.* **155**, 527.
Spek, A.L. (1982). The *EUCLID* package, In *Computational Crystallography*, p. 528, edited by D. Sayre. Oxford: Clarendon.
Strom, C.S. & Hartman, P. (1989). *Acta Cryst.* A**45**, 371.
Valleau, J.P. & Gardner, A.A. (1987). *J. Chem. Phys.* **86**, 4162
Van der Voort, E. (1990a). *J. Crystal Growth* **100**, 544.
Van der Voort, E. (1990b). The morphology of succinic acid crystals: the role of solvent interaction. Submitted to *J. Crystal Growth.*
Van Gunsteren, W.F. (1986). *GROMOS86*. Groningen Molecular Simulation program package. University of Groningen, The Netherlands.
Weiner, P.K. & Kollman, P.A. (1981). *J. Computational Chemistry* **2**, 287.
Wipff, G., Weiner, P.K. & Kollman, P.A. (1982). *J. Am. Chem. Soc.* **104**, 3249.
Woensdregt, C.F. (1971). *ENERGY*, a FORTRAN IV program to compute surface energies in an electrostatic point charge model. Geol. Mineral. Inst. Leiden State Univ. (unpublished).

CHAPTER 6

THE ROLE OF WATER IN THE HABIT CHANGE FROM CUBE TO OCTAHEDRON OF ALKALI HALIDE CRYSTALS

Abstract

The electrostatic field near the cube and octahedron faces of alkali halide crystals with the rocksalt structure was calculated. The results were used to recover the growth mechanisms of these faces. The solvent interaction with the kinks was assumed to determine the rate of integration of growth units in the kinks. With this assumption the habit change from cube to octahedron, which occurs when the supersaturation is increased or when one of the ions is present in excess, could be explained.

6.1 Introduction

NaCl-type crystals of alkali halides can undergo a habit change when they grow in a polar solvent (Kern, 1953; Bienfait, Boistelle & Kern, 1965). Octahedron faces {111} appear on the {100} cubic crystals when the supersaturation increases beyond a critical value, β_c. β is defined as c/c_s where c is the actual concentration and c_s is the saturation concentration. A KI crystal grown at a supersaturation between 1.10 and 1.14 has smooth {001} and {111} faces. When the supersaturation is increased above 1.14 the {001} faces become rough. The opposite happens when the supersaturation is lower than 1.10; the {111} faces become rough. It was also shown that once the (111) face has become rough, it can not become smooth any more. Bienfait, Boistelle & Kern (1965) observed that the critical supersaturation is not the same for all alkali halides considered. NaCl and KCl have a β_c of 1.23 and 1.25 respectively and RbCl and KI have a lower β_c (1.10 and 1.14).

The habit change has been explained in terms of growth rates of the faces that depend differently on the supersaturation. Other explanations were given earlier by Kern (1953), Hille, Jentsch & Stranski (1964) whose interpretations are based on a variation in solvation of the faces with the supersaturation.

Habit changes as those described above are also observed when there is excess of one of the ionic species in the solution. Examples are NaCl crystals grown from an aqueous HCl or NaOH solution and KCl crystals grown from an aqueous HCl or KOH solution (Groth, 1906). Kirov, Vesselinov & Cherneva (1972) observed a habit change of calcite crystals when one of the ionic species was present in excess. Calcite crystals are normally rhombohedral {211}. Steep rhombohedra {110} are formed when growth takes place from a solution containing an excess of Ca^{2+} ions. The basal plane {111} predominates when an excess of CO_3^{2-} is present. The combination of {110} and {111} corresponds to {111} of NaCl. The {110} faces are believed to grow by layers of thickness $\frac{1}{2}\, d_{110}$ (Heijnen, 1985). When one of the ions is present in excess, halving of the (011) slices is believed to be no longer possible so the {110} faces grow more slowly and appear on the crystals.

In the opinion of the present authors the solvent plays an important role in causing these habit changes. With more knowledge of the interaction of the solvent with the growing crystal faces one should be able to predict the growth mechanism, the relative growth rates of the faces and thus the habit changes. In this study the solvent interaction will be determined and with the help of the results, explanations for the observed phenomena will be given.

6.2 Method

The solvent considered in this study is water. Since a water molecule has a permanent dipole moment, the strength of the interaction of a water molecule with a crystal face can be derived from the electrostatic field strength at the adsorption site. Areas with a high field strength can be designated as preferential adsorption sites. Bienfait, Boistelle & Kern (1965) calculated the electrostatic field at lattice sites near the surface but we are also interested in the field strength at other positions as close as possible to the surface. Therefore a so-called solvent accessible surface was calculated (Connolly, 1981). The ions at the surface of the crystal faces are considered as spheres with radii equal to the ionic radii. A water molecule was taken as a sphere with a radius of 1.5 Å. The points of the solvent accessible surface are obtained by rolling the water molecule across the surface and taking the centre of the water molecule as a point. The surface point density was taken as 4 points per $Å^2$.

Contrary to Bienfait, Boistelle & Kern (1965) who took only nearest neighbours into account in the electrostatic field calculations, we calculated the potentials and fields with *SURFPOT* (Strom & Hartman, 1989). This program calculates Coulomb potentials and fields of stackings of infinite lattice slices based on the Ewald method (Ewald, 1921). Therefore it was necessary to describe the faces as structures with three-dimensional periodicity, using unit cells. The charges on the cations and anions are taken as +1 and -1 respectively.

6.3 Description of the faces

The (001) face is smooth, compact and contains both cations and anions in the uppermost layer. Because crystal growth processes on smooth faces involve the entering of growth units into steps and kinks, these were introduced on the face. On evaporation surfaces of NaCl steps of monatomic height (2.82 Å) and steps of double height (5.64 Å) are observed (Bethge & Keller, 1960). Figure 1 shows a model of the (001) face with a monatomic step and one with a double step. Two kinds of kinks can be discerned. One kink consists of anions and offers place to a cation and the other one consists of cations and offers place to an anion. The first kink is denoted as a "+" kink and the second one as a "-" kink.

The (111) face has alternating layers of cations and anions. Two slices of thickness d_{111} can be found, both containing a layer of cations and a layer of anions. In the electrostatic point charge model, both slices have the same slice energy and the same surface energy, which is infinite. So this surface is unstable as was shown earlier by Stranski (1928) and verified experimentally by Knoppik and Lösch (1976).

This face is stable if it is considered as a K (kinked) face. Then the uppermost two layers have vacant sites. The occupation in the uppermost layer is 25 % and in the second layer 75 %, so the face is rough on the atomic scale. This face is often referred to as the $(111)_2$ face. In figure 2 are shown a $(111)_2$ face with cations in the top layer and one with anions in the top layer. The first one has kinks offering place to cations, henceforth called octahedron "+", and the second one has kinks offering place to anions, henceforth called octahedron "-".

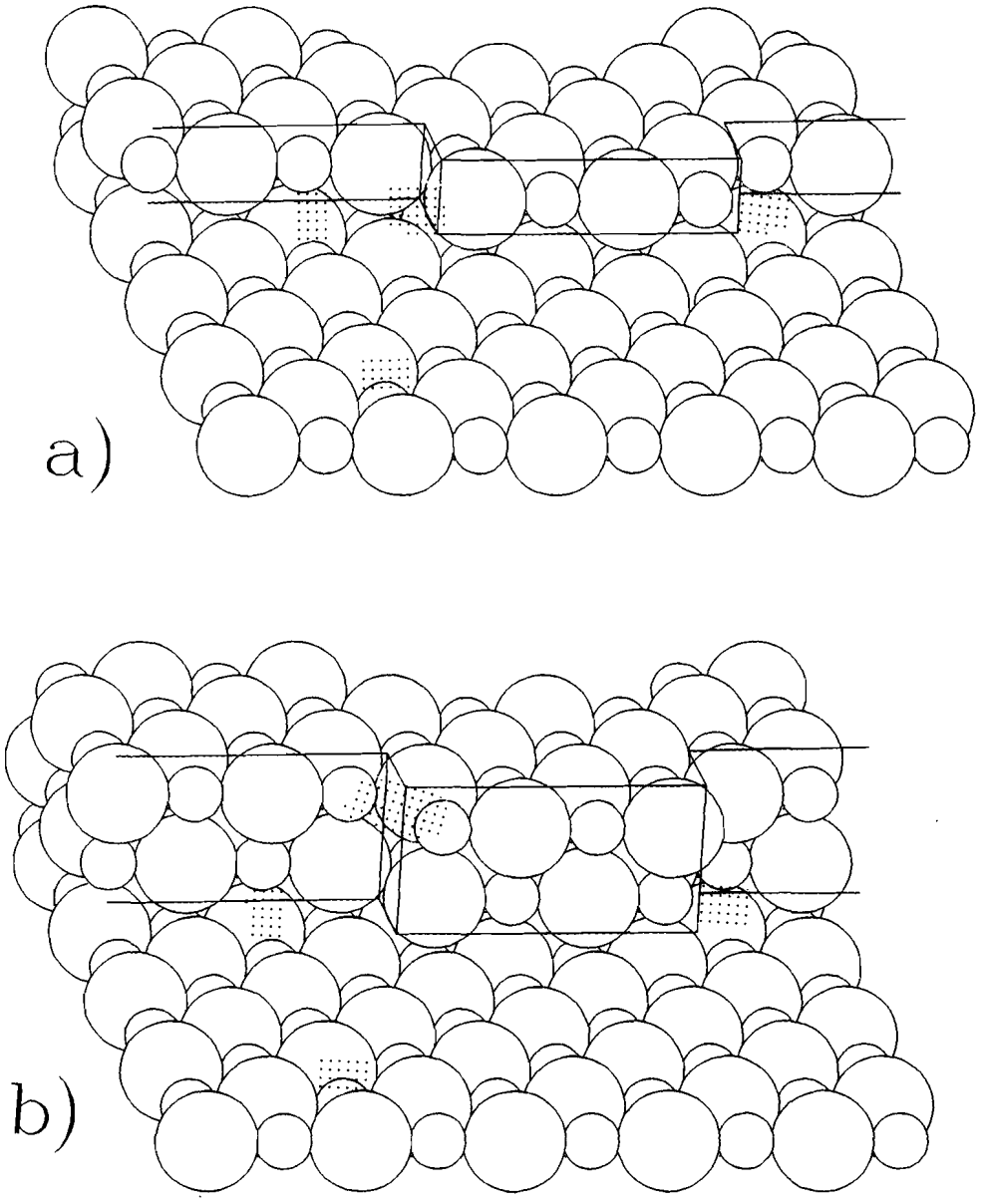

Figure 6.1 Cube {001} face of NaCl with a monoatomic step (a) and a double step (b). Solid line mark the steps and kinks. Large spheres are Cl^- ions. Small spheres are Na^+ ions. Dotted areas indicate maxima in electrostatic field.

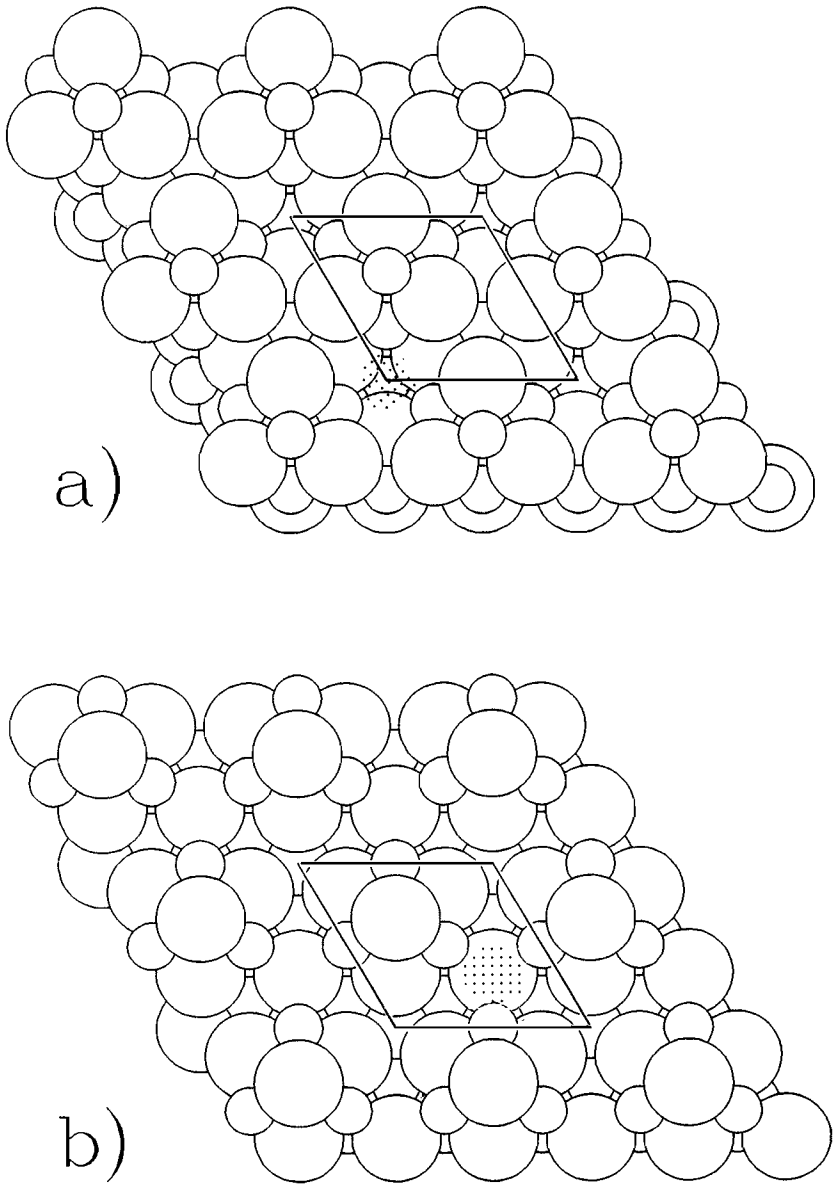

Figure 6.2 Octahedron "+" (a) and octahedron "-" (b) face of NaCl. Large spheres are Cl^- ions. Small spheres are Na^+ ions. Dotted areas indicate maxima in electrostatic field.

6.4 Results

6.4.1 The (001) face

Table 6.1 lists the electrostatic potentials at lattice sites just above the face, at the step and in the kinks of the NaCl (001) faces with the monatomic step and with the double step. The maximum electrostatic field strength on the solvent accessible positions near the face, step and kink are also listed in table 6.1 and indicated in figure 6.1 as dotted areas. The position with the maximum field on the face is located above the Na^+-ion. On the lower terrace of the step between two Na^+-ions there is another maximum. In the "-" kinks of the monatomic and double steps the maxima occur at the bottom of the step. In the "+" kinks on the monatomic step the maxima are also found at the bottom of the step. On the other hand, in the "+" kink on the double step the maxima are found on the edge of the upper terrace. Table 6.1 shows that the electrostatic potential and field are largest in and near the kinks and smallest on the face. There is a large difference between the potentials in the kinks in the monatomic and double step. In the case of the monatomic step, the contribution of the single row of four atoms converges very poorly. This means that the potentials in these kinks depend strongly on the distance between them. When the distance between the kinks is infinite the potentials will approach those in the kinks of the double step, where there is no convergence problem.

Table 6.2 shows the electrostatic field near the "+" and "-" kinks of the monatomic and double steps of NaCl, KCl, RbCl and KI. In general it can be said that the field in the NaCl and KCl kinks is somewhat stronger than in the kinks of RbCl and KI.

Table 6.1 Electrostatic potential (V, in e $Å^{-1}$) at lattice sites near face, step and kink of the NaCl (001) face and maximum electrostatic field ($|\bar{E}|$, in e $Å^{-2}$) near face, step and kink. Absolute values are given for the potentials at the face and step.

	monatomic step		double step	
	V	$\|\bar{E}\|$	V	$\|\bar{E}\|$
face	0.023	0.069	0.023	0.069
step	0.075	0.091	0.055	0.086
"-" kink	0.245	0.136	0.136	0.129
"+" kink	-0.245	0.107	-0.136	0.119

Table 6.2 Maximum electrostatic field strength (in e $Å^{-2}$) near the kinks of the (001) faces of the alkali halides.

	monatomic step		double step	
	"+"	"-"	"+"	"-"
NaCl	0.107	0.136	0.119	0.129
KCl	0.110	0.125	0.122	0.121
RbCl	0.101	0.116	0.110	0.114
KI	0.099	0.109	0.114	0.117

6.4.2 The (111) face

The electrostatic field of the octahedron "+" and octahedron "-" faces of the four alkali halides was also calculated. Table 6.3 lists the maximum values of the field strength. It appears that for the octahedron "+" faces the maximum field is not located in the kink but between the three cations next to the kink, as indicated in figure 6.2 by the dotted area. The octahedron "-" faces have their maxima right in the kink, where an anion can join the lattice. It should be noted that the field in the kinks of the (001) faces is stronger than the field on the octahedron faces.

Table 6.3 Maximum electrostatic field strength (in e $Å^{-2}$) on the octahedron faces of the alkali halides.

	octahedron "+"	octahedron "-"
NaCl	0.124	0.123
KCl	0.097	0.086
RbCl	0.091	0.086
KI	0.106	0.083

6.5 Discussion

The electrostatic field on the NaCl (001) face has its maximum just above the Na^+-ions. So these sites can be designated as preferential adsorption sites on the face. MD-simulations of water near a NaCl (001) face also show a strong Na-O attraction (Anastasiou, Fincham & Singer, 1983). The adsorption

energy is the inner product of the electrostatic field with the dipole moment. Polarization is taken into account so the dipole moment of 1.83 D (0.383 e Å) increases with $\mu_{ind} = \alpha \cdot |\bar{E}|$. The adsorption energy thus obtained is 46 kJ mole^{-1}. This agrees very well with the calculated values of Mikheikin *et al.* (1975) (43 kJ mole^{-1}), Korol & Posudievsky (1986) (43 kJ mole^{-1}), and the experimental values of Hugher (1967) (46 kJ mole^{-1}), and Estel *et al.* (1976) (43 kJ mole^{-1}).

Knowledge of the growth mechanism and the growth rate law is essential to understand and explain the habit changes and roughening of the faces.

The electrostatic field in the kinks of the (001) face and on the $(111)_2$ face is very strong and corresponds to an adsorption energy of more than 60 kJ mole^{-1} which suggests that the dehydration of the kinks is a slow step in the growth process.

The (001) face is a flat face (F), which indicates that it grows by layers. Bethge & Keller (1960) observed steps on the (001) face and the fact that the electrostatic potential and field on the face are much smaller than those near the steps and kinks is also indicative for layer growth. Furthermore it has been shown that the growth of NaCl and KCl crystals is reaction rate controlled (Peibst & Noack, 1962; Mullin, 1972). We assume that the integration of growth units in the kinks controls the growth of the (001) face, so it grows according to a parabolic rate law. Nielsen (1984) expresses the growth rate as

$$v_g = k_{int} (\beta - 1)^2 \tag{6.1}$$

where $(\beta - 1)$ is the relative supersaturation and k_{int} is the reaction rate constant which can be expressed as

$$k_{int} = \frac{0.1\ a\ \nu_{int}\ K_{ad}\ V_m\ c_s}{(\gamma/kT)\ \exp\ (\gamma/kT)} \tag{6.2}$$

where a is the length of a molecular jump (in the order of a few Å), K_{ad} is the adsorption constant, V_m is the molecular volume, c_s is the saturation concentration and γ is the edge energy. The integration frequency ν_{int} is expressed according to Eyrings formalism (Glasstone, Laidler & Eyring, 1941; Eyring & Eyring, 1963)

$$\nu_{int} = \nu_0 \exp(-\Delta G^{\neq}/kT) \tag{6.3}$$

where ν_0 is kT/h and $\Delta G^{\neq}$ is the activation energy for integration.

The $(111)_2$ face is rough on the atomic scale and in fact it consists entirely of kinks. Bienfait, Boistelle & Kern (1965), however, have shown that a step on the $(111)_2$ face is stable, which means that the face may grow by layers. The steps (in the $[0\bar{1}1]$ and $[01\bar{1}]$ direction) also consist entirely of kinks and therefore the growth of the face is most probably diffusion controlled. A linear rate law has been observed by Schüz (1969).

The growth rate of the $(111)_2$ face can be expressed by

$$v_g = k_D (\beta - 1) \tag{6.4}$$

where k_D is the rate constant.

$$k_D = D V_m c_s / r \tag{6.5}$$

D is the diffusion coefficient and r is the diffusion layer thickness.

Peibst & Noack (1962) observed an exponential rate law for KCl at higher supersaturations which suggests that the observed roughening of the (001) face upon increasing the supersaturation is connected with so-called kinetic roughening. At a higher supersaturation 2D nuclei develop on the terraces and the growth rate law becomes exponential.

The growth rate can then be expressed according to Nielsen (1984)

$$v_g = k_e \beta^{7/6} (\beta - 1)^{2/3} (\ln \beta)^{1/6} \exp(-K_e/\ln \beta) \tag{6.6}$$

with

$$k_e = 2 a \nu_{int} (K_{ad} c_s V_m)^{4/3} \exp(-\gamma/kT) \tag{6.7}$$

and

$$K_e = \pi \gamma^2 / 3 k^2 T^2 \tag{6.8}$$

Figure 3 shows a graph with a parabolic and an exponential curve. When the supersaturation increases beyond β_1, the exponential rate law becomes rate

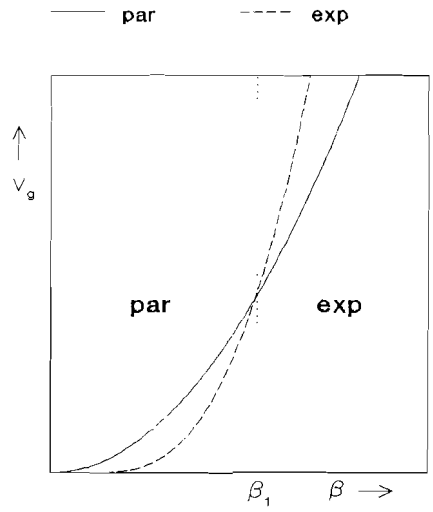

Figure 6.3 Examples of parabolic (solid) and exponential (dashed) rate laws.

determining because 2D nucleation and spiral growth occur simultaneously. The point of intersection β_1 can be found by equating (6.1) and (6.6) and solving β_1. We obtain

$$2(K_{ad}\, c_s\, V_m)^{1/3}\, \beta^{7/6}\, (\beta-1)^{2/3}\, (\ln \beta)^{1/6} \exp\,(-\pi\gamma^2/3k^2T^2\, \ln\beta) =$$

$$0.1\, (\beta-1)^2/(\gamma/kT) \qquad (6.9)$$

After substituting the parameters of Nielsen (1984), $K_{ad}\, c_s\, V_m = 0.1$ and $\gamma/kT = 0.5$ for both (001) and $(111)_2$, the equation was solved numerically. The rate determining mechanism changes (gradually) to 2D nucleation at $\beta_1 \approx 1.07$, which is in the same order of magnitude as the critical supersaturations for the habit changes.

When the supersaturation increases above β_{c1} the $(111)_2$ face appears on the crystal (see figure 4). The concentration of kinks on the (001) face has increased so much by the kinetic roughening that it has become comparable with the concentration of kinks on the $(111)_2$ face. When the supersaturation increases above β_{c2}, only the $(111)_2$ face is present. Bienfait, Boistelle & Kern (1965) found that steps on the $(111)_2$ face in a solution are stable and that the face can therefore grow in layers, although it consists of kinks.

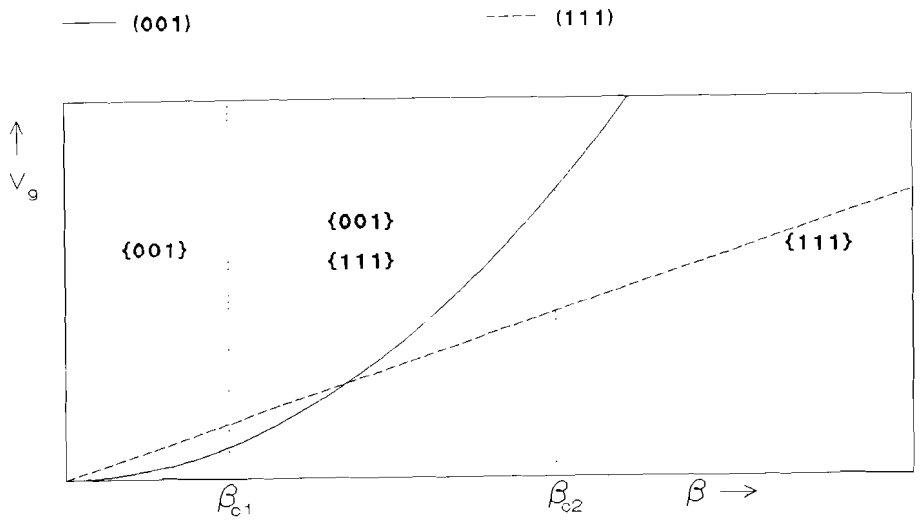

Figure 6.4 Growth rate laws of the (001) and $(111)_2$ faces.

When the supersaturation is decreased, it is found that the change in surface structure on the (001) face is reversible. The face becomes smooth again. The $(111)_2$ face, on the contrary, becomes rough and can not become smooth any more. This irreversible behaviour can be explained as follows. The electrostatic field in the kink in a step on the $(111)_2$ face is comparable with the field in a kink in a double step on the (001) face. The electrostatic field in a kink on a terrace on the $(111)_2$ face is somewhat smaller. Starting from the assumption that the dehydration is a slow step in the growth process, this means that the growth on a terrace increases more strongly with the supersaturation than growth at the step. At a high supersaturation the growth on the terrace is determined by volume diffusion whereas growth at the step is still determined by the dehydration of the kinks in the step. So at a high supersaturation growth at the step is easier than growth on the terrace (layer growth) whereas this is reversed at lower supersaturations. The face becomes rough and in that case it consists of pyramids with side faces (001) that can grow no longer by layers parallel to the (111) plane (see figure 6.5).

The $(111)_2$ face appears on the crystals when

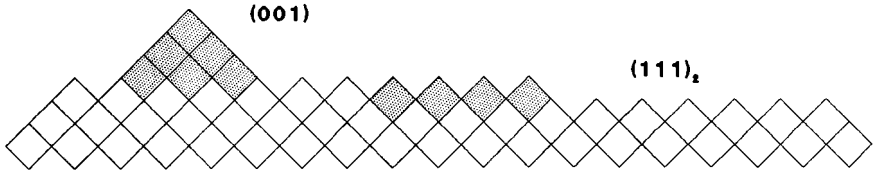

Figure 6.5 The $(111)_2$ face with growth (shaded squares) by layers (right) and on the terrace (left), which results in the formation of a pyramid with side faces {001}.

$$v_{g,D} = v_{g,int}\sqrt{3} \tag{6.10}$$

Combination of (6.1), (6.2), (6.4), (6.5) and (6.10) gives the point of intersection

$$(\beta_c - 1) = \frac{D\,(\gamma/kT)\,\exp\,(\gamma/kT)}{0.1\ r\ a\ K_{ad}\ \nu_{int}\ \sqrt{3}} \tag{6.11}$$

The critical supersaturation for the habit change, β_c, depends only on ν_{int} because the other variables have almost the same values for all alkali halides. So, the stronger the interaction of a water molecule with the kink site on the (001) face, the lower ν_{int} and therefore the higher β_c. From the data in table 6.2 a higher β_c is predicted for NaCl and KCl than for RbCl and KI, which is indeed observed by Bienfait, Boistelle & Kern (1965).

The habit change that happens when one of the ions is present in excess can be explained as follows. Nielsen & Toft (1984) have shown that the growth rate of an electrolyte is a function of the ionic product as long as this growth rate is reaction rate controlled (for instance by dehydration of kinks). This means that the growth rate of the (001) face increases when one of the ionic species is added to the solution.

When the growth rate is controlled by diffusion, it is a function of the concentration of the electrolyte and not of the ionic product. So the growth rate does not change when the concentration of one of the species is increased. The growth rate has become a function of the concentration of the deficient species. This is the case for the $(111)_2$ face. So, the growth rate of the (001)

face increases whereas the growth rate of $(111)_2$ does not change, which results in an increase in morphological importance of $(111)_2$.

6.6 Conclusions

The strong electrostatic field in the kinks on the faces of alkali halide crystals suggests that water molecules can adsorb strongly in the kinks and that dehydration of kinks is a slow step in the growth process. The habit change from cube to octahedron and the roughening of the cube and octahedron faces could be explained. The habit changes are, as already assumed by Bienfait, Boistelle & Kern (1965), indeed a consequence of the growth rates of (001) and $(111)_2$ that depend differently on the supersaturation. The roughening of the (001) face could be interpreted as kinetic roughening *i.e.* the formation of 2D nuclei on the terraces. The roughening of the $(111)_2$ face could be explained by the relatively high growth rate on the terrace at a low supersaturation.

References

Anastasiou, N., Fincham, D. & Singer, K. (1983). *J. Chem. Soc. Faraday Trans. 2* 79, 1639.

Bethge, H. & Keller, W. (1960). *Z. Naturforsch.* **15a**, 271.

Bienfait, M., Boistelle, R. & Kern, R. (1965). In *Adsorption et croissance cristalline*, Colloques Internationaux du CNRS, No. 152. Paris: CNRS.

Connolly, M.L. (1981). *"Molecular Surface Program", QCPE Bull.* **1**, 74. It may be obtained by writing to Quantum Chemistry Program Exchange, Department of Chemistry, Indiana University, Bloomington, IN 47405, USA.

Estel, J., Hoinkes, H., Kaarmann, H., Nahr, H. & Wilsch, H. (1986). *Surf. Sci.* **54**, 393.

Ewald, P.P. (1921). *Ann. Phys. (Leipzig)* **64**, 253.

Eyring, H. & Eyring, E.M. (1963). *Modern Chemical Kinetics*. London: Reinhold.

Glasstone, S.C., Laidler, K.J. & Eyring, H. (1941). *The Theory of Rate Processes*. London: McGraw-Hill.

Groth, P. (1906). *Chemische Krystallographie*, Vol. **1**, p. 176.

Heijnen, W.M.M. (1985). *Neues Jahrb. Mineral. Mh.* **1985**, 357.
Hille, M., Jentsch, C. & Stranski, I.N. (1964). *Z. Naturforsch.* **19a**, 133.
Hugher, M. (1967). *Compt. Rend B.* **264**, 243.
Kern, R. (1953). *Bull. Soc. Franç. Minér. Crist.* **76**, 325.
Kirov, G.K., Vesselinov, I. & Cherneva, Z. (1972). *Krist. Tech.* **7**, 497.
Knoppik, D. & Lösch, A. (1976). *J. Crystal Growth* **34**, 332.
Korol, E.N. & Posudievsky, O. Yu. (1986). *Surf. Sci.* **169**, 104.
Mikheikin, I.D., Abronin, I.A., Zhidomirov, G.M. & Kazanskii, V.B. (1975). *Russ. J. Phys. Chem.* **49**, 1306.
Mullin, J.W. (1972). *Crystallisation*, 2nd ed. London: Butterworths.
Nielsen, A.E. (1984). *J. Crystal Growth* **67**, 289.
Nielsen, A.E. & Toft, J.M. (1984). *J. Crystal Growth* **67**, 278.
Peibst, H. & Noack, J. (1962). *Z. Phys. Chem.* **221**, 115.
Schüz, W. (1969). *Z. Krist.* **128**. 36.
Stranski, I.N. (1928). *Z. Phys. Chem.* A**136**, 259.
Strom, C.S. & Hartman, P. (1989). *Acta Cryst.* A**45**, 371.

CHAPTER 7

MORPHOLOGY OF POLAR $ASO_3 \cdot 6H_2O$ CRYSTALS (A = Ni, Co, Mg) AND SOLVENT INTERACTION

Abstract

The PBC-analysis of the polar $ASO_3 \cdot 6H_2O$ structure leads to the F-forms {001}, {00$\bar{1}$}, {111}, {$\bar{1}\bar{1}\bar{1}$}, {011}, {0$\bar{1}\bar{1}$}, {0$\bar{1}$1} and {01$\bar{1}$}. Attachment energies and slice energies were calculated using an electrostatic point charge model. Two centrosymmetric theoretical habits are derived. One, based on slice energies, is prismatic with {0$\bar{1}$1} and {01$\bar{1}$} as main forms, the other, based on attachment energies, is isometric with only {001} and {00$\bar{1}$}.

The observed polar habit is explained in terms of the interaction of water molecules with the exposed oxygens of the sulphite ion. This interaction decreases the growth rate of ($\bar{1}\bar{1}\bar{1}$), {0$\bar{1}\bar{1}$} and {001}, while the {01$\bar{1}$} prism is more affected than {0$\bar{1}$1}, in qualitative agreement with the observed habit.

7.1 Introduction

The morphology of the compounds $ASO_3 \cdot 6H_2O$ with A = Ni, Co or Mg has been described by Klasens *et al.* (1936). The crystals grown from aqueous solutions have a clearly polar habit (point group 3) with the trigonal pyramid {001} and the pedion {$\bar{1}\bar{1}\bar{1}$} as main forms and with the trigonal pyramid {0$\bar{1}\bar{1}$} as less important form. Often the trigonal prisms {01$\bar{1}$} and {0$\bar{1}$1} appear as small faces (see figure 7.1).

Cadoret (1967) correlated the absolute crystal structure with the morphology and explained the habit using the PBC theory. The polar habit was explained in terms of deformation of the surfaces, which lowers the surface energy differently for each face.

In this paper a theoretical growth form of $MgSO_3 \cdot 6H_2O$ is derived by calculations based on an electrostatic point charge model. The results which are approximately also valid for $NiSO_3 \cdot 6H_2O$ and $CoSO_3 \cdot 6H_2O$, are compared to the observations. The discrepancies between observed habit and the theoretical

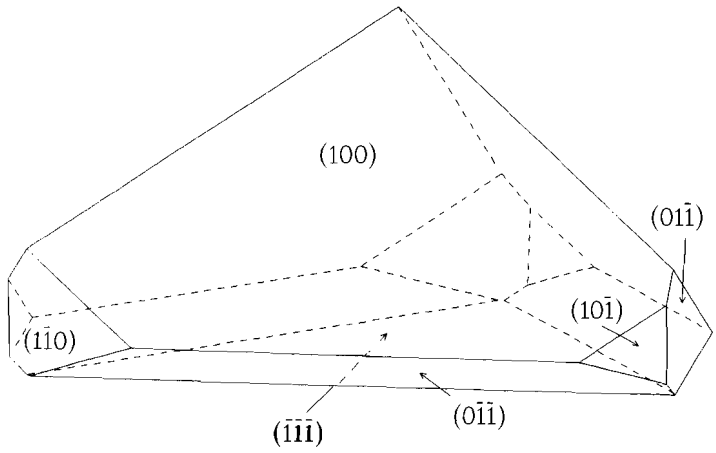

Figure 7.1 Crystal of $MgSO_3 \cdot 6H_2O$ grown from an aqueous solution (after Klasens et al., 1936).

habit are explained in terms of solvent interaction.

7.2 PBC-analysis and F-forms

Magnesium sulphite hexahydrate crystallizes in space group R3 with a = b = c = 5.933 Å and $\alpha = \beta = \gamma = 96.28°$ (Andersen & Lundqvist, 1984). Fractional atomic coordinates are given in table 7.1. The crystal structure is a trigonal distorted CsCl-type of packing of SO_3^{2-} ions and $Mg(H_2O)_6^{2+}$ cation complexes.

Table 7.1 Fractional atomic coordinates of $MgSO_3 \cdot 6H_2O$. a = b = c = 5.933 Å, $\alpha = \beta = \gamma = 96.28°$.

Atom	x	y	z
Mg	0	0	0
S	0.5021	0.5021	0.5021
O	0.5598	0.4826	0.2565
O1	-0.3165	-0.1254	0.0765
H11	-0.4523	-0.0624	0.0258
H12	-0.3632	-0.2635	0.1408
O2	0.3288	0.1464	-0.0496
H21	0.4036	0.2737	0.0651
H22	0.3672	0.1930	-0.1956

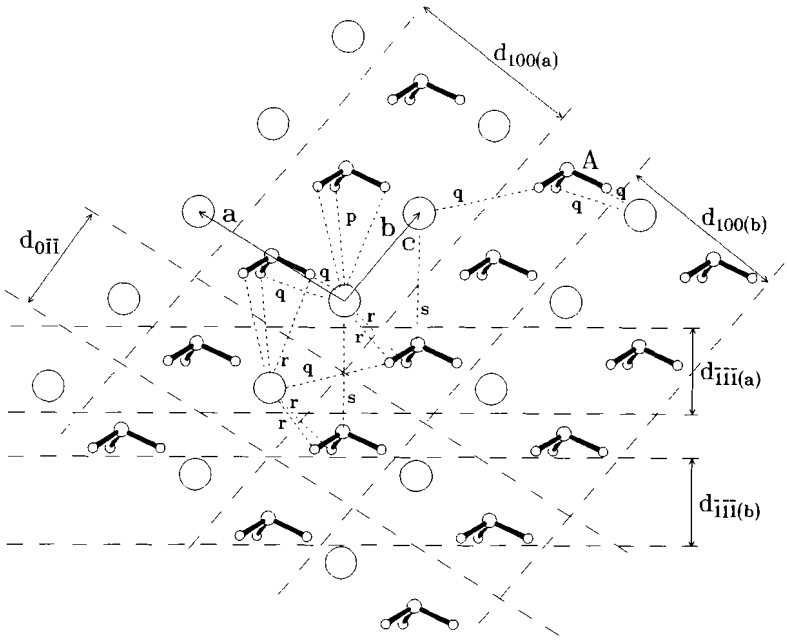

Figure 7.2 Projection along [01$\bar{1}$]. Large circles are $Mg(H_2O)_6^{2+}$ complexes. Slices of (0$\bar{1}\bar{1}$), (100)a, (100)b and (111)a and (111)b are shown.

Figure 7.2 shows a projection along [01$\bar{1}$], the hexagonal *b* axis. Each cation complex is surrounded by eight SO_3^{2-} ions. Because the SO_3^{2-} ions and the $Mg(H_2O)_6^{2+}$ cation complexes are present as such in the solution the strong bonds to be considered are those between a $Mg(H_2O)_6^{2+}$ complex and the SO_3^{2-} ions. In table 7.2 are given the $Mg(H_2O)_6^{2+}$ - SO_3^{2-} bond energies, which are calculated with charges on the atoms Mg(+2e), S(+1e), O(-1e), O_{water}(-0.82e) and H(+0.41e), which agree very well with charges determined with *MOPAC* (Merz & Besler, 1989). The bond *p* is the strongest one and involves three hydrogen bonds along with the Coulomb interaction. The three bonds *q* come next and then follow three bonds *r*. Finally the bond *s* is the weakest one, being not assisted by hydrogen bonds and having the positively charged sulphur atom turned towards the cation complex. The PBCs of CsCl are <111> and the only F-form is {011}. For the sulphites these correspond to the [111]

Table 7.2 Bonds between $Mg(H_2O)_6^{2+}$ and SO_3^{2-} ions in the first coordination sphere and their Coulomb energies (in kJ $mole^{-1}$). The bonds are shown in figures 7.2 and 7.3.

bond	energy (kJ $mole^{-1}$)
p	1389
q	1100
r	1007
s	948

(p + s) and <11$\bar{1}$> *(q + r)* PBCs, so {0$\bar{1}\bar{1}$}, {01$\bar{1}$} and {0$\bar{1}$1} are F-forms. The {01$\bar{1}$} and {0$\bar{1}$1} forms were not recognized by Cadoret (1967) as F-forms because bond *s* was not considered as a strong bond and therefore [111] not as a PBC. To explain the main forms Cadoret (1967) invokes other PBCs such as [01$\bar{1}$] *(q + q)*, indicated at A in figure 7.2 and a bond between two $Mg(H_2O)_6^{2+}$ complexes which is not considered by us because these repel each other. The PBC's *(q + q)* are bonded laterally in slices (100)a, ($\bar{1}\bar{1}\bar{1}$)a and (0$\bar{1}\bar{1}$), which are also shown in figure 7.2 together with the (100)b and ($\bar{1}\bar{1}\bar{1}$)b slices. Figure 7.3 is a projection along [100] which shows the {100}, {01$\bar{1}$} and {0$\bar{1}$1} slices. It is obvious that all F-slices except the {0$\bar{1}$1} and {01$\bar{1}$} slices have a dipole moment perpendicular to the slice.

7.3 Theory

The crystal structure is considered as a stacking of slices and the lattice energy is expressed as

$$E_{cr} = E_{slice} + E_{att} \tag{7.1}$$

where E_{slice} is the slice energy and E_{att} is the attachment energy, which is defined as the energy released when one slice of thickness d_{hkl} is attached to a face (hkl). If the slices have a dipole moment equation (7.1) no longer holds and must be replaced by

$$E_{cr} = E_{slice} + E_{att} + E_{corr} \tag{7.2}$$

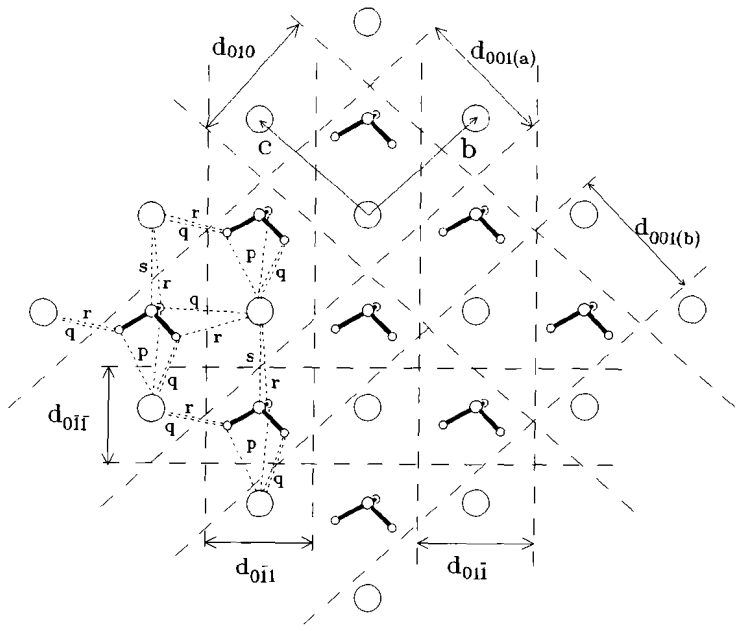

Figure 7.3 Projection along [100]. Large circles are $Mg(H_2O)_6^{2+}$ complexes. Slices of $(0\bar{1}1)$, $(01\bar{1})$, (010)a, (001)a and (001)b are shown.

where E_{corr} is a correction term which is necessary to obtain a constant value of E_{cr} independent of (hkl). The correction term is expressed, according to Smith (1981) and Hartman (1982) as

$$E_{corr} = 2\,\pi\,\mu^2/V \qquad (7.3)$$

where μ is the dipole moment of the slice per primitive unit cell contents and V is the volume of the primitive unit cell. The dipole moment is expressed as

$$\mu_{hkl} = d_{hkl} \sum_i q_i\,(hx_i + ky_i + lz_i) \qquad (7.4)$$

7.4 Results and discussion

Table 7.3 shows the dipole moments, correction energies, attachment energies and slice energies. The Coulomb interactions within the SO_3^{2-} ion and the $Mg(H_2O)_6^{2+}$ complex are subtracted from the calculated slice energies because these ions are believed to exist as such in the solution. The Coulomb energies were calculated with *SURFPOT* (Strom & Hartman, 1989). This program calculates the Coulomb energies of stackings of infinite lattice slices, based on the Ewald method (1921).

Hartman (1956) showed that the electrostatic potential near a slice with a dipole moment does not decrease to zero with the distance to that slice. The potential near the face becomes infinite and the surface becomes unstable. The surface can be stabilized by (1) polarization of bonds within the slice which results in a dipole moment that cancels the original one (2) statistically removing ions from the surface in order to obtain a slice without a dipole moment which has been applied to the (111) face of NaCl (Stranski, 1928; Hartman, 1959; Nosker, Mark & Levine, 1970) (3) a change in the charge or charge distribution within the ions.

Table 7.3 shows that the {001}b and $\{\bar{1}\,\bar{1}\,\bar{1}\}$b slices have larger dipole moments and smaller slices energies than the {001}a and $\{\bar{1}\,\bar{1}\,\bar{1}\}$a slices respectively. So the {001}b and $\{\bar{1}\,\bar{1}\,\bar{1}\}$b slices are unstable with respect to the {001}a and $\{\bar{1}\,\bar{1}\,\bar{1}\}$a slices.

To cancel the dipole moments of the $\{0\bar{1}\,\bar{1}\}$ and $\{\bar{1}\,\bar{1}\,\bar{1}\}$a slices a rearrangement of 5-10% of the ions at the surface is necessary. The {001}a slice has a relatively large dipole moment and a complete reconstruction of the slice is necessary. In figure 7.4 is shown the {001}' slice which is constructed by removing half of the SO_3^{2-} ions. The dipole moment of this slice is 1.22 eÅ

Table 7.3 Slice energies, attachment energies and correction energies (in kJ $mole^{-1}$) and dipole moment per unit cell (in eÅ) for $MgSO_3 \cdot 6H_2O$ (E_{cr} = 2350.3 kJ $mole^{-1}$).

face	E_{slice}	E_{cr}-E_{slice}	E_{att}	E_{corr}	μ
{001}a and $\{00\bar{1}\}$a	1407.6	942.7	26.8	915.9	4.64
{001}b and $\{00\bar{1}\}$b	219.4	2130.9	10.9	2120.0	7.05
$\{0\bar{1}1\}$ and $\{01\bar{1}\}$	1965.9	384.4	384.4	0	0
$\{0\bar{1}\bar{1}\}$ and {011}	1722.3	628.0	514.5	113.5	1.63
$\{\bar{1}\bar{1}\bar{1}\}$a and {111}a	1730.8	619.5	563.9	55.6	1.14
$\{\bar{1}\bar{1}\bar{1}\}$ and {111}b	1344.0	1006.3	-24.1	1030.4	4.92
{001}' and $\{00\bar{1}\}$'	1666.5	683.8	620.5	63.3	1.22

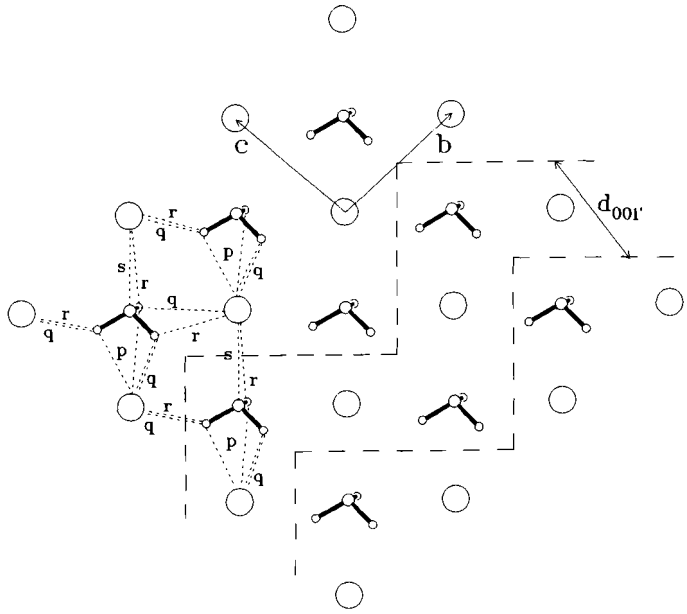

Figure 7.4 Projection along [100] which shows the reconstructed (001)' slice.

and the slice energy is 1666.5 kJ mole^{-1}. This smaller dipole moment can be cancelled in the same way as those of the $\{0\bar{1}\,\bar{1}\}$ and $\{\bar{1}\,\bar{1}\,\bar{1}\}$a slices. Because of these relatively small changes necessary to cancel the dipole moment, the reconstructed slice will be considered as such.

The attachment energies of the {100}a, $\{\bar{1}\,\bar{1}\,\bar{1}\}$a and $\{0\bar{1}\,\bar{1}\}$ slices agree with the estimations of Cadoret (1967), who found that $E_{att}\{100\} < E_{att}\{111\}$ and $E_{att}\{100\} < E_{att}\{0\bar{1}\,\bar{1}\}$.

Equation (7.2) shows that the attachment energy is no longer complementary to the slice energy when the slice has a dipole moment. The question arises which energy should be taken as habit controlling.

In the case of a non-polar crystal E_{att} is taken as the habit controlling factor. In the case of a polar crystal the complement of E_{slice}, which equals $E_{att} + E_{corr}$, can also be taken as habit controlling. Both choices can be defended. The importance of Jackson's α-factor (Jackson, 1958), which is proportional with the slice energy, is stressed when $E_{cr} - E_{slice}$ is taken as habit controlling. An argument for the choice of E_{att} is that it still is the interaction energy of the zeroth slice with an infinite stacking of slices but Table 7.3 shows that the attachment energies can become negative.

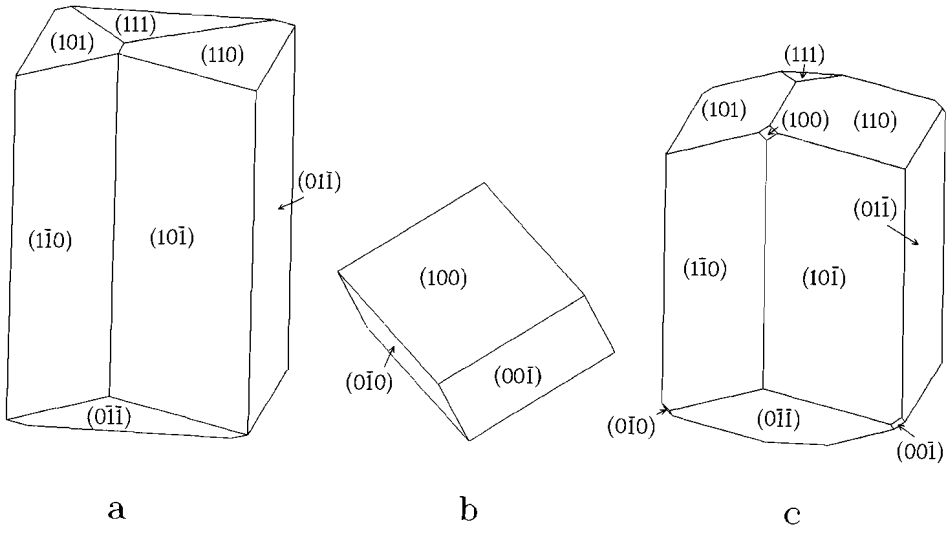

Figure 7.5 Theoretical habits constructed from (E_{att} + E_{corr}) (a), from E_{att} (b), and with reconstructed {001}' and {00$\bar{1}$}' face (c).

The slice energy of a {hkl} slice is of course exactly the same as the one of the {$\bar{h}\bar{k}\bar{l}$} slice. The same holds for the attachment energies. So on this basis one would expect that the growth rates of the {hkl} and {$\bar{h}\bar{k}\bar{l}$} face would be the same. Furthermore, the correction energy of the {001} F-slice is very large and therefore there is a very large difference between the growth forms constructed from E_{att} and the one constructed from E_{att} + E_{corr}. Figure 7.5 shows the theoretical habits of $MgSO_3 \cdot 6H_2O$. Habit a is constructed by taking the central distance of the faces proportional with (E_{att} + E_{corr}) of the F-faces. Habit b is constructed from E_{att} of the F-faces and habit c is constructed from the attachment energies of the F-faces and the reconstructed {001} face.

The polar habit of the crystal grown from an aqueous solution shows that the growth rates of two opposite faces are not the same. If habits are constructed from only the faces that appear on the crystals grown from solution, the non-centric forms shown in figure 7.6 are found. The form constructed from (E_{cr} - E_{slice}) does not agree and the one constructed from E_{att} agrees quite well.

The centric habits show that neither of the quantities (E_{cr} - E_{slice}) in their own can be taken as habit controlling. The observed non-centric habit can not

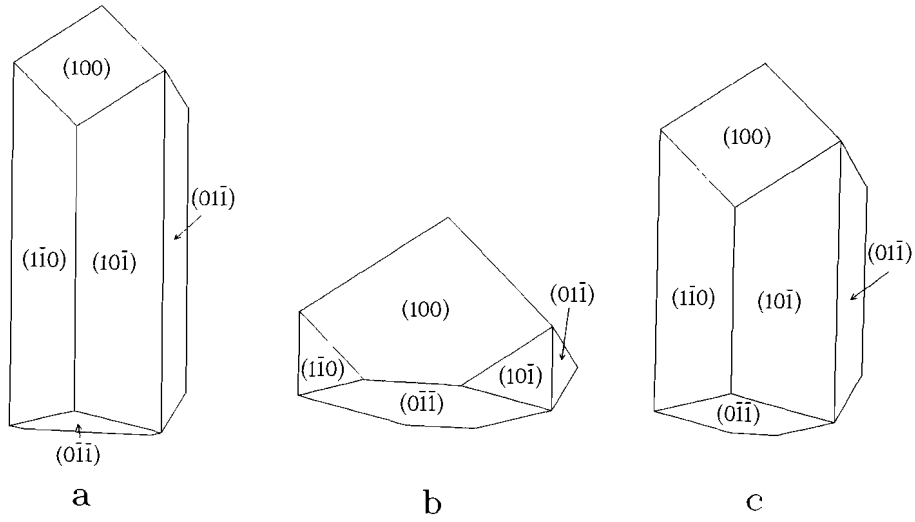

Figure 7.6 Theoretical habits constructed from (E_{att} + E_{corr}) (a), from E_{att} (b), and with reconstructed {001} face (c). Half of the faces are left out.

be predicted and understood by simply removing half of the faces.

Cadoret (1967) explains the polar habit in terms of surface relaxation. The faces are deformed by this relaxation and the mean free path of an adsorbed growth unit on the face decreases due to the deformation. The deformation depends on the polarizability of the ions at the surface. The larger the polarizability the larger the deformation and the larger the reduction of the growth rate. It is not known how large this relaxation effect is in aqueous solutions.

However, the present authors believe that solvent interaction with the faces plays a prominent role. The solvation of the faces changes their growth rate by reducing the surface energy and by changing kinetic factors such as the concentration of adsorbed growth units, the mean free path of the adsorbed growth units and their rate of integration in the lattice. In general it can be stated that the stronger the solvent interaction, the larger the reduction in growth rate. Berkovitch-Yellin (1985) studied the growth of polar crystals of α-resorcinol from different solvents. Crystals obtained from polar solvents exhibit large polar faces and crystals grown from non-polar solvents exhibit large non-polar faces.

Table 7.4 Exposed parts of the sulphite ions of the F-faces of $MgSO_3 \cdot 6H_2O$.

{001}	2 O and 1 S	{00$\bar{1}$}	none
{0$\bar{1}$1}	1 O	{01$\bar{1}$}	2 O
{0$\bar{1}\bar{1}$}	3 O	{011}	1 O and 1 S
{$\bar{1}\bar{1}\bar{1}$}	3 O	{111}	1 S
{001}'	2 O and 1 S	{00$\bar{1}$}'	1 S

The faces of the $MgSO_3 \cdot 6H_2O$ crystals have sulphite ions and water molecules of the hydrated Mg^{2+} ions in their outer layers. The interaction of the solvent (water) with the sulphite ion is stronger than with the hydrated Mg^{2+} ion and therefore a lower growth rate is expected for the faces with exposed sulphite ions. In table 7.4 are listed the exposed parts of the sulphite ions at the surfaces of the F-slices. The {001} face has two oxygens of each sulphite ion in its outer layer, whereas the {00$\bar{1}$} face has water molecules of the hydrated Mg^{2+} ion in its outer layer. On the {$\bar{1}\bar{1}\bar{1}$} and {0$\bar{1}\bar{1}$} faces three oxygens appear. The {111} face has sulphur atoms on its outside and the {011} face one oxygen. The {01$\bar{1}$} face has two oxygens in the outer layer, whereas the {0$\bar{1}$1} face has only one.

From these data on the surface structure of the F-slices it can be predicted that R{001} < R{00$\bar{1}$}, R{$\bar{1}\bar{1}\bar{1}$} < R{111}, R{0$\bar{1}\bar{1}$} < R{011} and R{01$\bar{1}$} < R{0$\bar{1}$1}, which agrees with the observed habit. And indeed it is found that {01$\bar{1}$} is somewhat more developed than {0$\bar{1}$1}. The results do not agree completely with the predictions from Cadoret (1967). He predicted that the {$\bar{1}\bar{1}\bar{1}$} face grows faster than the {111} face, because the sulphite ions on the outside of the {111} face are more polarizable than the $Mg(H_2O)^{2+}$ complexes that appear on the outside of the {$\bar{1}\bar{1}\bar{1}$} face. However, the {111} face is not present on the crystal because the {001} faces grow too slowly and no comparison with experiment is thus possible if final growth forms are studied.

Table 7.5 Required growth rate reductions to fit the theoretical habit constructed from $E_{cr} - E_{sl}$ with the observed habit.

{001} > {011}
{001} > {111}
{$\bar{1}\bar{1}\bar{1}$} > {00$\bar{1}$}
{$\bar{1}\bar{1}\bar{1}$} > {0$\bar{1}\bar{1}$}
{0$\bar{1}$1} < {0$\bar{1}\bar{1}$}, {$\bar{1}\bar{1}\bar{1}$}, {001}
{01$\bar{1}$} < {0$\bar{1}\bar{1}$}, {$\bar{1}\bar{1}\bar{1}$}, {001}

If we consider the theoretical forms in figure 7.5 we see that these are centrosymmetric and that some growth rate reductions are required to match it with the observed habit. These required growth rate reductions, that are listed in table 7.5, agree very well with the strength of the solvent interaction that can be deduced from table 7.4.

These results show that the polar habit of the $ASO_3 \cdot 6H_2O$ crystals can be explained satisfactorily when the interaction of the solvent (water) is taken into account, but only in a qualitative way.

7.5 Conclusions

1. The $ASO_3 \cdot 6H_2O$ structure can be considered as a distorted CsCl-like arrangement, leading to the F-forms {001}, {00$\bar{1}$}, {011}, {0$\bar{1}\bar{1}$}, {01$\bar{1}$}, {0$\bar{1}$1}, {111}, and {$\bar{1}\bar{1}\bar{1}$}.

2. Because the PBC-theory can not distinguish between {hkl} and {$\bar{h}\bar{k}\bar{l}$} forms the theoretical habit is centrosymmetric. Two theoretical habits have been derived. One, based on slice energies, is elongated along the three-fold axis with the prisms {01$\bar{1}$} and {0$\bar{1}$1} as main forms and is terminated by {011}, {0$\bar{1}\bar{1}$}, {111} and {$\bar{1}\bar{1}\bar{1}$}. The other,based on attachment energies is isometric with only {100} and {$\bar{1}$00}.

3. It is suggested that the growth rates of non-equivalent opposite faces (hkl) and ($\bar{h}\bar{k}\bar{l}$) are different because of their different interaction with the solvent. For $ASO_3 \cdot 6H_2O$ the interaction with the exposed oxygens of the sulphite ion is the habit controlling factor. It leads to a qualitative explanation of the observed habit.

References

Andersen, L. & Lundqvist, O. (1984). *Acta Cryst.* C**40**, 584.
Berkovitch-Yellin, Z. (1985). *J. Am. Chem. Soc.* **107**, 8239.
Cadoret R. (1967). *Bull. Soc. Franç. Minér. Crist.* **90**, 44.
Ewald, P.P. (1921). *Ann. Phys. (Leipzig)* **64**, 253.
Hartman, P. (1956). *Acta Cryst.* **9**, 569.
Hartman, P. (1959). *Bull. Soc. Franç. Minér. Crist.* **82**, 158.
Hartman, P. (1982). *Z. Krist.* **161**, 259.

Jackson, K.A. (1958). in: *Liquid Metals and Solidification* (Amer. Soc. Metals, Cleveland), p. 174.

Klasens, H.A., Perdok, W.G. & Terpstra, P. (1936). *Z. Krist.* **94**, 1.

Merz, K.M. & Besler, B.H. (1989). *MOPAC.* QCPE Program 589. It may be obtained by writing to Quantum Chemistry Program Exchange, Department of Chemistry, Indiana University, Bloomington, IN 47405, USA.

Nosker, R.W., Mark, P. & Levine, J.D. (1970). *Surf. Sci.* **19**, 291.

Smith, E.R. (1981). *Proc. Roy. Soc. London* **A375**, 475.

Stranski, I.N. (1928). *Z. Phys. Chem.* **136**, 259.

Strom, C.S. & Hartman, P. (1989). *Acta Cryst.* A**45**, 371.

CHAPTER 8

THE HABIT OF GYPSUM AND SOLVENT INTERACTION

Abstract

In this work the hydrated faces of gypsum crystals are studied. Two kinds of water molecules can be present on the faces. One kind is a part of the crystal structure and does not have to be removed before growth can continue. The other kind does not belong to the crystal structure and has to be removed, thereby lowering the growth rate.

Starting from this hypothesis it is found that the growth rate of the $\{\bar{1}11\}$ face is affected more than that of the {011} face, which agrees well with the observed habit. When organic impurities are present the growth rates of the $\{\bar{1}11\}$ and {011} faces are equally reduced, which is in agreement with the observed habit from solutions with organic impurities.

8.1 Introduction

The effect of the crystal structure on the habit of gypsum, $CaSO_4 \cdot 2H_2O$, has been studied by several authors. Simon & Bienfait (1965) carried out a PBC analysis and calculated electrostatic attachment energies. The theoretical habit is platy {010} with side faces {120} and {011} (figure 8.1a). Crystals of gypsum grown from aqueous solutions exhibit a large {020} basal plane with {120} and $\{\bar{1}11\}$ side faces, The {011} face is usually absent (figure 8.1b). They explain this discrepancy in terms of solvent interaction. The solvent (water) probably interacts more strongly with the Ca^{2+} ions that protrude from the $\{\bar{1}11\}$ face than with the {011} face that is bounded by SO_4^{2-} ions. This leads to a relatively large decrease in growth rate of the $\{\bar{1}11\}$ face.

Weijnen *et al.* (1987) calculated Ising temperatures and took these as a measure for the relative growth rates of the faces. The {011} and $\{\bar{1}11\}$ slices were believed to grow in slices of thickness $\frac{1}{2}d_{011}$ and $\frac{1}{2}d_{\bar{1}11}$ respectively. The result was a platy habit {010} with side faces {120} and {011} which is elongated along the c-axis, because of the higher relative growth rates of {011}

and {$\bar{1}11$}. They mention that the discrepancy between theory and practice can not be attributed to solvent adsorption because the {$\bar{1}11$} and {011} face are probably bounded by water molecules that are attached to Ca^{2+} ions. Furthermore, they show that the charge density along the reciprocal vectors $[\bar{1}11]^*$ and $[011]^*$ gives no obvious reason for a stronger solvent interaction with the {$\bar{1}11$} face.

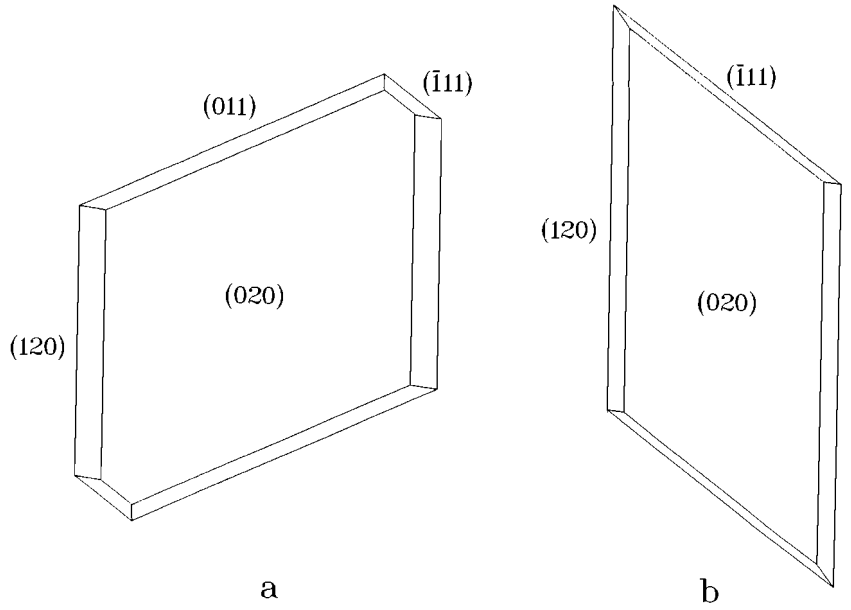

Figure 8.1 Theoretical habit as derived by Heijnen and Hartman (1990) (a) and observed habit of gypsum from an aqueous solution (b) (after Simon & Bienfait, 1965).

A computerized PBC-analysis of Heijnen & Hartman (1990) revealed five F-forms {020}, {011}, {$\bar{1}11$}, {120} and {$\bar{1}22$} of which the latter has not been found earlier. They calculated electrostatic attachment energies for several charge distributions in the SO_4^{2-} ion and in the water molecules. They found that the charge distribution on the water molecules is determinative for the theoretical habit, in this case the relative morphological importance of {011} and {$\bar{1}11$}. They mention that the difference in attachment energy of both slice configurations of {011} is smaller than for {$\bar{1}11$}. The {011} face,

therefore, starts to grow in half slices at a lower supersaturation than $\{\bar{1}11\}$. The {011} face thus grows faster and disappears from the crystal.

This explanation is only valid if 2D-nucleation determines the growth rate. Christoffersen *et al.* (1982), however, show that growth at moderate supersaturations is controlled by a screw dislocation mechanism.

The theoretical habits from these studies have in common that the morphological importance of $\{\bar{1}11\}$ is much less than that of {011}. There is no consensus about the origin of the discrepancies.

The present authors agree with Weijnen *et al.* (1987) that the gypsum faces must be bounded by water molecules. After all, the crystals grow from aqueous solutions.

The charge density in the crystal structure along a reciprocal vector is, however not a measure for the strength of the solvent interaction as was mentioned by Weijnen *et al.* (1987). This is because the charge density in the crystal structure gives no information about the electrostatic potential and field strength near the surface. So this is not an argument to rule out the influence of solvent interaction.

The purpose of this paper is to provide an explanation for the discrepancy between observed and theoretical habit by studying the hydrated crystal faces and the influence of the hydration on the growth rate.

8.2 Hydration of the surface

The faces of a crystal in an aqueous solution are hydrated. In general these water molecules have to be removed before growth can continue. When the water molecules are adsorbed very strongly the dehydration of the surface determines the growth kinetics.

When the crystal is a hydrate the situation may be different. Water molecules at the interface between crystal and solution may belong to the crystal structure because they are adsorbed on crystallographic positions. The bivalent cations in hydrates such as $MgSO_3 \cdot 6H_2O$ (Van der Voort & Hartman, 1990), $MgSO_4 \cdot 7H_2O$ (Rubbo, Aquilano, Franchini-Angela & Sgualdino, 1985), $K_2Mg(SO_4)_2 \cdot 6H_2O$ (Hartman, 1990), and $NiSO_4 \cdot 6H_2O$ (Hottenhuis, 1988) have a complete first coordination sphere. The $A(H_2O)_6^{2+}$ cation complexes in the crystal are also present as such in the solution. So dehydration of the cation

Table 8.1 Electrostatic p, q, r, s, and t bond energies.

bond	bond energy (kJ $mole^{-1}$)
p	1736
q	1577
r	249.5
s	88
t	90

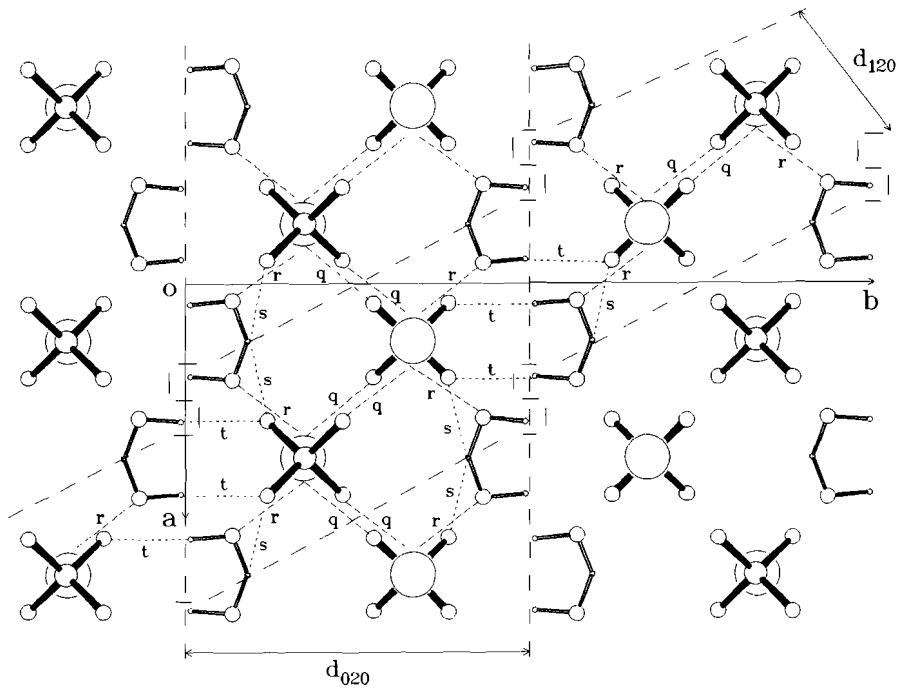

Figure 8.2 F-slices as established by Heijnen and Hartman (1990) in a [001] projection of gypsum with slices (020) and (120). Large circles are Ca^{2+} ions. Smaller circles are S and O atoms and smallest circles are H atoms.

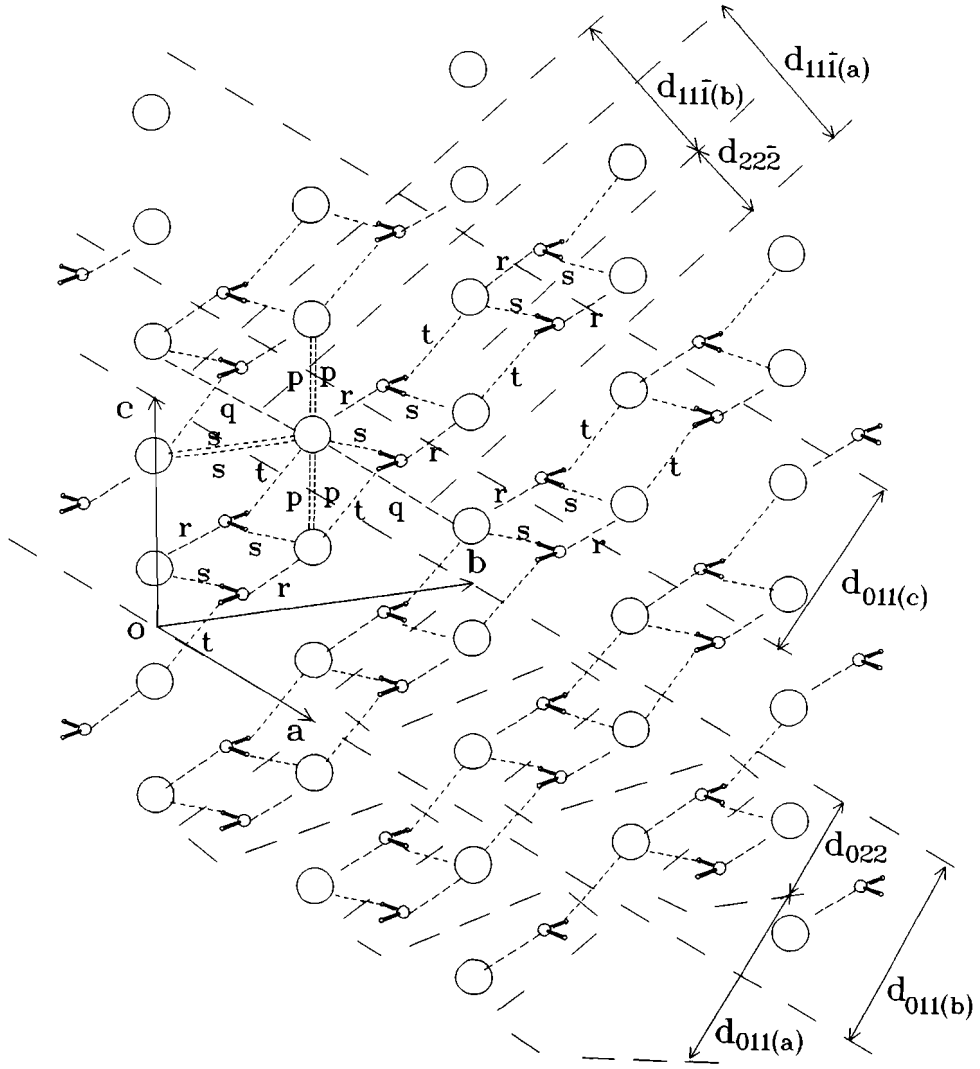

Figure 8.3 F-slices as established by Heijnen and Hartman (1990) in a [2$\bar{1}$1] projection with (011)a, (011)b (011)c, (022), (11$\bar{1}$)a, (11$\bar{1}$)b and (22$\bar{2}$) slices. Large circles represent the chain Ca - SO_4 - H_2O - Ca along [2$\bar{1}$1].

in the solution and at the surface is not necessary and a strong bond between a water molecules and a cation will not lower the growth rate.

In the case of gypsum the Ca^{2+} ions are surrounded by two water molecules while in the solution a much higher coordination is possible. The coordination is far from complete and coordination water of a Ca^{2+} ion at the surface can belong to the crystal structure *i.e.* is present on crystallographic positions or it belongs to the solution. In the latter case it has to be removed. If the dehydration of the surface determines the growth kinetics then the "solution water" lowers the growth rate. An application of this hypothesis to gypsum is discussed in this paper.

8.3 Results and discussion

Figure 8.2 and 8.3 show a [001] and [2$\bar{1}$1] projection of the crystal structure of gypsum with the (020), (120), (011) and ($\bar{1}$11) slices and the bonds *p*, *q*, *r*, *s*, and *t*. Bond *p* is a Ca-SO_4 bond in which Ca^{2+} is bonded to two oxygens of the SO_4^{2-} ion. In bond *q* Ca^{2+} is bonded to one oxygen. Bond *r* is a short contact between Ca^{2+} and water. Bonds *s* and *t* are two non-equal hydrogen bonds between water and the SO_4^{2-} ion. Table 8.1 shows the electrostatic bond energies of the *p*, *q*, *r*, *s*, and *t* bonds. These bond energies were calculated based on the crystal structure determination by Cole and Lancucki (1974) by Heijnen and Hartman (1990). The charges on the ions were taken as Ca^{2+}, S^{2+}, O^{1-} and $H^{\frac{1}{2}+}$. Bonds *p* and *q* are the strongest because they are contacts between a positive and negative ion charged +2 and -2 respectively. Bonds *r*, *s* and *t* are much weaker.

In this study it is assumed that the slices are bounded by water molecules that belong to the crystal structure. These water molecules are bonded to Ca^{2+} and SO_4^{2-} ions in the slice. In figures 8.4 and 8.5 these hydrated slices are shown which are constructed by moving water molecules along lattice translations. This has consequences for the slice energies because bonds are made and broken when the water molecules are moved. If we consider nearest neighbour interactions only, the bonds made and broken can be expressed in terms of bonds *r*, *s*, and *t* so an energy balance can be made. Table 8.2 shows the bonds to be made and broken and the energy involved to transform an F-slice into a hydrated slice. In the nearest neighbour approximation (NNA) the energy involved in this slice transformation corresponds to the increase in attachment energy.

Table 8.2 Attachment energies of the F-faces of gypsum as determined by Heijnen and Hartman (1990) and attachment energies of the hydrated slices.

face	E_{att}	bonds broken	bonds made	E_{att}'(NNA)	E_{att}'
{020}	75.8	2r + 2s	2t	199.7	199.6
{120}	292.4	2r + t	2s + t	373.2	357.2
{011}a	286.7	2r	2s + 2t	322.5	311.2
{$\bar{1}$11}	472.4	-	-	-	-

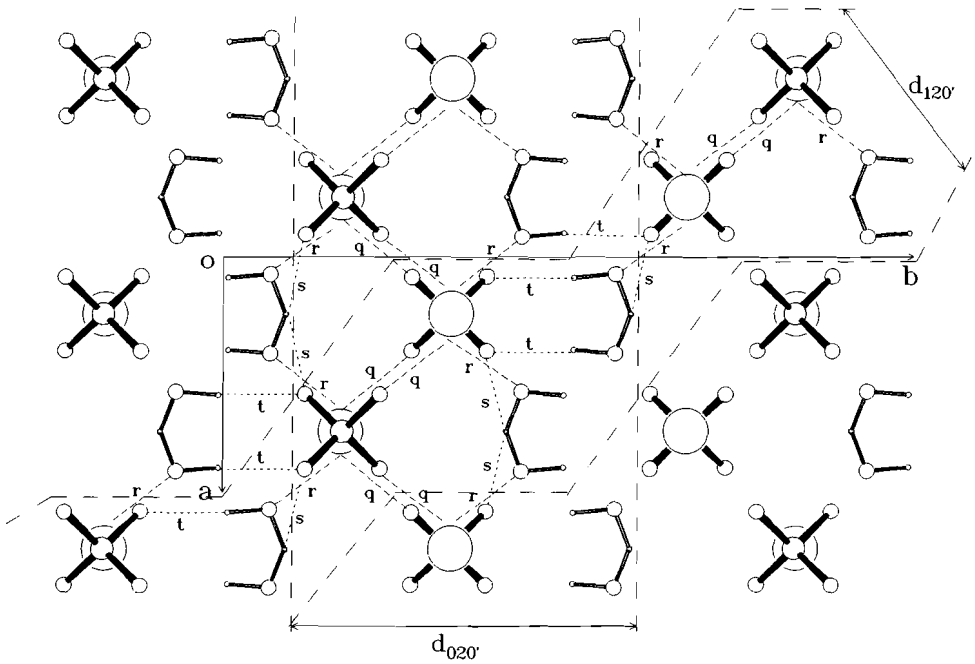

Figure 8.4 Hydrated slices (020)' and (120)' in a [001] projection.

For the {$\bar{1}$11} face no hydrated slices were constructed because there are no strong bonds *r*, *s*, and *t* between the slices. The attachment energies of the hydrated slices are shown in table 8.2 as well as the attachment energies that were calculated by Heijnen and Hartman (1990).

The attachment energies were also calculated with *SURFPOT* (Strom & Hartman, 1989), a program that calculates Coulomb energies of infinite lattice slices, based on the Ewald method (1921), and are also listed in table 8.2. The

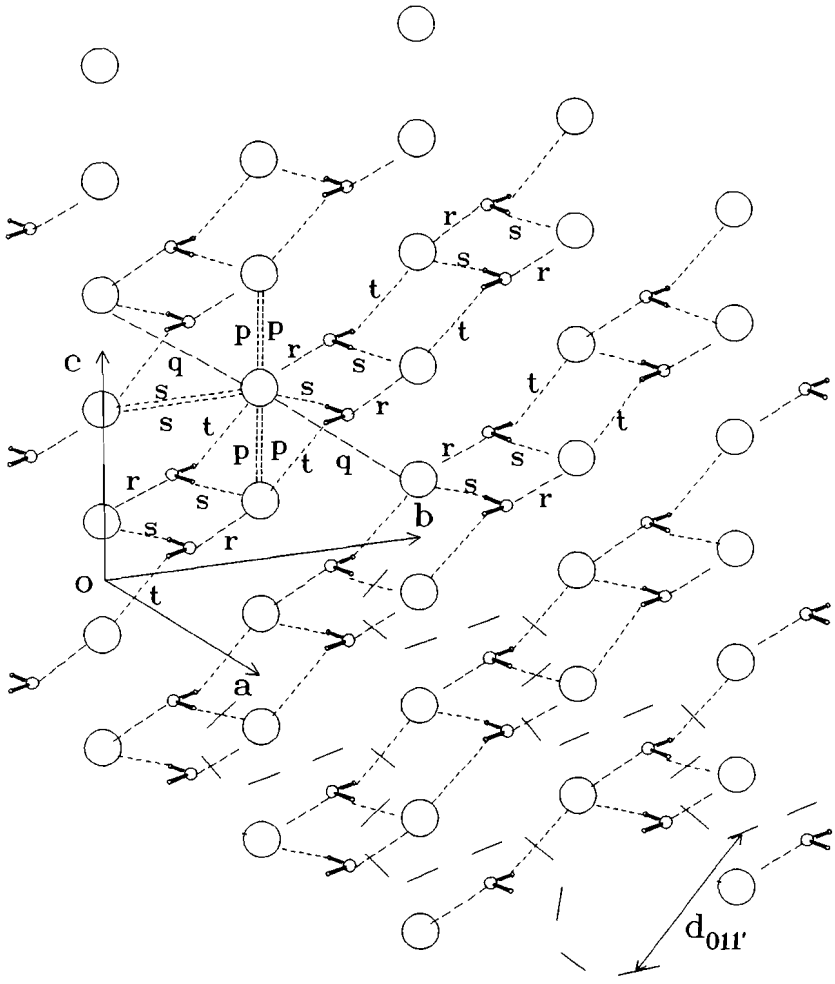

Figure 8.5 Hydrated (011)' slice in a $[2\bar{1}1]$ projection.

agreement between the attachment energies calculated in these two different ways is good, which shows that the nearest neighbour approximation can be used in this case. This is because the slice transformation involves translations of water molecules which are electrically neutral. The theoretical habit, that is constructed by taking the central distances of the faces proportional with the attachment energies of the $\{\bar{1}11\}$ face and of the hydrated {020}, {120} and {011} faces, is shown in figure 8.6. This theoretical habit does not differ much from the one determined by Heijnen and Hartman (1990) (figure 8.1a).

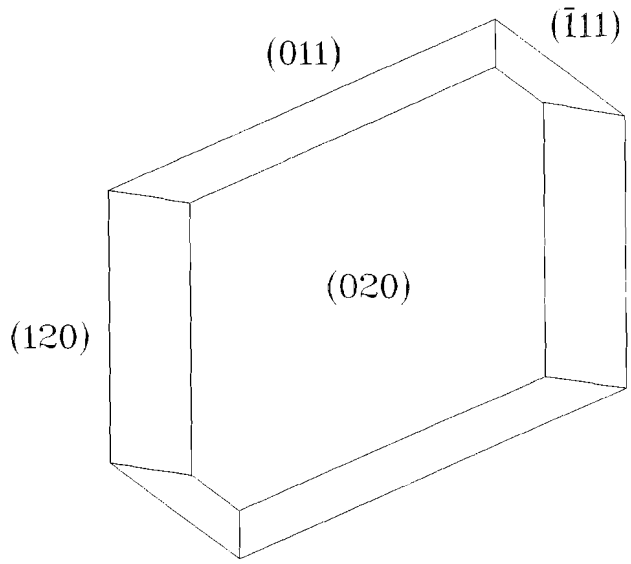

Figure 8.6 Theoretical habit of gypsum based on the attachment energies of the $\{\bar{1}11\}$ and the hydrated {020}, {011}, and {120} faces.

Although the hypothesis that the (011) face grows in layers $\frac{1}{2}d_{011}$ does improve the habit, a better agreement can be obtained by taking the hydration of the surfaces into account even when growth in half layers is not considered.

When growth takes place from a solution, water molecules are also present on other than crystallographic positions at the surface. As was already presumed in section 8.2 these water molecules reduce the growth rate. Table 8.3 shows which sites are available for water adsorption on non-crystallographic positions. The solvent interaction with the Ca^{2+} ions, of which the strength is approximately the same as bond r, is stronger than that

with the SO_4^{2-} ions, the strength of the latter being similar to that of bond *s* or *t*. The largest growth rate reduction is expected for {120} and {$\bar{1}$11} faces, which have Ca^{2+} and SO_4^{2-} ions available for solvent adsorption. The growth rate reduction of the (011) face is substantially smaller than that of the ($\bar{1}$11) face, so the latter can become the dominant terminal face in agreement with the observed habit (figure 8.1b).

When organic impurities are present in the solution, that interact more strongly with the faces than water, they may replace adsorbed water molecules on both crystallographic and non-crystallographic positions. The growth rates of the side faces {011} and {$\bar{1}$11} will be affected equally and the theoretical habit like the one shown in figure 8.1a may be obtained. Indeed, the {011} face is found to prevail over the {$\bar{1}$11} face on crystals grown from aqueous solutions with organic impurities (Weijnen & van Rosmalen, 1985).

8.4 Conclusions

The habit of gypsum crystals grown from a pure aqueous solution can be explained in a qualitative way when solvent interaction is taken into account. The habit of gypsum from solutions with organic impurities can be explained by the adsorption of the impurities. The solvent (water) should also be considered as an impurity, but in the case of a solvate (hydrate like gypsum) one should be very careful. On some of the faces water seems to act as an impurity, lowering the growth rate and on other faces it adsorbs on crystallographic natural water positions thus leaving the growth rate more or less unaltered.

References

Christoffersen, M.R., Christoffersen, J. Weijnen, M.P.C. & van Rosmalen, G.M. (1982). *J. Crystal Growth* **58**, 585.

Cole, W.F. & Lancucki, C.J. (1974). *Acta Cryst.* B**30**, 921.

Ewald, P.P. (1921). *Ann. Phys. (Leipzig)* **64**, 253.

Hartman, P. (1990). Private communication.

Heijnen, W.M.M. & Hartman, P. (1990). In preparation.

Hottenhuis, M.H.J. (1988). Ph.D. Thesis, Nijmegen.

Rubbo, M., Aquilano, D., Franchini-Angela, M. & Sgualdino, G. (1985). *J. Crystal Growth* 71, 470.

Simon, B. & Bienfait, M. (1965). *Acta Cryst.* **19**, 750.

Strom, C.S. & Hartman, P. (1989). *Acta Cryst.* A**45**, 371.

Van der Voort, E. & Hartman, P. (1990). Accepted for publication in *J. Crystal Growth.*

Weijnen, M.P.C. & van Rosmalen, G.M. (1985). *Desalination* **54**, 239.

Weijnen, M.P.C., van Rosmalen, G.M., Bennema, P. & Rijpkema, J.J.M. (1987). *J. Crystal Growth* **82**, 509.

SUMMARY

The agreement between theoretical habits of crystals obtained from PBC-analyses and observed habits is often remarkably good, even though only the internal crystalline structure is taken into account. Sometimes discrepancies are observed. The purpose of the research described in this thesis is to explain these discrepancies mainly in terms of interaction of solvent with the crystal and to improve the theoretical habits. Most of the discrepancies are observed when the crystals are grown from a solution. Solvent interaction with the crystal surfaces is believed to play an important role in reducing the growth rate of the faces.

Chapter 1 provides the reader with an introduction to the problem and a survey on what research has been done on solvent interaction with surfaces. In this thesis we focus on water as a solvent.

In Chapter 2 calculations of the electrostatic field near the cleavage rhombohedron of calcite are reported. It is shown that the electrostatic field is very strong and therefore the interaction of water with the face too.

The influence of previously reported oscillations with temperature in the growth rate of the faces of potassium nitrate crystals on the habit of these crystals is investigated. The oscillations are believed to be caused by changes in the structure of the solution near the faces. Habit changes were indeed observed but smaller and in a different way as was expected (Chapter 3).

In Chapters 4, 5, 6, 7 and 8 some case studies in which theory and practice do not agree are reported.

The interaction of water with the faces of succinic acid crystals was determined with the aid of Molecular Mechanics calculations (Chapter 4). The strength of the solvent interaction was included in the calculation of the theoretical growth rates. It appeared possible to explain the habit from water as well as from *iso*-propanol.

The same method was applied to potassium nitrate (Chapter 5). It was found that on certain positions on the crystal faces water molecules can adsorb very strongly. The removal of these water molecules is a slow step in the growth process and this step is believed to determine the growth rate. Only a qualitative explanation appeared feasible, due to the complexity of the system. In this case it is not known whether the growth units are single ions, ion pairs or larger complexes because of the high concentration of the saturated solution.

The relatively simple crystal structure of alkali halides such as sodium chloride made it possible to study also solvent interaction with steps and kinks. It was possible to establish the growth rate law and the rate of integration of growth units (ions). With the results it was possible to explain the habit change, when the supersaturation increases, from cube to octahedron.

Two case studies involving hydrates are presented in Chapters 7 and 8. The first one involves the polar habit of $MgSO_3 \cdot 6H_2O$, which can not be predicted by the PBC-theory. The second study deals with the habit of gypsum crystals. Several theoretical habits have been derived already, but none of them agrees with the habit from pure aqueous solutions. The polar habit of $MgSO_3 \cdot 6H_2O$ could be explained by taking the interaction of water with the sulphite oxygens as a habit controlling factor. The habit of gypsum and the (different) habit from solutions with organic impurities could also be explained in terms of solvent interaction by making a distinction between water molecules adsorbed on crystallographic, natural, positions and on non-crystallographic positions.

We have been able to explain several habits which could not be predicted with the current methods. However, in some cases is still not yet possible to predict good theoretical habits of crystals grown from solutions.

The solvent interaction with the crystal faces should anyway be considered as an important habit controlling factor.

Improvements can be made by further study of the structure of, especially, solutions of electrolytes in the adsorption layer on crystal faces in order to understand the complex growth mechanism of electrolyte crystals. Furthermore, taking surface relaxation in the presence of solvent molecules into account may provide more accurate values of solvent interaction energies.

SAMENVATTING

De overeenstemming tussen theoretische groeivormen van kristallen, verkregen uit PBC-analyses, en waargenomen vormen is vaak opvallend goed, ondanks het feit dat alleen de interne kristallijne structuur in beschouwing genomen wordt. Soms worden er toch verschillen waargenomen. Het doel van het in dit proefschrift beschreven onderzoek is om deze verschillen te verklaren met behulp van de interactie tussen oplosmiddel en kristalvlakken, en om zo de theoretische groeivormen te verbeteren. De meeste discrepanties worden waargenomen als de kristallen uit een oplossing gegroeid worden. De oplosmiddel/kristalvlak-interactie speelt vermoedelijk een belangrijke rol bij het verlagen van de groeisnelheid van de vlakken.

Hoofdstuk 1 geeft de lezer een inleiding tot het probleem en een overzicht van het onderzoek dat reeds gedaan is aan oplosmiddel/oppervlak-interactie. In dit proefschrift concentreren we ons op water als oplosmiddel.

In hoofdstuk 2 worden berekeningen van het elektrostatisch veld aan het splijtingsrhomboëdervlak van calciet gepresenteerd. Het blijkt dat het veld zeer sterk is en dus de interactie van watermoleculen met het veld ook.

De invloed van oscillaties in de groeisnelheid van kristalvlakken van kaliumnitraat als functie van de temperatuur op de habitus van deze kristallen is onderzocht. Deze oscillaties worden vermoedelijk veroorzaakt door veranderingen in de structuur van de oplossing grenzend aan de vlakken. Er werden inderdaad veranderingen in de habitus waargenomen maar kleiner en op een andere manier dan was verwacht (Hoofdstuk 3).

In hoofdstukken 4, 5, 6, 7 en 8 worden een aantal gevallen waarbij theorie en praktijk niet overeenkomen bestudeerd.

De interactie van water met de vlakken van barnsteenzuurkristallen werd bepaald met behulp van moleculaire mechanica berekeningen (Hoofdstuk 4). De sterkte van de oplosmiddel-interactie werd meegenomen in de berekening van de theoretische groeisnelheden. Het bleek mogelijk om de habitus uit zowel water als *iso*-propanol te verklaren.

Dezelfde methode werd toegepast op kaliumnitraat (Hoofdstuk 5). Er werd gevonden dat watermoleculen zeer sterk kunnen adsorberen op bepaalde plaatsen op de kristalvlakken. Het verwijderen van deze watermoleculen is een langzame stap in het groeiproces en bepaalt vermoedelijk de groeisnelheid. Alleen een kwalitatieve uitleg bleek mogelijk, hetgeen te wijten is aan de

complexiteit van het systeem. Het is niet bekend of de groei-eenheden ionen, ionenparen of grotere complexen zijn. Dit komt door de hoge concentratie van de verzadigde oplossing.

De relatief eenvoudige kristalstructuur van alkalihalides zoals natriumchloride maakt het mogelijk om ook de oplosmiddel-interactie met steps en kinks te bestuderen. Het was mogelijk om de groeiwet vast te stellen en de integratiesnelheid van de groeieenheden (ionen). Met de resultaten was het mogelijk om de habitusverandering, als de oververzadiging toeneemt, van kubus naar octaëder te verklaren.

Twee gevallen die hydraten betreffen worden beschreven in hoofdstukken 7 en 8. In het eerste geval gaat het om de polaire habitus van $MgSO_3 \cdot 6H_2O$, die niet voorspeld kan worden met de PBC theorie. In het tweede geval gaat het om de habitus van gipskristallen. Verschillende theoretische groeivormen hiervoor zijn al afgeleid, maar geen van alle komt overeen met de habitus uit waterige oplossingen. De polaire vorm van de $MgSO_3 \cdot 6H_2O$ kristallen kon verklaard worden door aan te nemen dat de interactie van water met de zuurstofatomen van de sulfietionen bepalend voor de groeisnelheid is. De habitus van gips en de (verschillende) habitus uit oplossingen met organische verontreinigingen konden ook met oplosmiddel-interactie verklaard worden door onderscheid te maken tussen watermoleculen geadsorbeerd op kristallografische en niet-kristallografische posities.

We zijn in staat om verschillende kristalvormen te verklaren die niet voorspeld konden worden met de gangbare methoden. Echter in sommige gevallen is het nog steeds niet mogelijk om goede theoretische groeivormen van kristallen uit oplossingen te voorspellen.

De oplosmiddel-interactie met de kristalvlakken moet in elk geval gezien worden als een belangrijke habitus-bepalende factor.

Verbeteringen kunnen worden gemaakt door verdere studie van, in het bijzonder, de structuur van electrolyt-oplossingen in de adsorptielaag op kristalvlakken om het complexe groei-mechanisme van kristallen van electrolyten te begrijpen. Verder kunnen betere waarden voor oplosmiddel-interactie energieën verkregen worden door oppervlakte-relaxatie in aanwezigheid van oplosmiddel mee te nemen.

CURRICULUM VITAE

De auteur van dit proefschrift werd op 11 december 1962 geboren te Utrecht. In 1981 behaalde zij het Atheneum-B diploma aan de Rijksscholengemeenschap "Schoonoord" te Zeist. In hetzelfde jaar werd begonnen met de Scheikunde studie aan de Rijksuniversiteit Utrecht. Het kandidaatsexamen (S_2) werd afgelegd in september 1984. Het doctoraalexamen met hoofdvak organische chemie en bijvak kristal- en structuurchemie werd afgelegd in mei 1986 (cum laude). Van augustus 1986 tot augustus 1990 was zij werkzaam bij de afdeling Kristallografie van het Instituut voor Aardwetenschappen van de Rijksuniversiteit Utrecht, waar het in dit proefschrift beschreven onderzoek werd verricht. Sinds 1 augustus 1990 is zij werkzaam als wetenschappelijk medewerker bij het Philips Natuurkundig Laboratorium te Eindhoven.